Pattern Formation in Magnetic Thin Films: Analysis and Numerics

D I S S E R T A T I O N

zur Erlangung des akademischen Grades

Dr. rer. nat.
im Fach Mathematik

eingereicht an der
Mathematisch-Naturwissenschaftlichen Fakultät II
Humboldt-Universität zu Berlin

von
Herr Nicolas Condette

Präsident der Humboldt-Universität zu Berlin:
Prof. Dr. Christoph Markschies

Dekan der Mathematisch-Naturwissenschaftlichen Fakultät II:
Prof. Dr. Peter Frensch

Gutachter:
1. Prof. Dr. Christof Melcher
2. Prof. Dr. Andreas Griewank
3. Prof. Dr. Endre Süli

eingereicht am: 22. Februar 2010
Tag der mündlichen Prüfung: 05. Oktober 2010

To my grandmother.

Abstract

This thesis is concerned with the study of a class of variational problems arising in the context of ferromagnetism. More precisely, it aims at providing a numerical and analytical background to the study of hard magnetic thin films with perpendicular anisotropy. Magnetic thin films are sheets of magnetic materials with thicknesses of a few micrometers down to a few nanometers used mainly in electronic industry, for example as magnetic data storage media for computers.

Our initial considerations are based on a model of Landau and Lifshitz that associates the ground states of the magnetization within a three-dimensional body to the minimizers of a nonconvex and nonlocal energy functional, the so-called micromagnetic energy. Under film thickness considerations (thin film regime), we first reduce the aforementioned model to two dimensions and then carry out a Γ-limit for a sharp-interface model. The resulting energy functional features a competition between an interfacial and a dipolar energy contribution.

The second part of the thesis is concerned with the analysis of a numerical method to approximate solutions of the previously derived sharp-interface model. We base our considerations on a relaxed model in which we replace the interfacial energy contribution by its Modica–Mortola approximation, and then study the associated L^2 gradient flow. The resulting evolution equation, a nonlinear and nonlocal parabolic equation, is discretized by a Crank–Nicolson approximation for the time variable and a Fourier collocation method for the space variable. We prove the existence and uniqueness of the solutions of the numerical scheme, the convergence of these solutions towards solutions of the initial continuous model and also derive a-priori error estimates for the numerical method. Finally, we illustrate the analytical results by a series of numerical experiments.

Zusammenfassung

Die vorliegende Arbeit beschäftigt sich mit einer Klasse von Variationsproblemen, die im Kontext des Ferromagnetismus entstehen. Es soll hierbei ein numerischer und analytischer Hintergrund zur Behandlung von harten magnetischen dünnen Filmen mit senkrechter Anisotropie gegeben werden. Bei magnetischen dünnen Filmen handelt es sich um Schichten von magnetischen Materialien mit Dicken von wenigen Mikrometern bis hin zu einigen Nanometern, die hauptsächlich in der Elektronikindustrie, zum Beispiel als Speichermedien in Computern, verwendet werden.

Ausgangspunkt der Betrachtungen ist ein Modell von Landau und Lifshitz, das die Grundzustände der Magnetisierung in einem dreidimensionalen Körpers mit den Minimierer eines nichtkonvexen und nichtlokalen Energiefunktionals, der sogenannten mikromagnetischen Energie, verbindet. Unter der Annahme sehr kleiner Filmdicken wird aus dem betrachteten Modell ein zwei-dimensionales Modell hergeleitet. Anschließend wird mit Hilfe der Γ-Konvergenz die Konvergenz zu einem Sharp-Interface-Modell gezeigt. Das resultierende Energiefunktional besteht aus konkurrierenden Interface- und Dipolenergieanteilen.

Der zweite Teil der Arbeit beschäftigt sich mit der Analyse einer numerischen Methode, die die Lösungen des vorher hergeleiteten Modells approximiert. Hierbei stützen sich die Betrachtungen auf ein relaxiertes Modell, in dem der Interfaceenergiebeitrag durch seine Modica–Mortola Approximation ersetzt und dann der entsprechende L^2 Gradientenfluß betrachtet wird. Die daraus resultierende nichtlineare und nichtlokale parabolische Gleichung wird anschließend durch ein Crank–Nicolson-Verfahren in der Zeitvariablen und einem Fourieransatz für die Raumvariablen diskretisiert. Wir beweisen die Existenz und Eindeutigkeit von Lösungen des numerischen Verfahrens, sowie deren Konvergenz zu Lösungen des anfänglich betrachteten stetigen Modells. Ferner werden auch a priori Fehlerabschätzungen für die numerische Methode hergeleitet. Abschließend werden die analytischen Resultate anhand numerischer Experimente illustriert.

Contents

List of Figures

1. Introduction

Pattern Forming Mechanisms

Stripes and bubble patterns are a paradigm of phase separation phenomena observed in nature, and appear in a large variety of physical problems such as the study of diblock copolymers [17] or hard magnetic films [36]. The formation of such patterns is a rather complex process that can often be understood through energy minimization. We investigate effective energies of the form

$$E_0(v) = \frac{\gamma}{2} \int_{\mathbb{T}^d} |\nabla v| + \frac{1}{2} \sum_{k \in \mathbb{Z}^d} \sigma(k) |\hat{v}(k)|^2 \tag{1.1}$$

for phase parameters $v : \mathbb{T}^d \to \{\pm 1\}$ defined on L-periodic domains $\mathbb{T}^d = (0, L)^d$ (flat torus of dimension $d = 2, 3$). The first energy term represents the interfacial energy. Here the parameter $\gamma > 0$ denotes the domain wall energy per unit length of area, for $d = 2$ and $d = 3$ respectively. The term $\frac{1}{2} \int_{\mathbb{T}^d} |\nabla v| = \mathrm{Per}(\{v = 1\}; \mathbb{T}^d)$ corresponds to the total length (respectively area) of the interfaces on the domain $\mathbb{T}^d$. The interfacial energy penalizes jumps of v, and thus favours the formation of coarse domains. The second energy term is a dipolar interaction energy based on a nonnegative Fourier multiplier $\sigma : \mathbb{Z}^d \to \mathbb{R}$ that decays to zero at infinity. From a variational point of view, this type of self interaction prefers high frequencies, and thus tends to create oscillations of v. The two energy contributions can never simultaneously achieve their minimum value zero and their competition gives rise to a pattern formation process. Understanding the resulting patterns and their morphology amounts to understanding the interplay between interfacial and dipolar energy as well as their scaling behaviour in terms of all system parameters involved.

Micromagnetic Model

Main Problem

In the context of ferromagnetism, (1.1) stems from a reduction of a more general model from micromagnetics. According to a well accepted theory of Landau and Lifshitz, cf. [42], in the absence of an external applied field, the ground states of the magnetization within a ferromagnetic body occupying a three-dimensional domain $\Omega_\delta = \Omega \times (-\frac{\delta}{2}, +\frac{\delta}{2})$ correspond to minimizers of the micromagnetic energy functional

$$d^2 \int_{\Omega_\delta} |\nabla \mathbf{m}|^2 + Q \int_{\Omega_\delta} \varphi(\mathbf{m}) + \int_{\mathbb{R}^3} |\nabla u|^2 \quad \text{for} \quad \mathbf{m} : \Omega_\delta \to \mathbb{S}^2. \tag{1.2}$$

The three summands in the above energy formulation each favour specific orientations or properties for the magnetization. The Dirichlet part, so called exchange energy, is a

quantum mechanical effect. It captures the property of a ferromagnet to favour constant equilibrium magnetization by penalizing deviations. The crystalline anisotropy, which is represented through the even polynomial function $\varphi : \mathbb{S}^2 \to [0, +\infty)$, models the preference for the crystal to favour certain magnetization easy axes. Finally, the nonlocal stray-field (or magnetostatic) energy is connected with the self-induced magnetic field. The magnetostatic potential u is related to the magnetization by Maxwell's equation

$$\Delta u = \nabla \cdot (\mathbf{m}\chi_{\Omega_\delta}) \quad \text{in} \quad \mathbb{R}^3.$$

There are two material parameters involved in the formulation of the micromagnetic energy: the exchange length $d > 0$, which characterizes the strength of the exchange energy relative to the stray-field energy and the quality factor $Q > 0$ which measures the relative strength of the anistropy and magnetostatic energies. The latter is a dimensionless quantity that enables to separate ferromagnetic materials into two broad classes: soft magnetic materials characterized by $Q \ll 1$, and hard magnetic materials for which we consider $Q \gg 1$. A further lentgh scale of interest in the study of the micromagnetic model is the ratio $d/\sqrt{Q}$ which defines the typical width of the Bloch wall transition to be introduced afterwards.

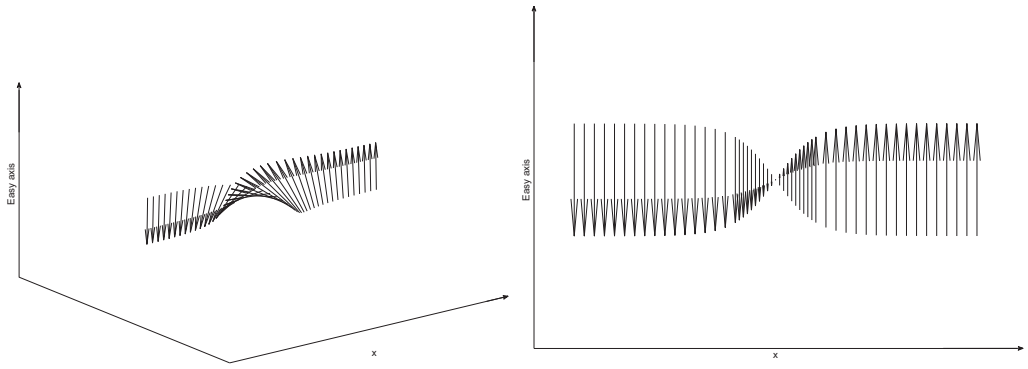

Figure 1.1.: Bloch wall transition.

Magnetic Domains and Domain Walls

The micromagnetic energy features a large variety of metastable states (local minimizers), as well as the development of microstructures. The minimizing configurations are typically composed of large uniformly magnetized regions, so called magnetic domains, separated by thin transition layers, referred to as domain walls, in which the magnetization changes rapidly. The structure of these interfaces can be rather complex, yet when considering oppositely magnetized domains separated by a plane and one-dimensional layer, there are two basic types of walls that we shall refer to:

- The one-dimensional Bloch wall where the magnetization performs a 180 degree rotation within the domain wall plane, see Figure 1.1. With such a rotation, there are no magnetic charges inside the wall (i.e. $\nabla \cdot \mathbf{m} = 0$) and therefore no internal stray fields are generated.

- The Néel wall where the magnetization rotates entirely within the surface plane, see Figure 1.2. The Néel wall transition allows to avoid surface charges but yet generates internal stray fields.

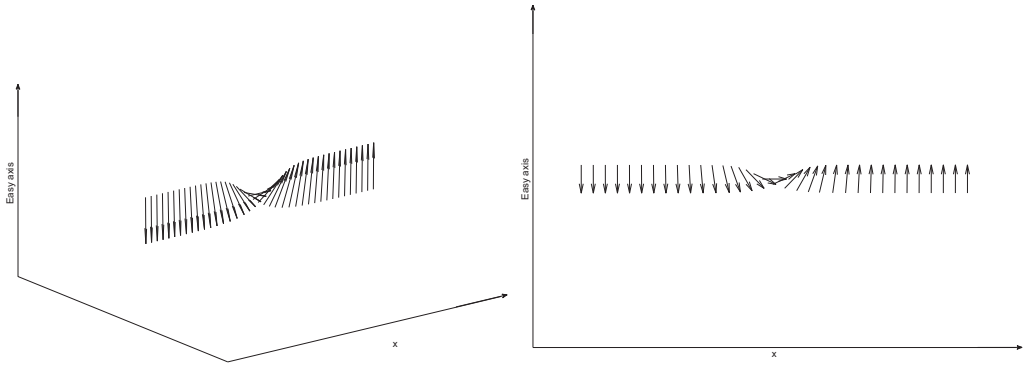

Figure 1.2.: Néel wall transition.

The characteristics of the observed patterns (e.g. morphology or typical length scales) are decided by the relative strentgh of the three competiting summands in (1.2) and hence also depend on the values of the material parameters balancing these terms.

Soft Magnetic Films

In the case of soft magnetic films, the contribution of the magnetic anisotropy is effectively negligible. The pattern selection is then mainly driven by the nonconvex constraint $|\mathbf{m}|^2 = 1$ and the competiting exchange and magnetostatic energies. For large samples of two-dimensional thin films, closed-flux magnetizations with vanishing stray field are favoured if possible. Basic examples of these type of configurations are depicted on Figure 1.3. In the case of larger crystals, one observes a domain refinement (branching) near the

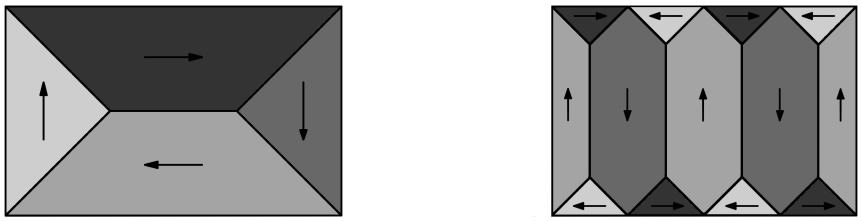

Figure 1.3.: Examples of closed flux magnetization patterns arising in soft magnetic films.

surface in order to reduce the closure energy. In the bulk however, wide uniform patterns are favoured in order to reduce the domain wall energy. An extensive treatment of soft magnetic films is given by Hubert and Schäfer in [36]. From a mathematical point of view,

DeSimone, Kohn, Müller and Otto develop in [23] a reduced theory for soft thin films. See also [24] from the same authors for an extensive review of analytical developments in micromagnetics.

Hard Magnetic Films

The main concern of this thesis will bear on the study of thin films with high perpendicular anisotropy. For these kind of magnetic films, the strong crystal anisotropy forces an out of plane magnetization perpendicular to the plane of the sample while the exchange energy contribution favours the formation of coarse domains. Yet a coherent state of uniform in- or out-of-plane magnetization is destabilized by the presence of the dipolar self-interaction which leads to the formation by heterogenous nucleation of various domain patterns such as stripes, bubbles or labyrinths. In these cases, the unfavourable storage of magnetostatic energy at the surface due to the out of plane magnetization can be compensated by adding more and more oscillations to the magnetization. Yet this subdivision process induces simultaneously an increase of the exchange energy due to the inversion of the magnetization. Equilibrium states correspond to a stable balance between the different energy contributions. This means for example that any further domain subdivision would cause a greater increase in exchange energy than decrease in magnetostatic energy and conversely. Figure 1.4 shows some examples of typical patterns arising in hard perpendicular films: the black and white areas are magnetized in and out of the image plane.

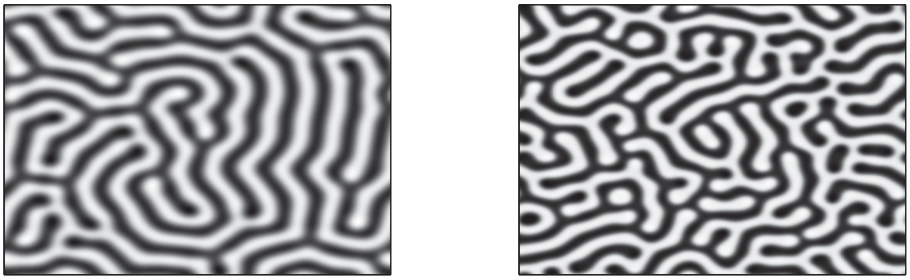

Figure 1.4.: Examples of typical magnetization patterns arising in the study of magnetic garnet films.

The oppositely magnetized domains are separated from each other by domain walls of rather complex structure, cf. [36, p256]. Indeed, the stray-field due to the surface magnetic poles distorts the internal structure of the domain walls in such a way that the magnetization is parallel to the wall plane only in the midplane of the film. Near the film surfaces, the magnetization vector is twisted in a direction perpendicular (or nearly perpendicular) to the plane of the wall. The domain wall therefore combines a regular Bloch wall structure in the center of the film with a Néel wall structure towards the surface of the film. The amount of twisting is related to the thickness of the film, or more precisely to the ratio of the film thickness to the Bloch wall width parameter, cf. [35]. In particular, for films of vanishing thickness, Schlömann predicted in [48] a decreasing of the value of the twist angle towards 0, which corresponds to a Bloch wall transition.

Questions and Goals

A direct prediction of an actual magnetic state for given parameter values is the ultimate challenge in the study of magnetic films. Yet, due to the complexity of the model, this is from a theoretical point of view nearly impossible. However, the study of pattern selection in magnetic films raises a lot of interesting questions, amongst others for example:

- What kind of patterns can be observed?
- Can we predict the morphology of the patterns (typical size of domains) by means of system parameters?

In view of this questions, the aim of this thesis is to provide an analytical and numerical background in order to understand some of the mechanisms of pattern formation in magnetic thin films with high perpendicular anisotropy. More precisely, our goals include:

- the derivation of a manageable reduced variational principle to apprehend the pattern formation process in hard magnetic thin films;
- the design and analysis of an efficient numerical method to approximate local minimizers of the energy functional (1.1).

Results

Our initial considerations are based on an averaged version of the micromagnetic model (1.2) presented previously. It is given by the variational formulation

$$E_1(\mathbf{m}) = \frac{d^2}{2} \fint_{\Omega_\delta} |\nabla \mathbf{m}|^2 + \frac{Q}{2} \fint_{\Omega_\delta} (1 - m_3^2) + \frac{1}{2\delta} \int_{\mathbb{R}\times\Omega} |\nabla u|^2 \to \min$$

for the nonconvex class of magnetization fields

$$\mathbf{m} = (m_1, m_2, m_3) : \Omega_\delta = \Omega \times (-\frac{\delta}{2}, +\frac{\delta}{2}) \to \mathbb{S}^2.$$

Derivation of a Reduced Theory for Hard Perpendicular Thin Films

In the first part of the work, we derive a reduced theory for the case of a film of vanishing thickness. More precisely, assuming under film thickness considerations (thin film regime) that the magnetization has no vertical variation within the sample, we base our considerations on the reduced variational problem

$$E_1^\varepsilon(\mathbf{m}) = \gamma \int_\Omega \Big(\frac{\varepsilon}{4} |\nabla \mathbf{m}|^2 + \frac{1}{4\varepsilon}(1 - m_3^2) \Big) \mathrm{d}x + \frac{1}{2\delta} \int_{\mathbb{R}\times\Omega} |\nabla u|^2 \to \min \tag{1.3}$$

for the periodic domain $\Omega = (0,1)^2$ and with the parameters $\varepsilon = d/\sqrt{Q}$ and $\gamma = 4d\sqrt{Q}$ denoting respectively the Bloch wall width and Bloch wall energy per unit length.

Considering the singularly perturbed part of the above energy functional, we carry out a Γ-limit for a sharp interface model (i.e. for $\varepsilon \to 0$). The result reads as follows:

Theorem 1.1. *Let* $\mathrm{X} := \mathrm{L}^2(\Omega, \mathbb{R}^3)$. *We consider the variational problems*

$$F_\varepsilon(\mathbf{m}) = \begin{cases} \frac{\varepsilon}{4} \int_\Omega |\nabla \mathbf{m}|^2 \mathrm{d}x + \frac{1}{4\varepsilon} \int_\Omega (1 - m_3^2) \mathrm{d}x & \text{if } \mathbf{m} \in \mathrm{H}^1(\Omega, \mathbb{S}^2), \\ +\infty & \text{elsewhere in } \mathrm{X}. \end{cases}$$

Given sequences (ε_n) *and* (v_n) *such that* $\varepsilon_n \to 0$ *and* $F_{\varepsilon_n}(v_n)$ *is bounded, then* (v_n) *is pre-compact in* X. *Moreover, the functionals* F_ε Γ*-converge to the following functional:*

$$F_0(\mathbf{m}) = \begin{cases} \frac{1}{2} \int_\Omega |\nabla v| & \text{if } \mathbf{m} = (0, 0, v),\ v \in \mathrm{BV}(\Omega; \{\pm 1\}), \\ +\infty & \text{elsewhere in } \mathrm{X}. \end{cases}$$

Following the approach of Melcher in [43], we further derive a Fourier representation for the averaged stray-field energy contribution $\frac{1}{2\delta} \int_{\Omega \times \mathbb{R}} |\nabla u|^2$. The latter acts as a continuous perturbation on the aforementioned Γ-limit, so that finally we obtain the following nonconvex and nonlocal sharp-interface model for (1.3):

$$E_0(v) = \frac{\gamma}{2} \int_\Omega |\nabla v| + \frac{1}{2} \sum_{k \in \mathbb{Z}^2} \sigma(\delta k) |\hat{v}(k)|^2 \to \min \tag{1.4}$$

for solutions $v \in \mathrm{BV}(\Omega; \{\pm 1\})$ defined on a space of functions of bounded variation and the Fourier multiplier σ given by

$$\sigma(k) = \frac{1 - \exp(-2\pi |k|)}{2\pi |k|} \quad \text{for all } k \in \mathbb{Z}^2.$$

Note that the contribution $\frac{1}{2} \int_\Omega |\nabla v| = \mathrm{Per}(\{v = 1\}; \Omega)$ agrees with the perimeter functional; it corresponds to the length of the interface on Ω.

Numerical Analysis and Simulation

The second part of the thesis is concerned with the analysis of a numerical method to approximate local minimizers of the energy functional (1.1). In order to bypass the difficulties due to the nonconvexity of the problem we consider a reduced model in which we relax the nonconvex constraint $v = \pm 1$ and replace up to a surface tension constant the perimeter functional by its Modica–Mortola approximation, cf. e.g. [2, 10, 21], and then study the associated $\mathrm{L}^2(\Omega)$ gradient flow. The resulting singular perturbation problem reads

$$E_\varepsilon(u) = \gamma \int_\Omega \Big(\frac{\varepsilon}{2} |\nabla u|^2 + \frac{1}{\varepsilon} W(u) \Big) \mathrm{d}x + \frac{1}{2} \sum_{k \in \mathbb{Z}^2} \sigma(\delta k) |\hat{u}(k)|^2 \to \min, \tag{1.5}$$

where W denotes the nonnegative double-well potential given by $W(u) = c_0(1 - u^2)^2$ with $c_0 > 0$. The parameter $\varepsilon > 0$ can be understood as the typical width of a transition layer within the sample; we shall consider its value to be small but fixed. Note further that a renormalization of the generic double well by a positive constant in the Modica–Mortola approximation allows to realize every value of γ; thus, for more clearness in the analysis, we shall set $\gamma = 1$. This variational problem is very similar to the initial two-dimensional

micromagnetic problem, but with the main difference of being now scalar and therefore more likely to be implemented numerically. The associated gradient flow with variational formulation

$$\partial_t u + \nabla_u E_\varepsilon(u) = 0 \quad \text{for} \quad u(\cdot,t) : \Omega \to \mathbb{R} \quad \text{and} \quad t > 0,$$

leads, on long time asymptotics, to local minimizers that approximate those of the sharp interface problem (1.4). It reads in fact as the following nonlinear parabolic equation

$$u_t + \mathcal{L}_\varepsilon u = \mathcal{N}_\varepsilon(u) \tag{1.6}$$

with $\mathcal{L}_\varepsilon$ a symmetric elliptic operator and $\mathcal{N}_\varepsilon$ a nonlinear operator derived from the double-well potential W by $\mathcal{N}_\varepsilon(u) = -\frac{1}{\varepsilon}\mathrm{D}W(u)$. We assume that equation (1.6) is subject to periodic boundary conditions and the initial condition $u(\cdot,0) = u_0(\cdot)$ with u_0 a given periodic function defined and continuous on Ω.
Our numerical approach to the initial-boudary-value problem (1.6) is based on a modified Crank–Nicolson approximation for the time variable and a Fourier collocation method for the space variable. The scheme has the particularity of inheriting the energy dissipation property of the gradient flow equation in a discretized fashion: indeed, the solutions of the numerical scheme generate local minimizers for the discrete counterpart of the energy functional E_ε.

The main results in this part of the thesis concern the analysis of the numerical scheme. In particular, following the approach of Melcher, Süli and C. in [19], we show that for a given restriction on the size of the time step Δt in terms of the number of Fourier modes N used for the collocation approximation, the numerical scheme has a unique solution at each time iteration. More precisely, we prove:

Theorem 1.2. *Considering as initial condition a trigonometric polynomial with finite associated discrete energy, then for $\Delta t \lesssim 1/N^2$, the formulated numerical scheme has a unique solution at each time iteration.*

Using a weighted residual approach for the collocation scheme, we further prove the subconvergence of our numerical solutions towards weak solutions of the continuous equation (1.6).

Theorem 1.3. *Let $(u_N^n)_{n=0}^J$ be a solution of the numerical scheme on a time interval $(0,T)$ and with bounded associated inital discrete energy. Then as we send the gridsize $N \to \infty$ and the time step $\Delta t \to 0$ with the rate $(\Delta t)^{1/2} \leq 1/N^2$, the numerical solution subconverges to a weak solution of the continuous equation* (1.6).

Under appropriate assumptions on the regularity of the analytical solution u of (1.6), we additionaly estimate the error in the $\ell^\infty(0,T;\mathrm{L}^2(\Omega))$ norm between u and its numerical approximation $(u_N^n)_{n=0}^J$ generated by our fully discrete scheme. More precisely, we show:

Theorem 1.4. *Suppose that $u \in \mathrm{H}_t^3\mathrm{L}_x^2 \cap \mathrm{H}_t^2\mathrm{H}_x^2 \cap \mathrm{L}_t^\infty\mathrm{H}_x^s((0,T)\times\Omega)$, $s \geq 2$; then there exists a positive constant C depending on s, T and ε such that*

$$\max_{0\leq n\leq J} \|u_N^n - u(t^n)\|_{\mathrm{L}^2(\Omega)} \leq C\big(N^{-s}\log N + (\Delta t)^2\big).$$

Finally, we illustrate the previous analytical results by a series of numerical experiments.

2. Preliminaries and Notation

2.1. Introduction

This chapter introduces some basic notation as well as some notions that we shall use throughout the manuscript.

2.2. Basic Notation

2.2.1. Euclidean Structure and Periodic Domains on $\mathbb{R}^n$

Let $n > 0$ denote a positive integer. A n-dimensional real vector x will be written $x = (x_1, \ldots, x_n)$ where all entries $x_1, \ldots, x_n$ are real numbers. We denote by $\mathbb{R}^n$ the Euclidean space of all such vectors equipped with the classical scalar product $x \cdot y = x_1 y_1 + \ldots + x_n y_n$ for $x, y \in \mathbb{R}^n$. The corresponding norm $|x|$ of a vector $x \in \mathbb{R}^n$ is given by $|x| = (x \cdot x)^{1/2}$. Throughout all the thesis, we shall base our considerations on 1-periodic domains

$$\Omega = (0,1)^n \subset \mathbb{R}^n,$$

so called flat torus of dimension n. Practically, we shall mainly focus on the physically relevant dimension $n = 2$.

2.2.2. Fourier Transform

Concerning the Fourier transform, we make the following convention: considering the periodic domain $\Omega = (0,1)^n$ with $n > 1$ and a square-integrable 1-periodic function $u \in \mathrm{L}^2(\Omega)$, we denote by $u \mapsto \mathcal{F}u = \hat{u} : \mathbb{Z}^n \to \mathbb{C}$ the Fourier transform on Ω. The Fourier coefficients are given for discrete frequencies $k \in \mathbb{Z}^n$ by

$$\mathcal{F}u(k) = \hat{u}(k) = \int_\Omega \mathrm{e}^{-2\mathrm{i}\pi\, k \cdot x} u(x) \mathrm{d}x, \tag{2.1}$$

where $k \cdot x$ denotes the inner product on $\mathbb{R}^n$ mentioned in the previous section. We denote the inverse Fourier transform by $\mathcal{F}^{-1}$. According to Parseval's formula, there holds

$$\int_\Omega |u(x)|^2 \mathrm{d}x = \sum_{k \in \mathbb{Z}^2} |\hat{u}(k)|^2 \quad \text{for all } u \in \mathrm{L}^2(\Omega).$$

In Section 3.2, we shall also use a continuous version of the Fourier transform, but only for a square-integrable function $u \in \mathrm{L}^2(\mathbb{R})$ defined on the real line. In this case, we take the following unitary transformation for the Fourier transform:

$$\mathcal{F}u(\xi) = \hat{u}(\xi) = \frac{1}{(2\pi)^{1/2}} \int_{\mathbb{R}} \mathrm{e}^{-\mathrm{i}x\xi} u(x) \mathrm{d}x, \tag{2.2}$$

for all $\xi \in \mathbb{R}$. Note that as previously, Parseval's formula holds here without additional constants, i.e. we have

$$\int_{\mathbb{R}} |u(x)|^2 \mathrm{d}x = \int_{\mathbb{R}} |\hat{u}(\xi)|^2 \mathrm{d}\xi \quad \text{for all } u \in \mathrm{L}^2(\mathbb{R}).$$

The fully discrete counterpart of the Fourier transform shall be presented in Section 5.2.

2.3. Sobolev Spaces

In this section, we give only a short introduction to Sobolev spaces, presenting a few definitions or properties that we will need throughout the thesis. See Adams [1] for full discussion of definitions, properties and proofs on Sobolev spaces.

Basic Definitions

Let us consider the previously introduced periodic domain $\Omega \subset \mathbb{R}^n$ and let $1 < p \leq \infty$ be an extended real number. We shall first introduce the space $\mathrm{L}^p(\Omega)$ of all Lebesgue measurable 1-periodic functions $u : \Omega \to \mathbb{C}$ for which the $\mathrm{L}^p(\Omega)$ norm $\|u\|_{\mathrm{L}^p(\Omega)}$ exists and is finite. In the case $1 < p < \infty$, we have

$$\|u\|_{\mathrm{L}^p(\Omega)} = \left(\int_\Omega |u(x)|^p \mathrm{d}x \right)^{\frac{1}{p}},$$

in particular for $p = 2$, we shall use the notation $\|u\| := \|u\|_{\mathrm{L}^2(\Omega)}$. In the case $p = \infty$, we have

$$\|u\|_{\mathrm{L}^\infty(\Omega)} = \operatorname{ess\,sup}_{x \in \Omega} |u(x)|.$$

We shall now turn to the case of Sobolev spaces. Given $k \in \mathbb{N}$ and $1 \leq p \leq \infty$, one defines formally the Sobolev space $\mathrm{W}^{k,p}(\Omega)$ as the set of all functions $u : \Omega \to \mathbb{C}$ such that for every multi index $\alpha = (\alpha_1, \ldots, \alpha_n)$ with $|\alpha| \leq k$, the mixed partial derivative (defined in a weak sense)

$$\mathrm{D}^\alpha u = \frac{\partial^{|\alpha|} u}{\partial x_1^{\alpha_1} \ldots \partial x_n^{\alpha_n}}$$

exists and is in $\mathrm{L}^p(\Omega)$. In this thesis, we shall be particularly interested in the case $k = 1$ and $p = 2$ for which we denote the Sobolev space $\mathrm{H}^1(\Omega) := \mathrm{W}^{1,2}(\Omega)$, more generally we shall also use at some point the notation $\mathrm{H}^p(\Omega) := \mathrm{W}^{1,p}(\Omega)$. These spaces, defined by

$$\mathrm{H}^p(\Omega) = \left\{ u \in \mathrm{L}^p(\Omega) \, : \, \frac{\partial u}{\partial x_1}, \ldots, \frac{\partial u}{\partial x_n} \in \mathrm{L}^p(\Omega) \right\},$$

and endowed for $1 < p < \infty$ with the norm

$$\begin{aligned} \|u\|_{\mathrm{H}^p(\Omega)} :&= \left(\|u\|^p_{\mathrm{L}^p(\Omega)} + \left\| \frac{\partial u}{\partial x_1} \right\|^p_{\mathrm{L}^p(\Omega)} + \ldots + \left\| \frac{\partial u}{\partial x_n} \right\|^p_{\mathrm{L}^p(\Omega)} \right)^{\frac{1}{p}} \\ &= \left(\|u\|^p_{\mathrm{L}^p(\Omega)} + \|\nabla u\|^p_{\mathrm{L}^p(\Omega)} \right)^{\frac{1}{p}} \end{aligned}$$

indeed form a Banach space. We shall write $\mathrm{H}^p(\Omega)^*$ for their dual space. Strong and weak convergence on $\mathrm{H}^p(\Omega)$ are understood in the usual way. Given $u, u_N \in \mathrm{H}^p(\Omega)$, we write $u_N \to u$ strongly in $\mathrm{H}^p(\Omega)$ whenever $\|u - u_N\|_{\mathrm{H}^p(\Omega)} \to 0$, and $u_N \rightharpoonup u$ weakly in $\mathrm{H}^p(\Omega)$ if we have

$$\langle u_N, f \rangle_{\mathrm{H}^p(\Omega)} \to \langle u, f \rangle_{\mathrm{H}^p(\Omega)}$$

for every $f \in \mathrm{H}^p(\Omega)^*$. Here $\langle \cdot, \cdot \rangle_{\mathrm{H}^p(\Omega)}$ denotes the dual pairing defined on $\mathrm{H}^p(\Omega) \times \mathrm{H}^p(\Omega)^*$.

Sobolev Embeddings

We shall present here some embedding properties of various Sobolev spaces that will be used at some points within the manuscript. These are based on so-called "Sobolev type inequalities", see the aforementioned reference and also [11] for more details or proofs. In the one dimensional case i.e., for $\mathrm{I} \subset \mathbb{R}$, there holds the embedding

$$\mathrm{W}^{1,p}(\mathrm{I}) \subset \mathrm{L}^\infty(\mathrm{I}).$$

Hence on the real line, boundedness on $\mathrm{H}^1(\mathrm{I})$ implies uniform boundedness on $\mathrm{L}^\infty(\mathrm{I})$. However, this implication does usually not hold in higher dimensions. Indeed, given the periodic domain $\Omega = (0,1)^n$ and $1 \leq p \leq \infty$, then

- if $1 \leq p < n$, there holds

$$\mathrm{W}^{1,p}(\Omega) \subset \mathrm{L}^{p^*} \quad \text{where} \quad \frac{1}{p^*} = \frac{1}{p} - \frac{1}{n}.$$

  Additionaly, there exists a constant C depending only on p, n and Ω such that we have the estimate

$$\|u\|_{\mathrm{L}^{p^*}(\Omega)} \leq C \|u\|_{\mathrm{W}^{1,p}(\Omega)} \quad \text{for all } u \in \mathrm{W}^{1,p}(\Omega);$$

- if $p = n$, we have

$$\mathrm{W}^{1,p}(\Omega) \subset \mathrm{L}^q(\Omega) \quad \text{for all } q \in [p, +\infty[;$$

- finally, if $p > n$, there holds

$$\mathrm{W}^{1,p}(\Omega) \subset \mathrm{L}^\infty(\Omega).$$

Compactness

Some of the embedding presented previously actually appear to be compact.

Definition 2.1. *Let* X *and* Y *be Banach spaces with* $\mathrm{X} \subset \mathrm{Y}$. *We say that* X *is compactly embedded in* Y, *written* $\mathrm{X} \subset\subset \mathrm{Y}$ *provided*

(i) there exists a constant C *such that* $\|x\|_{\mathrm{Y}} \leq C\|x\|_{\mathrm{X}}$ *for all* $x \in \mathrm{X}$;

(ii) each bounded sequence in X *is precompact in* Y.

Indeed, the Rellich–Kondrachov theorem states the following compactness results:

Theorem 2.2 (Rellich–Kondrachov Compactness Theorem)**.** *Suppose* $1 \leq p < n$*. Then*

$$\mathrm{W}^{1,p}(\Omega) \subset\subset \mathrm{L}^q(\Omega) \quad \textit{for all} \quad 1 \leq q < p^*.$$

Further, for the case $p = n$*, there holds in fact*

$$\mathrm{W}^{1,p}(\Omega) \subset\subset \mathrm{L}^q(\Omega) \quad \textit{for all} \quad q \in [1, +\infty[.$$

2.4. Γ-Convergence: Definition and Properties

Γ-convergence is a notion of convergence for functionals aiming at describing the asymptotic behaviour of families of variational problems depending on some e.g constitutive or geometric parameters. It was introduced by De Giorgi and Franzoni [22] in the 1970's and has since then much developed especially in connection with various applied problems in the Calculus of Variations. We refer to the book of Dal Maso [21] for an extensive treatment of variational convergence, see also Attouch [6], as well as Braides [10] for a description of the main features and properties of Γ-convergence and a broad spectrum of application examples. The paper of Alberti [2], based on lecture notes, also gives a well presented introduction to the theory of Γ-convergence as well as a presentation of the Modica-Mortola example, which is closely related to the example treated in Chapter 3.

We shall nevertheless recall here an abstract definition of the notion of Γ-convergence on a metric space and present as well some of its main properties.

Definition 2.3. *Let* X *be a metric space, and for every* $\varepsilon > 0$ *let* $F_\varepsilon : \mathrm{X} \to [0, +\infty]$ *be a function defined on* X*. We say that the sequence of functions* (F_ε) Γ*-converges to* F *on* X *as* $\varepsilon \to 0$ *(and we write* $F_\varepsilon \xrightarrow{\Gamma} F$*) if the following conditions hold:*

(LB) Lower-bound inequality: for every $u \in \mathrm{X}$ *and every sequence* (u_ε) *such that* $u_\varepsilon \to u$ *in* X *there holds*

$$\liminf_{\varepsilon \to 0} F_\varepsilon(u_\varepsilon) \geq F(u);$$

(UB) Upper-bound inequality: for every $u \in \mathrm{X}$ *there exists a sequence* (u_ε) *such that* $u_\varepsilon \to u$ *in* X *and*

$$\lim_{\varepsilon \to 0} F_\varepsilon(u_\varepsilon) = F(u)$$

or equivalently

$$\limsup_{\varepsilon \to 0} F_\varepsilon(u_\varepsilon) \leq F(u).$$

The notion of Γ-convergence enjoys important properties, such as:

(i) The Γ-limit F is a lower semicontinuous functional on X; this is a very useful structure property that usually implies the existence of minimizers of F.

(ii) Stability under continuous perturbations: if $F_\varepsilon \xrightarrow{\Gamma} F$ and G is continuous, then $F_\varepsilon + G \xrightarrow{\Gamma} F + G$.

The main motivation of Γ-convergence though is to define the convergence of variational problems through the convergence of minimizers in the following sense: if $F_\varepsilon \xrightarrow{\Gamma} F$ and

v_ε is a minimizer of F_ε on X, then every cluster point of (v_ε) is a minimizer of F on X. But this only makes sense if we know a-priori that the the minimizing sequence (v_ε) is pre-compact in X. For this reason, one usually pairs the Γ-convergence result for the functionals F_ε with a compactness result for the corresponding minimizing sequences by trying to prove the following asymptotical equi-coercivity property of F_ε:

(C) Compactness: Let be given sequences (ε_n) and (u_n) such that $\varepsilon_n \to 0$ and $F_{\varepsilon_n}(u_n)$ is bounded; then (u_n) is pre-compact in X.

An equivalent way of formulating the equi-coercivity of a sequence of functionals is following: we say that a sequence $F_\varepsilon : \mathrm{X} \to [0; +\infty]$ is equi-coercive if there exists a compact set K independent of ε such that

$$\inf\{F_\varepsilon(u) : u \in \mathrm{X}\} = \inf\{F_\varepsilon(u) : u \in \mathrm{K}\}.$$

The aforementioned convergence of minimizers property of Γ-convergence is summarized in the following fundamental theorem of Γ-convergence:

Theorem 2.4. *Let (F_ε) be an equi-coercive sequence of functions that Γ-converges on* X *to the function F. Then we have convergence of minima*

$$\min\{F(u) : u \in \mathrm{X}\} = \lim_{\varepsilon \to 0} \inf\{F_\varepsilon(u) : u \in \mathrm{X}\}.$$

Moreover we have also convergence of minimizers: if $u_\varepsilon \to u$ in X *and $\lim_\varepsilon F_\varepsilon(u_\varepsilon) = \liminf_\varepsilon F_\varepsilon(u_\varepsilon)$ then u is a minimizer for F.*

2.5. Functions of Bounded Variation

In this section, we shall give a short introduction to the space of functions of bounded variation $\mathrm{BV}(\mathbb{T}^n)$ on the n-dimensional flat torus $\mathbb{T}^n = (0,1)^n$. We shall refer to [5],[27] or [28] for a full discussion on measure theory and functions of bounded variation. From a formal point of view, functions of bounded variation (or BV functions) are functions whose distributional derivative is a finite Radon measure. They can represent discontinuous functions and are well adapted to problems with singularities or discontinuities such as domain walls. In non-periodic situations, when considering phase separation problems with solutions defined on a space of bounded variation and featuring interfaces, the regularity of the domain boundary as well as the treatment of the boundary values of these BV functions is a subtle topic to be taken into account. For example, the paper of Modica [45] contains a transversality condition for interface and domain boundary that is crucial to perform a smooth approximation of sets of bounded perimeter. This kind of condition allows to restrict solutions of minimal interface problems or more general variational problems. On the other hand, problems with interfaces on the boundary are much more difficult to handle. In view of these aspects, the periodic case we are considering is particularly convenient as there are no boundaries to be taken into account.

We shall start with a formal definition of the space $\mathrm{BV}(\mathbb{T}^n)$ on the torus.

Definition 2.5. *We say that a locally integrable function $u \in \mathrm{L}^1(\mathbb{T}^n)$ has a bounded variation on $\mathbb{T}^n$ and we write $u \in \mathrm{BV}(\mathbb{T}^n)$, if there exists a finite vector-valued Radon*

measure $Du \in \mathcal{M}(\mathbb{T}^n, \mathbb{R}^n)$ *such that*

$$\int_{\mathbb{T}^n} u(x)\,\mathrm{div}\phi(x)\,\mathrm{d}x = -\int_{\mathbb{T}^n} \langle \phi(x), Du(x)\rangle \quad \textit{for every } \phi \in \mathrm{C}^1_c(\mathbb{T}^n;\mathbb{R}^n).$$

The measure Du represents here the distributional derivative of u. Note that the request that the test functions ϕ in the above definition have compact support is redundant as we base our considerations on the compact manifold $\mathbb{T}^n$. We shall however keep this redundancy in the notation as this condition is fundamental when considering non-periodic situations. Equivalently, $\mathrm{BV}(\mathbb{T}^n)$ can be defined as the space of real-valued functions with finite total variation:

Definition 2.6. *Given* $u \in \mathrm{L}^1(\mathbb{T}^n)$*, the total variation of* u *in* $\mathbb{T}^n$ *is defined as*

$$\mathrm{V}(u,\mathbb{T}^n) := \sup\Big\{ \int_{\mathbb{T}^n} u(x)\,\mathrm{div}\phi(x)\,\mathrm{d}x \,:\, \phi \in \mathrm{C}^1_c(\mathbb{T}^n;\mathbb{R}^n), \|\phi\|_{\mathrm{L}^\infty(\mathbb{T}^n)} \le 1\Big\}.$$

The space of functions of bounded variation can then be defined as

$$\mathrm{BV}(\mathbb{T}^n) := \{u \in \mathrm{L}^1(\mathbb{T}^n) \,:\, \mathrm{V}(u,\mathbb{T}^n) < +\infty\}.$$

Note that the Sobolev space $\mathrm{W}^{1,1}(\mathbb{T}^n)$ is a subset of $\mathrm{BV}(\mathbb{T}^n)$. Indeed, for $u \in \mathrm{W}^{1,1}(\mathbb{T}^n)$ one can choose the measure $\mu := \nabla u \mathcal{L}$ (with $\mathcal{L}$ the Lebesgue measure on $\mathbb{T}^n$) such that the equality

$$\int_{\mathbb{T}^n} u(x)\,\mathrm{div}\phi(x)\,\mathrm{d}x = -\int_{\mathbb{T}^n} \phi\,\mathrm{d}\mu = -\int_{\mathbb{T}^n} \phi\,\nabla u,$$

which is nothing else than the definition of weak derivative, holds for every $\phi \in \mathrm{C}^1_c(\mathbb{T}^n)$.

In view of Chapter 3, interesting properties of the space $\mathrm{BV}(\mathbb{T}^n)$ include:

(i) The total variation $\mathrm{V}(\cdot,\mathbb{T}^n) : \mathrm{BV}(\mathbb{T}^n) \to \mathbb{R}^+$ is lower semi-continuous in the $\mathrm{L}^1(\mathbb{T}^n)$ topology i.e., for a Cauchy sequence of BV functions $(u_n)_{n\in\mathbb{N}}$ converging to u in $\mathrm{L}^1(\mathbb{T}^n)$ there holds the following inequality

$$\liminf_{n\to\infty} \mathrm{V}(u_n,\mathbb{T}^n) \ge \mathrm{V}(u,\mathbb{T}^n);$$

(ii) the space $\mathrm{BV}(\mathbb{T}^n)$ endowed with the norm $\|u\|_{\mathrm{BV}(\mathbb{T}^n)} := \|u\|_{\mathrm{L}^1(\mathbb{T}^n)} + \mathrm{V}(u,\mathbb{T}^n)$ is a Banach space.

On can also define the $\mathrm{BV}(\mathbb{T}^n)$ has the space of functions for which the sum of the perimeters of the level sets is finite. Given a measurable subset $\mathrm{E} \subset \mathbb{T}^n$, the perimeter of E in $\mathbb{T}^n$ is defined as the total variation of its characteristic function χ_E in $\mathbb{T}^n$, i.e.

$$\begin{aligned}\mathrm{Per}(\mathrm{E};\mathbb{T}^n) :&= \int_{\mathbb{T}^n} |D\chi_\mathrm{E}| = \mathrm{V}(\chi_\mathrm{E},\mathbb{T}^n)\\ &= \sup\Big\{ \int_\mathrm{E} \mathrm{div}\phi(x)\,\mathrm{d}x \,:\, \phi \in \mathrm{C}^1_c(\mathbb{T}^n;\mathbb{R}^n), \|\phi\|_{\mathrm{L}^\infty(\mathbb{T}^n)} \le 1\Big\}.\end{aligned}$$

Hence precisely in the sense of definition 2.5, the set E has a finite perimeter if the characteristic function χ_E belongs to $\mathrm{BV}(\mathbb{T}^n)$.

3. Gamma Limit for a Sharp-Interface Model

3.1. Introduction

The model for hard magnetic films with perpendicular anisotropy presented in Chapter 1 is studied in some of his mathematical aspects in this chapter. Recall that it can be formulated as the following variational problem

$$E_1(\mathbf{m}) = \frac{d^2}{2} \fint_{\Omega_\delta} |\nabla \mathbf{m}|^2 + \frac{Q}{2} \fint_{\Omega_\delta} (1 - m_3^2) + \frac{1}{2\delta} \int_{\mathbb{R}\times\Omega} |\nabla u|^2 \to \min$$

for the class of magnetization fields

$$\mathbf{m} = (m_1, m_2, m_3) : \Omega_\delta = \Omega \times (-\frac{\delta}{2}, +\frac{\delta}{2}) \to \mathbb{S}^2.$$

defined on the cylindrical domain Ω_δ. The parameter δ stands here for the relative thickness of the magnetic film while $\Omega = (0,1)^2$ will denote the two-dimensional unit torus. Note that the above variational problem is nonconvex and nonlocal in view of the nonconvex constraint $|\mathbf{m}|^2 = 1$ and the nonlocal differential constraint linking the magnetostatic potential u with the magnetization vector $\mathbf{m}$.

Assuming under film thickness considerations (thin film regime) that the magnetization has no vertical variation within the sample, we first derive a reduced formulation for the above variational problem. We then carry out a Γ-limit for a sharp interface model. The resulting energy functional is defined on the space of functions of bounded variation $\mathrm{BV}(\Omega; \{\pm 1\})$ and driven only by the competition of a domain wall energy and a reduced stray-filed interaction.

3.2. Model Reduction

Magnetic films are defined as thin if their thickness is comparable with the typical width of the Bloch wall introduced in Chapter 1. Based on a rigorous mathematical framework, Gioia and James showed in [32] that the magnetization associated with a film of vanishing thickness can be derived from the minimization of a certain limiting free energy, and that it is independent of the space coordinate normal to the film, therefore that the limiting problem is two dimensional. A somehow less rigorous scaling argument suggests that in the case of a thin film regime (for $\delta/d \ll 1$), the vertical variation of the magnetization within the sample can be neglected. Indeed, assuming that the quantity $d^2 \fint_{\Omega_\delta} |\nabla \mathbf{m}(\mathbf{x})|^2 \mathrm{d}\mathbf{x}$ is bounded as the ratio of the thickness on the exchange length tends to 0 and setting

$\nabla' = (\partial_1, \partial_2)^T$, $\mathbf{x} = (x, x_3)$, we have

$$\frac{d^2}{2} \fint_{\Omega_\delta} |\nabla \mathbf{m}(\mathbf{x})|^2 \mathrm{d}\mathbf{x} = \frac{d^2}{2} \fint_{\Omega_\delta} |\nabla' \mathbf{m}(\mathbf{x})|^2 \mathrm{d}\mathbf{x} + \frac{d^2}{2} \fint_{\Omega_\delta} |\partial_3 \mathbf{m}(\mathbf{x})|^2 \mathrm{d}\mathbf{x}.$$

In order to perform a rescaling of the above quantity, we set $\tilde{\mathbf{m}}(\mathbf{x}) = \mathbf{m}(x, \delta x_3)$. On denoting $\Omega_1 := \Omega \times (-\frac{1}{2}, +\frac{1}{2})$ the rescaled domain, this yields

$$\begin{aligned} \frac{d^2}{2} \fint_{\Omega_\delta} |\nabla \mathbf{m}(\mathbf{x})|^2 \mathrm{d}\mathbf{x} &= \frac{d^2}{2} \int_{\Omega_1} |\nabla' \tilde{\mathbf{m}}(\mathbf{x})|^2 \mathrm{d}\mathbf{x} + \frac{d^2}{2\delta} \int_\Omega \int_{-\frac{1}{2}}^{+\frac{1}{2}} \frac{1}{\delta^2} |\partial_3 \tilde{\mathbf{m}}(\mathbf{x})|^2 \, \delta \, \mathrm{d}x_3 \mathrm{d}x \\ &= \frac{d^2}{2} \int_{\Omega_1} |\nabla' \tilde{\mathbf{m}}(\mathbf{x})|^2 \mathrm{d}\mathbf{x} + \frac{1}{2} \frac{d^2}{\delta^2} \int_\Omega \int_{-\frac{1}{2}}^{+\frac{1}{2}} |\partial_3 \tilde{\mathbf{m}}(\mathbf{x})|^2 \, \mathrm{d}x_3 \mathrm{d}x. \end{aligned}$$

As δ/d tends to 0, the ratio d^2/δ^2 becomes infinite. Therefore, the only way for the exchange energy contribution $d^2 \fint_{\Omega_\delta} |\nabla \mathbf{m}(\mathbf{x})|^2 \mathrm{d}\mathbf{x}$ to remain bounded is that

$$|\partial_3 \tilde{\mathbf{m}}(\mathbf{x})|^2 = 0 \quad \text{i.e.} \quad \frac{\partial \mathbf{m}(\mathbf{x})}{\partial x_3} = 0 \quad \text{on } \Omega_\delta.$$

We shall assume from now on that the magnetization within the sample is independent of the space coordinate normal to the film. Based on this first statement, we can carry out the integration over the third spatial coordinate for the exchange and anisotropy contributions of the energy. This yields the following reduced formulation

$$E_1(\mathbf{m}) = \frac{d^2}{2} \int_\Omega |\nabla \mathbf{m}|^2 + \frac{Q}{2} \int_\Omega (1 - m_3^2) + \frac{1}{2\delta} \int_{\mathbb{R} \times \Omega} |\nabla u|^2.$$

We shall now derive a reduced form for the averaged stray field energy. In order to separate the vertical component of the magnetization, we first set $m := (m_1, m_2)$ and thus we have

$$\mathbf{m} = (m, m_3).$$

We now closely follow the argument of Melcher in [43] in order to derive a Fourier representation for the magnetostatic energy. Recall that the magnetostatic potential u is given as a solution of $\nabla \cdot (\mathbf{m} \chi_{\{x_3 \in (-\frac{\delta}{2}, +\frac{\delta}{2})\}}) = \Delta u$ in the space of functions on $\Omega \times \mathbb{R}$ with $\int_{\Omega \times \mathbb{R}} |\nabla u|^2 < \infty$.

Proposition 3.1. *For a magnetization vector $\mathbf{m} = (m, m_3) : \Omega_\delta \to \mathbb{S}^2$ extended to 0 outside the domain Ω_δ and such that $\frac{\partial \mathbf{m}}{\partial x_3} = 0$ on Ω_δ, the averaged stray field contribution can be reduced in a form given by*

$$\frac{1}{2\delta} \int_{\mathbb{R} \times \Omega} |\nabla u|^2 = \frac{1}{2} \sum_{k \in \mathbb{Z}^2} \sigma(\delta k) \, |\hat{m}_3(k)|^2 + \frac{1}{2} \sum_{k \in \mathbb{Z}^2} (1 - \sigma(\delta k)) \Big| \frac{k}{|k|} \cdot \hat{m}(k) \Big|^2 \tag{3.1}$$

with the Fourier multiplier σ given by

$$\sigma(k) = \frac{1 - \exp(-2\pi|k|)}{2\pi|k|} \quad \textit{for} \quad k \neq 0 \quad \textit{and} \quad \sigma(0) = 1.$$

Note that the continuous version of the Fourier multiplier σ is symmetric-decreasing and decays rapidly for high frequencies, see Figure 3.1 for a one-dimensional representation. Hence the reduced stray-field interaction will favour an oscillatory behaviour of the vertical component m_3 of the magnetization.

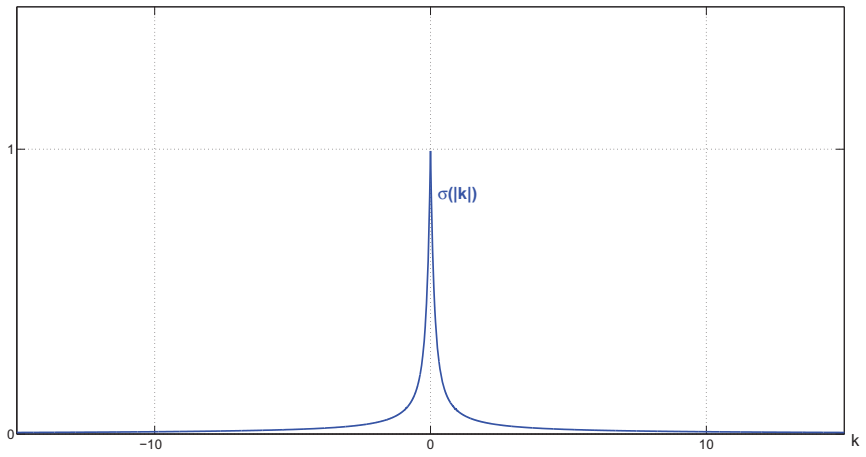

Figure 3.1.: The Fourier multiplier $\sigma(k) = (1 - \exp(-2\pi|k|))/(2\pi|k|)$.

Proof. The considered magnetization field $\mathbf{m}$ has no vertical variation within the sample, hence we have the following representation for its zero extension

$$\mathbf{m} : \mathbb{R}^3 \ni (x_1, x_2, x_3) \mapsto \begin{pmatrix} m \\ m_3 \end{pmatrix} (x_1, x_2)\, \chi_\delta(x_3) \in \mathbb{R}^3$$

with the characteristic function $\chi_\delta(z) := \begin{cases} 1 & \text{if } z \in (-\frac{\delta}{2}, +\frac{\delta}{2}) \\ 0 & \text{else} \end{cases}$.

Using the above representation of the magnetization field $\mathbf{m}$, we obtain that

$$\nabla \cdot \mathbf{m} = \left(\frac{\partial m_1}{\partial x_1} + \frac{\partial m_2}{\partial x_2} \right) (x_1, x_2)\, \chi_\delta(x_3) + m_3(x_1, x_2) \frac{\mathrm{d}\chi_\delta}{\mathrm{d}x_3}(x_3) \tag{3.2}$$

in the sense of distributions. Now recall the formulation of the averaged magnetostatic energy

$$E_{\mathrm{mag}}(\mathbf{m}) = \frac{1}{2\delta} \int_{\mathbb{R}\times\Omega} |\nabla u|^2.$$

By virtue of Green's formula applied in three dimensions, this can be equivalently be written

$$E_{\mathrm{mag}}(\mathbf{m}) = \frac{1}{2\delta} \int_{\mathbb{R}} \int_{\Omega} \nabla \cdot \mathbf{m}\, (-\Delta)^{-1} \nabla \cdot \mathbf{m}\, \mathrm{d}x\, \mathrm{d}x_3.$$

We now decompose this formulation of the magnetostatic energy into two parts: the first one, denoted $E^{[1]}_{\mathrm{mag}}(\mathbf{m})$, involving the normal component m_3 of the magnetization, and the other one, denoted $E^{[2]}_{\mathrm{mag}}(\mathbf{m})$, involving the tangential part m of the magnetization.

To this end, we use the decomposition of Equation (3.2). This yields

$$E^{[1]}_{\mathrm{mag}}(\mathbf{m}) = \frac{1}{2\delta}\int_{\mathbb{R}}\int_{\Omega}\left(m_3\frac{d\chi_\delta}{dx_3}\right)(-\Delta)^{-1}\left(m_3\frac{\mathrm{d}\chi_\delta}{\mathrm{d}x_3}\right)\,\mathrm{d}x\,\mathrm{d}x_3.$$

Let now $\xi \in \mathbb{R}$ denote the frequency variable for x_3 and $k \in \mathbb{Z}^2$ the discrete frequency variable for $x{=}(x_1,\, x_2)$. By virtue of Parseval's formula, cf. Section 2.2.2, we obtain the following Fourier representation

$$\begin{aligned} E^{[1]}_{\mathrm{mag}}(\mathbf{m}) &= \frac{1}{2\delta}\int_{\mathbb{R}}\sum_{k\in\mathbb{Z}^2}|\hat{m}_3(k)|^2\frac{\xi^2}{|2\pi k|^2+\xi^2}\left[\sqrt{\frac{2}{\pi}}\frac{\sin(\delta\xi/2)}{\xi}\right]^2\,\mathrm{d}\xi \\ &= \frac{1}{\delta\pi}\int_{\mathbb{R}}\sum_{k\in\mathbb{Z}^2}|\hat{m}_3(k)|^2\left[\frac{\sin^2(\delta\xi/2)}{|2\pi k|^2+\xi^2}\right]\,\mathrm{d}\xi. \end{aligned}$$

Carrying out the integration over ξ (see e.g.,[12]) yields

$$E^{[1]}_{\mathrm{mag}}(\mathbf{m}) = \frac{1}{2}\sum_{k\in\mathbb{Z}^2}\left[\frac{1-\exp(-2\pi\delta|k|)}{2\pi\delta|k|}\right]|\hat{m}_3(k)|^2.$$

We now proceed similarly with the second part of the magnetostatic energy. We have

$$E^{[2]}_{\mathrm{mag}}(\mathbf{m}) = \frac{1}{2\delta}\int_{\mathbb{R}}\int_{\Omega}\nabla\cdot\begin{pmatrix} m\chi_\delta \\ 0\end{pmatrix}(-\Delta)^{-1}\nabla\cdot\begin{pmatrix} m\chi_\delta \\ 0\end{pmatrix}\mathrm{d}x\mathrm{d}x_3.$$

Again, Parseval's formula yields the Fourier representation

$$\begin{aligned} E^{[2]}_{\mathrm{mag}}(\mathbf{m}) &= \frac{1}{2\delta}\int_{\mathbb{R}}\sum_{k\in\mathbb{Z}^2}\frac{|2\pi k\cdot\hat{m}(k)|^2}{|2\pi k|^2+\xi^2}\left[\sqrt{\frac{2}{\pi}}\frac{\sin(\delta\xi/2)}{\xi}\right]^2\,\mathrm{d}\xi \\ &= \frac{1}{\delta\pi}\int_{\mathbb{R}}\sum_{k\in\mathbb{Z}^2}\left[\frac{\sin^2(\delta\xi/2)}{\xi^2}-\frac{\sin^2(\delta\xi/2)}{|2\pi k|^2+\xi^2}\right]\frac{|2\pi k\cdot\hat{m}(k)|^2}{|2\pi k|^2}\,\mathrm{d}\xi \end{aligned}$$

which, after integration over the frequency variable ξ, becomes

$$E^{[2]}_{\mathrm{mag}}(\mathbf{m}) = \frac{1}{2}\sum_{k\in\mathbb{Z}^2}\left[1-\frac{1-\exp(-2\pi\delta|k|)}{2\pi\delta|k|}\right]\left|\frac{k\cdot\hat{m}(k)}{|k|}\right|^2.$$

On denoting the Fourier multiplier

$$\sigma(k) := \frac{1-\exp(-2\pi|k|)}{2\pi|k|},$$

we obtain the following Fourier representation for the averaged magnetostatic energy

$$E_{\mathrm{mag}}(\mathbf{m}) = \frac{1}{2}\sum_{k\in\mathbb{Z}^2}\sigma(\delta k)|\hat{m}_3(k)|^2 + \frac{1}{2}\sum_{k\in\mathbb{Z}^2}(1-\sigma(\delta k))\left|\frac{k\cdot\hat{m}(k)}{|k|}\right|^2.$$

□

We shall now define the following characteristic parameters

$$\varepsilon := \frac{d}{\sqrt{Q}} \qquad \text{and} \qquad \gamma_\varepsilon := 2d\sqrt{Q};$$

these can be interpretated respectively as the Bloch wall width and the Bloch wall energy per unit length. Based on the previous results, our energy functional can up to this point be written in the following reduced form involving the Fourier representation for the averaged stray-field energy and a two dimensional representation for the exchange and anisotropy energies

$$\begin{aligned} E_1(\mathbf{m}) = E_1^\varepsilon(\mathbf{m}) &= \gamma_\varepsilon \int_\Omega \left(\frac{\varepsilon}{4} |\nabla \mathbf{m}|^2 + \frac{1}{4\varepsilon}(1 - m_3^2) \right) \mathrm{d}x + E_{\mathrm{mag}}(\mathbf{m}) \\ &= \gamma_\varepsilon F_\varepsilon(\mathbf{m}) + E_{\mathrm{mag}}(\mathbf{m}). \end{aligned}$$

3.3. Bloch Wall Construction

Even though the structure of the domain walls in the case of magnetic films with perpendicular anisotropy is rather complex, cf. [50], we shall show in the next section that it is sufficient for our construction to implant a one-dimensional Bloch wall structure.

The Bloch wall transition between two domains of opposite magnetization is a transition in which the magnetization performs a continous 180 degree rotation perpendicularly to the transition axis. With such a rotation, there are no magnetic charges inside the wall (i.e. $\nabla \cdot \mathbf{m} = 0$) and therefore no stray-field interactions.

It will be useful to consider the functional F_ε of Equation (3.2) as a function of the integration domain; hence we set

$$F_\varepsilon(\mathbf{m}, A) = \frac{\varepsilon}{4} \int_A |\nabla \mathbf{m}(x)|^2 \mathrm{d}x + \frac{1}{4\varepsilon} \int_A (1 - m_3^2(x)) \mathrm{d}x,$$

for every measurable set A and every magnetization vector $\mathbf{m} \in \mathrm{H}^1(A)$. In particular, we have $F_\varepsilon(\mathbf{m}) := F_\varepsilon(\mathbf{m}, \Omega)$.

From a qualitative aspect, on denoting (e_1, e_2, e_3) an orthonormal vector basis of $\mathbb{R}^3$, the Bloch wall transition can be described as a parametrized transition along the transition axis $\mathbb{R}e_1$ connecting two antipodal points on the anisotropy easy axis $\mathbb{R}e_3$, i.e.

$$\mathbf{m} : \mathbb{R} \to \mathbb{S}^2, \quad \mathbf{m}(\pm\infty) = (0, 0, \pm 1)$$

and with a corresponding induced energy $\gamma_\varepsilon F_\varepsilon(\mathbf{m}, \mathbb{R})$. Considering the optimal profile problem

$$\rho := \inf\{F_\varepsilon(\mathbf{m}, \mathbb{R}) : \mathbf{m} : \mathbb{R} \to \mathbb{S}^2, \mathbf{m}(\pm\infty) = \pm(0, 0, 1)\},$$

the number ρ represents the minimal cost in term of the energy F_ε for a Bloch wall transition from $(0, 0, -1)$ to its antipodal point $(0, 0, 1)$ on the entire real line. The corresponding optimal profile as well as the minimal energy cost for the transition can be determined by solving the Euler–Lagrange equation related to the variational problem

$$F_\varepsilon(\mathbf{m}, \mathbb{R}) = \frac{\varepsilon}{4} \int_{\mathbb{R}} |\mathbf{m}'(x)|^2 \mathrm{d}x + \frac{1}{4\varepsilon} \int_{\mathbb{R}} W_1(\mathbf{m}(x)) \mathrm{d}x = \int_{\mathbb{R}} f_\varepsilon(x, \mathbf{m}, \mathbf{m}') \mathrm{d}x,$$

where $W_1(\mathbf{m}) = 1 - m_3^2$ and $f_\varepsilon(x, \mathbf{m}, \mathbf{m}') := \frac{\varepsilon}{4}|\mathbf{m}'(x)|^2 + \frac{1}{4\varepsilon}W_1(\mathbf{m}(x))$.
Using the constraint $g(\mathbf{m}) = 1 - |\mathbf{m}|^2 = 0$ with a Lagrange multiplier λ, the Euler–Lagrange equation reads

$$\frac{\partial f_\varepsilon}{\partial \mathbf{m}} - \frac{\partial}{\partial x}\Big(\frac{\partial f_\varepsilon}{\partial \mathbf{m}'}\Big) + \lambda \frac{\partial g(\mathbf{m})}{\partial \mathbf{m}} = 0.$$

This yields

$$\frac{1}{4\varepsilon}W_1'(\mathbf{m}(x)) - \frac{1}{2}\varepsilon \mathbf{m}''(x) = -\lambda \mathbf{m}(x) \quad \text{for all } x \in \mathbb{R}.$$

Since $\mathbf{m}$ takes values on the unit sphere, the vectors $\mathbf{m}$ and $\mathbf{m}'$ are orthogonal in $\mathbb{R}^3$, thus there holds $\mathbf{m} \cdot \mathbf{m}' = 0$ in terms of the usual scalar product on $\mathbb{R}^3$. Consequently, taking the inner product of the previous equation with $\mathbf{m}'$ yields

$$\frac{1}{4\varepsilon}W_1'(\mathbf{m}(x)) \cdot \mathbf{m}'(x) - \frac{1}{2}\varepsilon\, \mathbf{m}''(x) \cdot \mathbf{m}'(x) = -\lambda\, \mathbf{m}(x) \cdot \mathbf{m}'(x) = 0,$$

which can equivalently be written

$$\frac{1}{\varepsilon}\frac{\mathrm{d}}{\mathrm{d}x}W_1(\mathbf{m}(x)) - \varepsilon \frac{\mathrm{d}}{\mathrm{d}x}|\mathbf{m}'(x)|^2 = 0 \quad \text{for all } x \in \mathbb{R}.$$

On integrating over the entire real line with the constraints $\mathbf{m}(\pm\infty) = \pm(0, 0, 1)$, we obtain

$$\varepsilon^2 |\mathbf{m}'(x)|^2 = 1 - m_3^2(x) \quad \text{for all } x \in \mathbb{R}.$$

For a Bloch wall transition, the magnetization rotates parallel to the wall plane, hence we have that $m_1(x) = 0$ for all $x \in \mathbb{R}$ and thus there holds

$$|\mathbf{m}'(x)|^2 = \frac{|m_3'(x)|^2}{1 - m_3^2(x)}.$$

Substituting this identity in the previous equation yields

$$\varepsilon^2 |m_3'(x)|^2 = (1 - m_3^2(x))^2.$$

Under the further assumption that m_3 is monotone increasing on $\mathbb{R}$, we obtain the ordinary differential equation

$$\varepsilon\, m_3'(x) = 1 - m_3^2(x),$$

which, under the constraints $\mathbf{m}(+\infty) = (0, 0, 1)$ and $\mathbf{m}(-\infty) = (0, 0, -1)$, has as solution the optimal profile given for all $x \in \mathbb{R}$ by

$$\mathbf{m}(x) = \left(0, \frac{1}{\cosh(x/\varepsilon)}, \tanh\left(x/\varepsilon\right)\right), \tag{3.3}$$

see Figure 3.2.

The corresponding minimal cost in term of the energy $F_\varepsilon(\mathbf{m})$ can be computed ex-

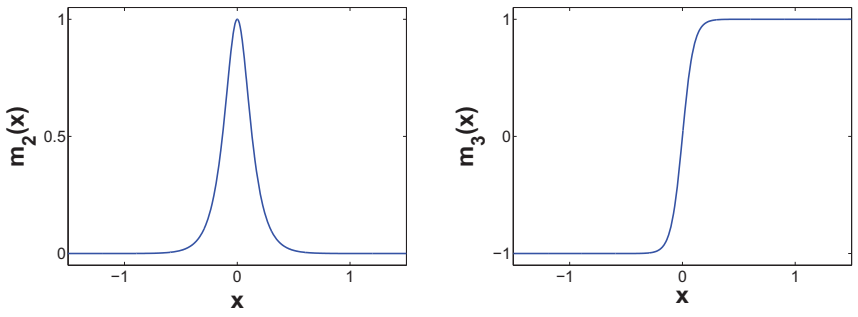

Figure 3.2.: Plot of the nonzero components of the optimal profile $m_2(x) = 1/\cosh(x/\varepsilon)$, $m_3(x) = \tanh(x/\varepsilon)$ for parameter value $\varepsilon = 1/10$.

plicitely. Indeed, we have

$$\begin{aligned} F_\varepsilon(\mathbf{m}, \mathbb{R}) &= \frac{\varepsilon}{4} \int_{\mathbb{R}} \frac{|m_3'(x)|^2}{1 - m_3^2(x)} \mathrm{d}x + \frac{1}{4\varepsilon} \int_{\mathbb{R}} (1 - m_3^2(x)) \mathrm{d}x \\ &= \frac{\varepsilon}{4} \int_{\mathbb{R}} \frac{1}{\varepsilon^2} \frac{(1/\cosh^2(x/\varepsilon))^2}{1 - \tanh^2(x/\varepsilon)} \mathrm{d}x + \frac{1}{4\varepsilon} \int_{\mathbb{R}} (1 - \tanh^2(x/\varepsilon)) \mathrm{d}x \\ &= \frac{1}{4\varepsilon} \int_{\mathbb{R}} \frac{1}{\cosh^2(x/\varepsilon)} \mathrm{d}x + \frac{1}{4\varepsilon} \int_{\mathbb{R}} \frac{1}{\cosh^2(x/\varepsilon)} \mathrm{d}x. \end{aligned}$$

Carrying out the integration, we obtain in fact that

$$\frac{1}{4\varepsilon} \int_{\mathbb{R}} \frac{1}{\cosh^2(x/\varepsilon)} \mathrm{d}x = \frac{1}{4} \big[\tanh(x/\varepsilon) \big]_{-\infty}^{+\infty} = \frac{1}{2},$$

so that finally the minimal cost for the optimal profile is given by

$$\rho = F_\varepsilon(\mathbf{m}, \mathbb{R}) = 1.$$

3.4. Γ-Convergence of the Exchange / Anisotropy Balance

We shall now prove the Γ-convergence of the energy functionals

$$E_1^\varepsilon(\mathbf{m}) = \gamma_\varepsilon F_\varepsilon(\mathbf{m}) + E_{\mathrm{mag}}^{[1]}(\mathbf{m}) + E_{\mathrm{mag}}^{[2]}(\mathbf{m})$$

under the assumptions that the parameter γ_ε remains bounded and that the parameter ε tends to 0.

As stated in Section 2.4, Γ-convergence enjoys the property of being stable with respect to continuous perturbations. In view of this property, we shall show that the ε-independent contributions $E_{\mathrm{mag}}^{[1]}$ and $E_{\mathrm{mag}}^{[2]}$ are continuous in $\mathrm{L}^2(\Omega)$, cf. Proposition 3.5, and thus do not affect the Γ-limit with respect to $\mathrm{L}^2(\Omega)$ convergence of the energy functional E_1^ε. Consequently, the we will only study the Γ-convergence of the functional F_ε under the constraint $|\mathbf{m}| = 1$.

Let $\mathrm{X} = \mathrm{L}^2(\Omega, \mathbb{R}^3)$ denote the set of all admissible configurations. We now consider the

variational problem

$$F_\varepsilon(\mathbf{m}) = \begin{cases} \frac{\varepsilon}{4}\int_\Omega |\nabla \mathbf{m}|^2 \mathrm{d}x + \frac{1}{4\varepsilon}\int_\Omega (1-m_3^2)\mathrm{d}x & \text{if } \mathbf{m} \in \mathrm{H}^1(\Omega,\mathbb{S}^2), \\ +\infty & \text{elsewhere in X.} \end{cases} \tag{3.4}$$

Theorem 3.2. *Let*

$$F_0(\mathbf{m}) = \begin{cases} \frac{1}{2}\int_\Omega |\nabla v| & \textit{if } \mathbf{m} = (0,0,v),\ v \in \mathrm{BV}(\Omega;\{\pm 1\}) \\ +\infty & \textit{elsewhere in X.} \end{cases} \tag{3.5}$$

Then the functionals F_ε Γ-converge to F_0 in X *and the following compactness condition is satisfied: given sequences (ε_n) and $(\mathbf{m}^{\varepsilon_n})$ such that $\varepsilon_n \to 0$ and $F_{\varepsilon_n}(\mathbf{m}^{\varepsilon_n})$ is bounded; then $(\mathbf{m}^{\varepsilon_n})$ is pre-compact in* X.

Note that the Γ-limit F_0 only depends on the total vertical variation of the magnetization on the domain Ω; it can be interpretated as the total length of the interface on Ω, see Section 2.5.

3.4.1. Lower Bound Inequality and Compactness Condition

A first step towards proving the Γ-convergence of the functionals F_ε involves showing that the following statements hold:

(LB) Lower-bound inequality: for every $\mathbf{m} = (0,0,v) \in \mathrm{H}^1(\Omega,\mathbb{S}^2)$ with $v \in \mathrm{BV}(\Omega;\{\pm 1\})$ and every sequence $(\mathbf{m}^{\varepsilon_n}) \in \mathrm{H}^1(\Omega,\mathbb{S}^2)$ such that $\varepsilon_n \to 0$ and $\mathbf{m}^{\varepsilon_n} \to \mathbf{m}$ in $\mathrm{L}^2(\Omega)$ there holds

$$\liminf_{n\to\infty} F_{\varepsilon_n}(\mathbf{m}^{\varepsilon_n}) \geq \frac{1}{2}\int_\Omega |\nabla v|;$$

(C) Compactness condition: given sequences (ε_n) and $(\mathbf{m}^{\varepsilon_n})$ such that $\varepsilon_n \to 0$ and $F_{\varepsilon_n}(\mathbf{m}^{\varepsilon_n})$ is bounded; then $(\mathbf{m}^{\varepsilon_n})$ is pre-compact in $\mathrm{L}^2(\Omega)$ and every limit point belongs to $\mathrm{BV}(\Omega;\{\pm 1\})$.

To this end, we shall use the following lemma.

Lemma 3.3. *For all $\mathbf{m} = (m, m_3) \in \mathrm{H}^1(\Omega,\mathbb{S}^2)$ we have*

$$F_\varepsilon(\mathbf{m}) \geq \frac{1}{2}\int_\Omega |\nabla m_3| \mathrm{d}x.$$

Proof. Let $\mathbf{m} = (m, m_3) \in \mathrm{H}^1(\Omega,\mathbb{S}^2)$. Then we have that $|m|^2 = 1 - m_3^2$ and also that $|\nabla \mathbf{m}|^2 = |\nabla m|^2 + |\nabla m_3|^2$, so that the functional F_ε can be formulated as

$$F_\varepsilon(\mathbf{m}) = \frac{\varepsilon}{4}\int_\Omega \left[|\nabla m|^2 + |\nabla m_3|^2\right]\mathrm{d}x + \frac{1}{4\varepsilon}\int_\Omega (1-m_3^2)\mathrm{d}x.$$

Using the following set of inequalities

$$|\nabla m|^2 \geq |\nabla |m||^2 = |\nabla(\sqrt{1-m_3^2})|^2 = \frac{m_3^2 |\nabla m_3|^2}{1-m_3^2},$$

we obtain that

$$|\nabla m|^2 + |\nabla m_3|^2 \geq \frac{m_3^2 |\nabla m_3|^2}{1 - m_3^2} + |\nabla m_3|^2 = \frac{|\nabla m_3|^2}{1 - m_3^2},$$

and hence the lower bound

$$F_\varepsilon(\mathbf{m}) \geq \frac{\varepsilon}{4} \int_\Omega \frac{|\nabla m_3|^2}{1 - m_3^2} \mathrm{d}x + \frac{1}{4\varepsilon} \int_\Omega (1 - m_3^2) \mathrm{d}x.$$

Furthermore, by virtue of Young's inequality there holds

$$\frac{\varepsilon}{4} \frac{|\nabla m_3|^2}{1 - m_3^2} + \frac{1}{4\varepsilon}(1 - m_3^2) \geq \frac{1}{2} |\nabla m_3|,$$

so that finally we obtain

$$F_\varepsilon(\mathbf{m}) \geq \frac{1}{2} \int_\Omega |\nabla m_3| \mathrm{d}x.$$

□

We shall first prove the L^2-compactness of the sequences $(\mathbf{m}^{\varepsilon_n})$. In all the following, (ε_n) will denote a positive decreasing sequence such that $\varepsilon_n \to 0$ as $n \to \infty$. We shall furthermore use as previously the notation $\mathbf{m}^{\varepsilon_n} = (m^{\varepsilon_n}, m_3^{\varepsilon_n})$ to separate the in-plane and vertical components of $\mathbf{m}^{\varepsilon_n}$.

Theorem 3.4 (Compactness)**.** *Suppose* $(\mathbf{m}^{\varepsilon_n}) \subset \mathrm{H}^1(\Omega; \mathbb{S}^2)$ *with* $F_{\varepsilon_n}(\mathbf{m}^{\varepsilon_n}) \leq C$ *for some universal constant* $C > 0$*. Then* $(\mathbf{m}^{\varepsilon_n})$ *is relatively compact in* $\mathrm{L}^2(\Omega; \mathbb{R}^3)$ *with* $m^{\varepsilon_n} \to 0$ *in* $\mathrm{L}^2(\Omega; \mathbb{R}^2)$ *as* $n \to \infty$*.*

Proof. Let $\mathbf{m}^{\varepsilon_n} = (m^{\varepsilon_n}, m_3^{\varepsilon_n}) \subset \mathrm{H}^1(\Omega; \mathbb{S}^2)$ with $F_{\varepsilon_n}(\mathbf{m}^{\varepsilon_n}) \leq C$. On the first hand, we have the following inequality

$$\|m^{\varepsilon_n}\|^2_{\mathrm{L}^2(\Omega)} = \int_\Omega \big(1 - (m_3^{\varepsilon_n})^2\big) \mathrm{d}x \leq \frac{4\varepsilon_n}{\gamma_{\varepsilon_n}} F_{\varepsilon_n}(\mathbf{m}^{\varepsilon_n}) \leq \frac{C}{\gamma_{\varepsilon_n}} \varepsilon_n.$$

This implies that $m^{\varepsilon_n} \to 0$ in $\mathrm{L}^2(\Omega; \mathbb{R}^2)$ as $n \to \infty$.
By Lemma 3.3, there further holds

$$\|m_3^{\varepsilon_n}\|_{\mathrm{W}^{1,1}(\Omega)} = \int_\Omega \big(|m_3^{\varepsilon_n}| + |\nabla m_3^{\varepsilon_n}|\big) \mathrm{d}x \leq \int_\Omega |m_3^{\varepsilon_n}| \mathrm{d}x + 2F_{\varepsilon_n}(\mathbf{m}^{\varepsilon_n}) \leq |\Omega| + 2C.$$

The domain Ω being bounded and $\mathrm{W}^{1,1}(\Omega)$ being compactly embedded in $\mathrm{L}^1(\Omega)$, the above inequality implies that for a subsequence, we have $m_3^{\varepsilon_n} \to v$ in $\mathrm{L}^1(\Omega)$. This implies the pointwise convergence almost everywhere of $m_3^{\varepsilon_n}$ for a further subsequence. Moreover, there holds $|m_3^{\varepsilon_n}|^2 \leq 1 \in \mathrm{L}^1(\Omega)$ for all $n \in \mathbb{N}$. By the generalized Lebesgue convergence theorem, cf. [4], we finally obtain that, up to a subsequence, $m_3^{\varepsilon_n} \to v$ in $\mathrm{L}^2(\Omega)$ as $n \to \infty$. Thus $(\mathbf{m}^{\varepsilon_n})$ is relatively compact in $\mathrm{L}^2(\Omega; \mathbb{R}^3)$. □

We shall now prove the $\mathrm{L}^2(\Omega)$-continuity of the contributions ${E_{\mathrm{mag}}}^{[1]}$ and ${E_{\mathrm{mag}}}^{[2]}$.

Proposition 3.5. *Let* $\mathbf{m}$ *and* $\mathbf{m}^{\varepsilon_n} \in \mathrm{H}^1(\Omega;\mathbb{S}^2)$*; suppose that* $\mathbf{m}^{\varepsilon_n} \to \mathbf{m}$ *in* $\mathrm{L}^2(\Omega;\mathbb{R}^3)$*. Then as* $n \to \infty$*, we have*

$$E_{\mathrm{mag}}{}^{[1]}(\mathbf{m}^{\varepsilon_n}) \to E_{\mathrm{mag}}{}^{[1]}(\mathbf{m}) \quad \textit{and} \quad E_{\mathrm{mag}}{}^{[2]}(\mathbf{m}^{\varepsilon_n}) \to E_{\mathrm{mag}}{}^{[2]}(\mathbf{m}).$$

In particular, if $\mathbf{m} = (0,0,v)$*, then* $E_{\mathrm{mag}}{}^{[2]}(\mathbf{m}) = 0$*.*

Proof. Note that the quadratic form $E_{\mathrm{mag}}{}^{[i]}$, for $i = 1,2$ respectively, is continuous on $\mathrm{L}^2(\Omega)$ if there exists a constant $C > 0$ such that $E_{\mathrm{mag}}{}^{[i]}(\mathbf{m}) \leq C\|\mathbf{m}\|^2_{\mathrm{L}^2(\Omega;\mathbb{R}^3)}$ for all $\mathbf{m} \in \mathrm{L}^2(\Omega)$.
For all $k \in \mathbb{Z}^2$, we have $0 \leq \sigma(\delta k) \leq 1$. Hence for all $\mathbf{m} \in \mathrm{L}^2(\Omega)$, there holds

$$E_{\mathrm{mag}}{}^{[1]}(\mathbf{m}) = \frac{1}{2}\sum_{k\in\mathbb{Z}^2} \sigma(\delta k)|\hat{m}_3(k)|^2 \leq \frac{1}{2}\sum_{k\in\mathbb{Z}^2} |\hat{m}_3(k)|^2.$$

By virtue of Parseval's formula, there further holds

$$\sum_{k\in\mathbb{Z}^2} |\hat{m}_3(k)|^2 = \|m_3\|^2_{\mathrm{L}^2(\Omega)} \leq \|\mathbf{m}\|^2_{\mathrm{L}^2(\Omega)},$$

so that we finally obtain the inequality

$$E_{\mathrm{mag}}{}^{[1]}(\mathbf{m}) \leq \frac{1}{2}\|\mathbf{m}\|^2_{\mathrm{L}^2(\Omega)} \quad \text{for all } \mathbf{m} \in \mathrm{L}^2(\Omega).$$

Proceeding identically with the second contribution, as $0 \leq 1 - \sigma(\delta k) \leq 1$ and $0 \leq \left|\frac{k\cdot\hat{m}(k)}{|k|}\right|^2 \leq 2|\hat{m}(k)|^2$ for all $k \in \mathbb{Z}^2$, we obtain the energy inequality

$$E_{\mathrm{mag}}{}^{[2]}(\mathbf{m}) \leq \|\mathbf{m}\|^2_{\mathrm{L}^2(\Omega)} \quad \text{for all } \mathbf{m} \in \mathrm{L}^2(\Omega).$$

□

Finally, we prove the lower-bound inequality:

Proposition 3.6. *Let* $\mathbf{m} = (0,0,v) \in \mathrm{H}^1(\Omega,\mathbb{S}^2)$ *and a let* $(\mathbf{m}^{\varepsilon_n}) \subset \mathrm{H}^1(\Omega,\mathbb{S}^2)$ *be a sequence such that* $\mathbf{m}^{\varepsilon_n} \to \mathbf{m}$ *in* $\mathrm{L}^2(\Omega)$ *and* $F_{\varepsilon_n}(\mathbf{m}^{\varepsilon_n}) \leq C$*. Then* $v \in \mathrm{BV}(\Omega;\{\pm 1\})$ *with*

$$\frac{1}{2}\int_\Omega |\nabla v| \leq \liminf_{n\to\infty} F_{\varepsilon_n}(\mathbf{m}^{\varepsilon_n}).$$

Proof. Note that, since the domain Ω is bounded, the $\mathrm{L}^2(\Omega)$-convergence of $(\mathbf{m}^{\varepsilon_n})$ implies the $\mathrm{L}^1(\Omega)$-convergence i.e. there holds $\mathbf{m}^{\varepsilon_n} \to \mathbf{m}$ in $\mathrm{L}^1(\Omega)$. It follows from Lemma 3.3 that

$$\frac{1}{2}\int_\Omega |m_3^{\varepsilon_n}|\mathrm{d}x \leq F_{\varepsilon_n}(\mathbf{m}^{\varepsilon_n}),$$

so that on passing to the limit $n \to \infty$, we obtain

$$\liminf_{n\to\infty} \frac{1}{2}\int_\Omega |m_3^{\varepsilon_n}|\mathrm{d}x \leq \liminf_{n\to\infty} F_{\varepsilon_n}(\mathbf{m}^{\varepsilon_n}).$$

The total variation being lower semi-continuous with respect to $\mathrm{L}^1(\Omega)$-convergence, cf.

Section 2.5, there further holds

$$\int_\Omega |\nabla v| \leq \liminf_{n\to\infty} \int_\Omega |m_3^{\varepsilon_n}| \mathrm{d}x$$

so that we finally obtain the lower-bound inequality

$$\frac{1}{2}\int_\Omega |\nabla v| \leq \liminf_{n\to\infty} F_{\varepsilon_n}(\mathbf{m}^{\varepsilon_n}).$$

□

3.4.2. Upper Bound Inequality

The second and last step towards proving the Γ-limit is to verify the following statement:

(UB) Upper-bound inequality: for every $v \in \mathrm{BV}(\Omega;\{\pm 1\})$ and $\mathbf{m} = (0,0,v) \in \mathrm{H}^1(\Omega,\mathbb{S}^2)$, there exists a sequence $(\mathbf{m}_\varepsilon) \subset \mathrm{H}^1(\Omega,\mathbb{S}^2)$ such that $\mathbf{m}_\varepsilon \to \mathbf{m}$ in $\mathrm{L}^2(\Omega)$ and

$$\limsup_{\varepsilon\to 0} F_\varepsilon(\mathbf{m}_\varepsilon) \leq \frac{1}{2}\int_\Omega |\nabla v|.$$

It is in fact enough to prove the inequality (UB) for a dense subset $\mathcal{D}$ of X. In that sense, we choose $\mathcal{D}$ as follows: setting $\mathrm{E} := \{x \in \Omega : v(x) = 1\}$ the subset of Ω where the magnetization vector $\mathbf{m}$ is pointing up and $\mathcal{F} := \{\mathrm{E} \subset \Omega\text{: } \partial\mathrm{E} \text{ piecewise affine}\}$, we define

$$\mathcal{D} := \{v = 2\chi_\mathrm{E} - 1, \mathrm{E} \in \mathcal{F}\}.$$

The set $\mathcal{D}$ is the class of all $v \in \mathrm{BV}(\Omega;\{\pm 1\})$ whose singular set S_v is a piecewise affine curve in Ω.

Remark 3.7. *We use the notation $\mathcal{H}^1(S_v)$ to denote the one-dimensional Hausdorff measure of the singular set S_v. Recall that it corresponds here to the total length of the interface on Ω and that it agrees with the perimeter functional*

$$\mathcal{H}^1(S_v) = \frac{1}{2}\int_\Omega |\nabla v| = \mathrm{Per}(\mathrm{E},\Omega).$$

Lemma 1 in the paper of Modica [45], see also Ambrosio [5, p147], states that for every E of finite perimeter in Ω, there exists a sequence (E_k) with smooth boundaries such that $\mathrm{E}_k \to \mathrm{E}$ in measure and $\mathrm{Per}(\mathrm{E}_k,\Omega) \to \mathrm{Per}(\mathrm{E},\Omega)$. In fact, the paper of Modica contains arguments for smooth approximation that easily imply the result for piecewise affine functions by interpolation.

Thus we take $\mathbf{m} = (0,0,v)$ with $v \in \mathcal{D}$ and we consider S_v the singular set of v in Ω as a piecewise affine curve. In order to prove the inequality (UB), we shall proceed as follows:

1. We decompose the interface S_v into a finite union of M line segments S_i (dotted lines on Figure 3.3) i.e., we have $S_v = \cup_{i=1}^M S_i$;

2. Given $\varepsilon > 0$, we cover the interface up to a set of small residual triangles (dark gray triangles on Figure 3.3) with a set of disjoint rectangles U_i, $i = 1,\ldots,M$, that

are each composed of a inner rectangle R_i (light gray rectangle on Figure 3.3) of width $\varepsilon^{4/5}$ and two smaller outer rectangles, the union of which we shall name K_i. Within the inner rectangles R_i, we set the magnetization $\mathbf{m}_\varepsilon$ to follow the optimal profile derived in Section 3.3. In the darker outer rectangles we take a quadratic extension of $\mathbf{m}_\varepsilon$ which agrees with the values taken by the magnetization on the sides which border the black and white regions. We follow the same approach within the residual regions L_i joining the rectangles;

3. Given $\mathcal{L} = \frac{1}{2}\int_\Omega |\nabla v|$ the length of the interface on Ω and $\rho = 1$ the minimal cost for the Bloch wall transition computed in Section 3.3, we shall show that $\rho\mathcal{L}$ yields an upper bound for the exchange and anisotropy energy contributions on the set of rectangles R_i i.e. $\rho\mathcal{L} \geq \sum_{i=1}^{M} F_\varepsilon(\mathbf{m}_\varepsilon, R_i)$;

4. As the exchange and anisotropy energy contributions are zero outside the set covering the interface S_v, we infer that

$$F_\varepsilon(\mathbf{m}_\varepsilon) = \sum_{i=1}^{M} F_\varepsilon(\mathbf{m}_\varepsilon, R_i) + \sum_{i=j}^{M} F_\varepsilon(\mathbf{m}_\varepsilon, K_j) + \sum_{k=1}^{M} F_\varepsilon(\mathbf{m}_\varepsilon, L_k),$$

which, combined with the previous inequality yields

$$\mathcal{L} \geq F_\varepsilon(\mathbf{m}_\varepsilon) - \sum_{i=j}^{M} F_\varepsilon(\mathbf{m}_\varepsilon, K_j) - \sum_{k=1}^{M} F_\varepsilon(\mathbf{m}_\varepsilon, L_k);$$

5. As a last step, we shall show that the energy contributions on all the rectangles K_j and all the joining triangles L_k vanish as we let ε tend to 0. This then yields the upper-bound inequality (UB).

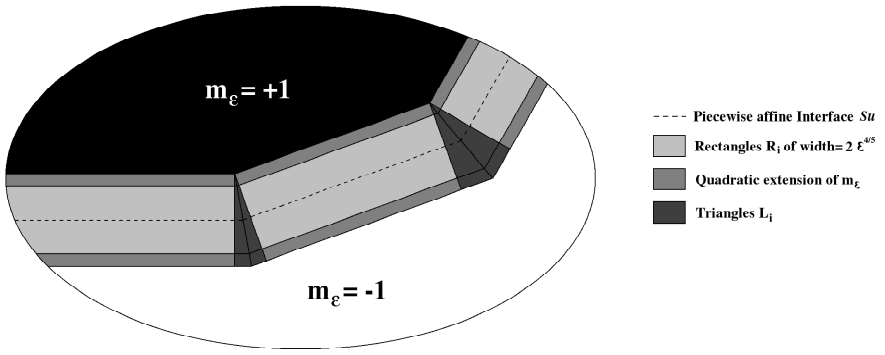

Figure 3.3.: Covering of the interface S_v.

Before beginning with the construction of the sequence $(\mathbf{m}_\varepsilon)$, we shall set a few notations. For all $i = 1, 2, \ldots, M$, we define around each line segment S_i a local set of coordinate axes as follows: the first coordinate axis $e_1^{[i]}$ is set perpendicular to the transition axis, oriented in the direction of the side of S_i where $m_3 = +1$. The second coordinate

axis $e_2^{[i]}$ is set on the transition axis whereas the third axis $e_3^{[i]}$ is set perpendicular to the domain Ω. Furthermore, on each rectangle U_i we set the coordinates

$$x = x^{[i]} = (x_1^{[i]}, x_2^{[i]}) \quad \text{with respect to the axes} \quad (e_1^{[i]}, e_2^{[i]}),$$

and the corresponding magnetization

$$\mathbf{m}_\varepsilon(x) = \mathbf{m}_\varepsilon(x^{[i]}) = (m_{\varepsilon 1}^{[i]}(x^{[i]}), m_{\varepsilon 2}^{[i]}(x^{[i]}), m_{\varepsilon 3}^{[i]}(x^{[i]})) \quad \text{with respect to} \quad (e_1^{[i]}, e_2^{[i]}, e_3^{[i]}).$$

Let now $i \in \{1, 2, \dots, N\}$ be given. For a sake of simplicity, we shall drop the indices $[i]$ and ε in the notation i.e., from now on we write $x = (x_1, x_2)$ for $x^{[i]} = (x_1^{[i]}, x_2^{[i]})$ and $\mathbf{m} = (m_1, m_2, m_3)$ for $\mathbf{m}_\varepsilon(x^{[i]}) = (m_{\varepsilon 1}^{[i]}, m_{\varepsilon 2}^{[i]}, m_{\varepsilon 3}^{[i]})$. We shall now proceed to the construction of the recovery sequence $(\mathbf{m}_\varepsilon)$.

On considering a one-dimensional Bloch-wall transition, the first component of the magnetization will remain zero on the whole domain i.e. $m_1 = 0$. As the magnetization vector takes values on the unit sphere, we have for the second component $|m_2| = \sqrt{1 - m_3^2}$ so that we only need to consider the variations of the third component m_3 along the transition axis. On the inner rectangles R_i i.e., for $x_1 \in (-\varepsilon^{4/5}, \varepsilon^{4/5})$, we set the magnetization equal to the optimal profile $m_3(x_1, x_2) = \tanh(x_1/\varepsilon)$. On the outer rectangles K_i, we take a quadratic extension of m_ε. This yields the profile

$$m_3(x_1, x_2) := \begin{cases} \frac{(1-\alpha_\varepsilon)}{(\varepsilon^{2/3} - \varepsilon^{4/5})^2} (x_1 + \varepsilon^{2/3})^2 - 1 & \text{if } x_1 \in (-\varepsilon^{2/3}, -\varepsilon^{4/5}), \\ \tanh(x_1/\varepsilon) & \text{if } x_1 \in (-\varepsilon^{4/5}, \varepsilon^{4/5}), \\ -\frac{(1-\alpha_\varepsilon)}{(\varepsilon^{2/3} - \varepsilon^{4/5})^2} (x_1 - \varepsilon^{2/3})^2 + 1 & \text{if } x_1 \in (\varepsilon^{4/5}, \varepsilon^{2/3}). \end{cases}$$

where $\alpha_\varepsilon := \tanh(\varepsilon^{-1/5})$, see Figure 3.4. Note that the quadratic extension of $\mathbf{m}_\varepsilon$ already reaches the values $+1$ (repectively -1) at the values $x_1 = \varepsilon^{2/3}$ (respectively $x_1 = -\varepsilon^{2/3}$), and therefore agrees with the values taken by the magnetization within the domains (black and white regions on Figure 3.3). The same construction procedure for the recovery sequence is applied within the linking triangles.

Remark 3.8. *Note that the values $\varepsilon^{4/5}$ and $\varepsilon^{2/3}$ are chosen so that the term $\alpha_\varepsilon = \tanh(\varepsilon^{-1/5})$ tends to 1 as ε goes to 0 and so that the energy contributions of the outer rectangles K_i and the small rectangles L_i vanish as ε goes to 0, cf. Lemma 3.9.*

Now that we have defined the recovery sequence on the whole interface, we shall proceed to the analysis. On all the inner rectangles R_i, $i = 1, \dots, M$, the magnetization follows the optimal profile but yet does not attain the asymptotic values. Hence it follows immediately that

$$F_\varepsilon(\mathbf{m}, R_i) \leq \rho \mathcal{H}^1(S_i) \quad \text{for all } i \in \{1, 2, \dots, M\}.$$

Summation over all $i \in \{1, 2, \dots, M\}$ yields

$$\sum_{i=1}^{M} F_\varepsilon(\mathbf{m}_\varepsilon, R_i) \leq \rho \mathcal{L} = \mathcal{L}$$

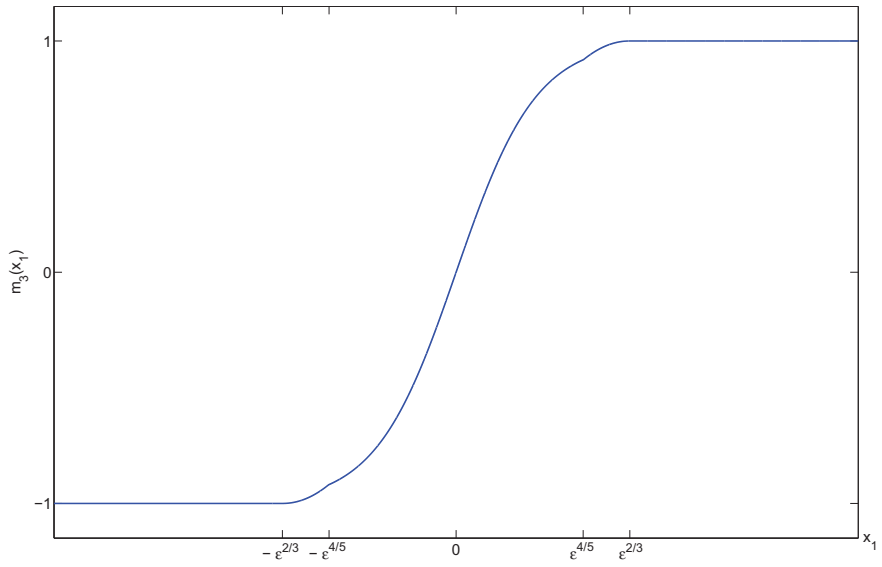

Figure 3.4.: Construction of the recovery sequence $\mathbf{m}_\varepsilon$ along the axis perpendicular to the wall.

with $\mathcal{L} := \mathcal{H}^1(S_v) = \frac{1}{2}\int_\Omega |\nabla v|$. Let $J = \bigcup_{i=1}^M (L_i \cup U_i)$ denote the union of all the rectangles and triangles used in our construction to cover the interface. Outside this covering area (black and white regions on Figure 3.3), the magnetization remains constant, pointing either up or down i.e.,

$$m_3(x) = \pm 1 \quad \text{for all } x \in \Omega \setminus J,$$

and hence cancels the exchange and anisotropy energy contributions. Consequently, we have that

$$F_\varepsilon(\mathbf{m}) = \sum_{i=1}^M F_\varepsilon(\mathbf{m}_\varepsilon, R_i) + \sum_{j=1}^M F_\varepsilon(\mathbf{m}_\varepsilon, K_j) + \sum_{k=1}^M F_\varepsilon(\mathbf{m}_\varepsilon, L_k),$$

which, substituted into the previous inequality, yields

$$\mathcal{L} \geq F_\varepsilon(\mathbf{m}) - \sum_{j=1}^M F_\varepsilon(\mathbf{m}_\varepsilon, K_j) - \sum_{k=1}^M F_\varepsilon(\mathbf{m}_\varepsilon, L_k). \tag{3.6}$$

We shall now show that the energy contributions on the outer rectangles L_i as well as on the linking triangles K_i vanish as we let the parameter ε go to 0.

Lemma 3.9. *Let $i \in \{1, 2, \ldots, M\}$. The exchange and anisotropy energy contributions of the areas K_i and L_i vanish as ε goes to 0 i.e.*

$$\lim_{\varepsilon \to 0} F_\varepsilon(\mathbf{m}, K_i) = 0 \quad \textit{and} \quad \lim_{\varepsilon \to 0} F_\varepsilon(\mathbf{m}, L_i) = 0 \quad \textit{for all } i = 1, \ldots, M.$$

Proof. Let $i \in \{1, 2, \ldots, M\}$. In a first instance, we shall prove the vanishing of the energy contributions on the rectangles K_i. In fact, we shall consider in the proof only the outer rectangle denoted K_{i_1} located on the side of the interface where the magnetization reaches the value $+1$ i.e., in terms of the local coordinates, for $x_1 \in [\varepsilon^{4/5}, \varepsilon^{2/3}]$. The proof

is exactly identical for the second rectangle. Recall first that S_i (respectively $\mathcal{H}^1(S_i)$) denotes the i-th line segment (respectively the length of the i-th line segment) of the piecewise affine interface S_v. In the rectangle K_{i_1}, the magnetization varies only in the direction normal to S_i, in that sense we have

$$F_\varepsilon(\mathbf{m}, K_{i_1}) \leq \mathcal{H}^1(S_i)\big[\frac{\varepsilon}{4}\int_{\varepsilon^{4/5}}^{\varepsilon^{2/3}} \frac{|m_3'(x)|^2}{1-m_3^2(x)}\mathrm{d}x_1 + \frac{1}{4\varepsilon}\int_{\varepsilon^{4/5}}^{\varepsilon^{2/3}}(1-m_3^2(x))\mathrm{d}x_1\big].$$

Let now $x = (x_1, x_2)$ be in the rectangle K_{i_1}. On the first hand, we have explicitely

$$m_3(x) = -\frac{(1-\alpha_\varepsilon)}{(\varepsilon^{2/3}-\varepsilon^{4/5})^2}\,(x_1-\varepsilon^{2/3})^2 + 1,$$

with $\alpha_\varepsilon = \tanh(\varepsilon^{-1/5})$, so that the first derivative of m_3 with respect to the variable x can be determined in a closed form. Indeed, we have

$$m_3'(x) = -\frac{2(1-\alpha_\varepsilon)}{(\varepsilon^{2/3}-\varepsilon^{4/5})^2}(x_1-\varepsilon^{2/3}) \quad \text{i.e.} \quad |m_3'(x)|^2 = \frac{4(1-\alpha_\varepsilon)}{(\varepsilon^{2/3}-\varepsilon^{4/5})^2}(1-m_3(x)).$$

Consequently, since $m_3(x) \geq 0$ on the rectangle K_{i_1}, we obtain the upper bound

$$\frac{|m_3'(x)|^2}{1-m_3^2(x)} = \frac{4(1-\alpha_\varepsilon)}{(\varepsilon^{2/3}-\varepsilon^{4/5})^2}\frac{1}{m_3(x)+1} \leq \frac{4(1-\alpha_\varepsilon)}{(\varepsilon^{2/3}-\varepsilon^{4/5})^2}.$$

On integrating the previous inequality between $\varepsilon^{4/5}$ and $\varepsilon^{2/3}$, we finally obtain

$$\frac{\varepsilon}{4}\int_{\varepsilon^{4/5}}^{\varepsilon^{2/3}} \frac{|m_3'(x)|^2}{1-m_3^2(x)}\mathrm{d}x_1 \leq (1-\alpha_\varepsilon)\frac{\varepsilon^{1/3}}{(1-\varepsilon^{2/15})}.$$

The right hand-side of previous inequality vanishes as ε tends to 0, hence have as well that

$$\lim_{\varepsilon\to 0}\frac{\varepsilon}{4}\int_{\varepsilon^{4/5}}^{\varepsilon^{2/3}} \frac{|m_3'(x)|^2}{1-m_3^2(x)}\mathrm{d}x_1 = 0.$$

On the other hand, we have

$$(1-m_3^2(x)) = (1-m_3(x))(1+m_3(x)) \leq 2(1-m_3(x)) = \frac{2(1-\alpha_\varepsilon)}{(\varepsilon^{2/3}-\varepsilon^{4/5})^2}(x_1-\varepsilon^{2/3})^2.$$

On integrating the above inequality between $\varepsilon^{4/5}$ and $\varepsilon^{2/3}$, we obtain

$$\frac{1}{4\varepsilon}\int_{\varepsilon^{4/5}}^{\varepsilon^{2/3}}(1-m_3^2(x))\mathrm{d}x_1 \leq \frac{1}{6}\frac{(1-\alpha_\varepsilon)}{\varepsilon}(\varepsilon^{2/3}-\varepsilon^{4/5}) \leq \frac{1}{6}\frac{(1-\alpha_\varepsilon)}{\varepsilon^{1/3}}.$$

Since the quantity α_ε converges exponentially to 0 as ε goes to 0, we immediately obtain that

$$\lim_{\varepsilon\to 0}\frac{(1-\alpha_\varepsilon)}{\varepsilon^{1/3}} = 0,$$

and hence the anisotropy term of the energy on the rectangle K_{i_1} vanishes as well as we let ε go to 0. As previously mentioned, the result is identical for the inner rectangle, so

that finally we obtain

$$\lim_{\varepsilon\to 0} F_\varepsilon(\mathbf{m}, K_i) = 0 \quad \text{for all } i = 1, 2, \ldots, M,$$

i.e. the energy contribution of the rectangle K_i vanishes as ε goes to 0.

We shall now show a similar result for the energy contribution on the triangles L_i (see Figure 3.3). Let $\beta_i \in [0, \pi]$ denote the angle between the segment lines S_i and S_{i+1} and let $\beta := \min_{i=1,\ldots,M} \beta_i$; To the angle β corresponds the biggest joining triangle in terms of domain size. Indeed, let $i \in \{1, 2, \ldots, M\}$. The area of the triangle L_i - in fact the ends of each segment line are covered by two triangles, but for obvious reasons of symmetry we will set our analysis only on one triangle per segment line - covering the joint of S_i and S_{i+1} is given by

$$|L_i| = \frac{2\varepsilon^{4/3}}{\tan(\beta_i/2)},$$

so that, on setting $C(\beta) = 2/\tan(\beta/2)$, we obtain the upper bound

$$|L_i| \leq C(\beta)\varepsilon^{4/3}.$$

In terms of the exchange energy, we therefore have

$$\frac{\varepsilon}{4}\int_{L_i} |\nabla \mathbf{m}(x)|^2 \mathrm{d}x \leq \frac{\varepsilon}{4}|L_i| \sup_{x\in L_i} |\nabla \mathbf{m}(x)|^2.$$

For $x_1 \in (-\varepsilon^{4/5}, \varepsilon^{4/5})$, the magnetization vector follows the optimal profile, hence there holds

$$\varepsilon^2 |\nabla \mathbf{m}(x)|^2 = 1 - m_3^2(x) \quad \text{i.e.} \quad |\nabla \mathbf{m}(x)|^2 \leq \frac{1}{\varepsilon^2}.$$

For $x_1 \in (-\varepsilon^{2/3}, -\varepsilon^{4/5}) \cup (\varepsilon^{4/5}, \varepsilon^{2/3})$, we have as well

$$|\nabla \mathbf{m}(x)|^2 = \frac{|\nabla m_3(x)|^2}{1 - m_3^2(x)} = \frac{4(1-\alpha_\varepsilon)}{\varepsilon^{2/3} - \varepsilon^{4/5}} \frac{1}{m_3(x) + 1} \leq \frac{1}{\varepsilon^2}$$

for ε sufficiently small. Consequently, we have

$$\sup_{x\in L_i} |\nabla \mathbf{m}(x)|^2 \leq \frac{1}{\varepsilon^2},$$

and therefore

$$\frac{\varepsilon}{4}\int_{L_i} |\nabla \mathbf{m}(x)|^2 \mathrm{d}x \leq \frac{C(\beta)}{4}\varepsilon^{1/3},$$

so that finally in the limit we obtain

$$\lim_{\varepsilon\to 0} \int_{L_i} |\nabla \mathbf{m}(x)|^2 \mathrm{d}x = 0.$$

Similarly, as $0 \leq 1 - m_3^2(x) \leq 1$ for all x, there holds

$$\frac{1}{4\varepsilon}\int_{L_i} (1 - m_3^2(x)) \mathrm{d}x \leq \frac{1}{4\varepsilon}|L_i| \leq \frac{C(\beta)}{4}\varepsilon^{1/3},$$

so that

$$\lim_{\varepsilon\to 0}\frac{1}{4\varepsilon}\int_{L_i}(1-m_3^2(x))\mathrm{d}x = 0.$$

Finally, we have shown that

$$\lim_{\varepsilon\to 0} F_\varepsilon(\mathbf{m}, L_i) = 0 \quad \text{for all } i = 1, 2, \ldots, M.$$

□

Using the results of Lemma 3.9 in Equation (3.6) we obtain

$$\frac{1}{2}\int_\Omega |\nabla v| = \mathcal{L} \geq F_\varepsilon(\mathbf{m}_\varepsilon) - o(1) - o(1).$$

On passing to the limit $\varepsilon \to 0$ in the above inequality yields the upper-bound inequality

$$\limsup_{\varepsilon\to 0} F_\varepsilon(\mathbf{m}_\varepsilon) \leq \frac{1}{2}\int_\Omega |\nabla v|.$$

3.4.3. Gamma-Limit for the Sharp Interface Model

According to the results of sections 3.2, 3.4.1 and 3.4.2, we now can claim that our initial energy functional E_1^ε Γ-converges in $\mathrm{X} = \mathrm{L}^2(\Omega;\mathbb{R}^3)$ to the functional E_0 given by

$$E_0(v) = \begin{cases} \frac{\gamma}{2}\int_\Omega |\nabla v| + \frac{1}{2}\sum_{k\in\mathbb{Z}^2}\sigma(\delta k)\,|\hat{v}(k)|^2 & \text{if } v \in \mathrm{BV}(\Omega;\{\pm 1\}), \\ \\ +\infty & \text{elsewhere in X.} \end{cases}$$

Since Γ-convergence ensures the convergence of minimizers, minimizing the energy functional $E_1^\varepsilon(\mathbf{m})$ on $\mathrm{H}^1(\Omega,\mathbb{S}^2)$ boils down to minimizing the functional $E_0(v)$ on $\mathrm{BV}(\Omega;\{\pm 1\})$. Our new energy functional $E_0(v)$ is then driven only by the competition of the reduced stray-field energy that favours a rapidly oscillating magnetization, and the domain wall energy that favours a small domain wall length and thus a slowly varying magnetization. This simplifies the analysis of the existence of local minimizers of the energy functional and therefore is a step towards the prediction of the formation of magnetic patterns in thin films. Based on a similar result and on the stripe domains theory developed by Kooy and Enz, Gehring and Kaplan [31] showed that in case of an ultrathin magnetic film with perpendicular anisotropy, a stripe pattern is a lower energy state than a checkerboard pattern.

3.4.4. Analogy with the Microphase Separation of Diblock Copolymers

The model previously derived presents similarities with the model commonly proposed to study the microphase separation of diblock copolymers. A diblock copolymer is linear-chain molecule consisting of two subchains made of different monomer units A and B, and bound covalently to each other. The repulsion between the unlike monomers induces a strong repulsion between the subchains of the polymer. Below a critical temperature, the latter tend to segregate. But the chemical bond between the chains of the copolymer empeaches a macroscopic segregation where the subchains would disassemble from each

other. Rather, the diblock copolymers undergo a microphase separation on a mesoscopic scale and self assemble into various ordered structures composed of domains rich in either A or B-monomers. Different pattern morphologies such as lamellae, spheres, cylinders or gyroids can bee observed, see e.g. [7].
Ohta and Kawasaki derived in [47] a density functional theory to model the microphase separation of diblock copolymers. It gives rise to a nonlocal variational problem of Cahn–Hilliard type, see [18, 46], which, after appropriate rescaling and under specific parameter regime, can be written in the following condensed form

$$\min_{v\in\mathcal{S}} E_{\varepsilon,\sigma}(v) := \int_\Omega \varepsilon|\nabla v| + \sigma \sum_{k\in\mathbb{Z}^3} \frac{1}{|k|^2}|\hat{v}(k)|^2$$

on the restricted class

$$\mathcal{S} := \{v \in \mathrm{BV}(\Omega;\{-1,+1\}) : \int_\Omega v\,\mathrm{d}x = 0\}$$

and with the three-dimensional domain $\Omega \subset \mathbb{R}^3$ and parameters $\varepsilon > 0$, $\sigma > 0$, cf. [17]. The variable v stands for the averaged macroscopic monomer density, i.e. $v = +1$ denotes a state of exclusively A-monomer while $v = -1$ denotes a pure B-monomer state. The interfacial energy term models the preference for the system to form structures minimizing the contacts between the monomers and hence favouring minimal interface. It is balanced by a nonlocal long-range interaction term modeling the entropy cost associated to the chain stretching. Note that the main difference with the model for hard magnetic films derived previously concerns a volume conservation constraint for the monomer density v that needs to be taken into account. We refer to the aforementioned literature and the references therein for a complete discussion about the physical as well as mathematical aspects of microphase separation of diblock copolymers.

4. Dynamical Model

4.1. Introduction

In this chapter we shall consider a dynamical model arising as the L^2 gradient flow for the Modica–Mortola regularization of the sharp interface Γ-limit functional

$$v \in \mathrm{BV}(\Omega;\{-1,1\}) \mapsto E_0(v) := \frac{\gamma}{2}\int_\Omega |\nabla v| + \frac{1}{2}\sum_{k\in\mathbb{Z}^2}\sigma(\delta k)|\hat{v}(k)|^2 \tag{4.1}$$

derived in the previous chapter. For more simplicity, the thickness parameter δ arising in the formulation of the reduced stray-field energy will be dropped in the following, more precisely it will be set to $\delta = 1$. We shall introduce a relaxed model, based on an approximation of the perimeter functional by a singular perturbation problem, and derive the associated $\mathrm{L}^2(\Omega)$ gradient flow equation, a nonlinear and nonlocal parabolic equation. We finally prove the existence of a unique global solution to this equation.

4.2. Relaxed Model

We are interested in the approximation of local minimizers of the energy functional E_0 on the space of functions of bounded variation $\mathrm{BV}(\Omega;\{\pm 1\})$. We shall to this end consider a dynamical approach based on a gradient flow equation for a relaxed model; indeed, the nonconvex constraint $v = \pm 1$ for the solutions of variational problem (4.1) is rather problematic in view of a later numerical implementation. Thus we shall base our considerations on a model in which we relax the aforementioned nonconvex constraint on v and substitute the line energy for domain walls $\frac{1}{2}\int_\Omega |\nabla v|$ for its Modica–Mortola approximation. Recall indeed that for the double-well potential

$$W(u) = c_0(1-|u|^2)^2, \quad c_0 > 0,$$

the functional

$$\int_\Omega \left(\frac{\varepsilon}{2}|\nabla u|^2 + \frac{1}{\varepsilon}W(u)\right)\mathrm{d}x$$

approximates the domain wall energy in the sense of Γ-convergence by finite layers of thickness $\varepsilon > 0$ and with associated surface tension

$$\gamma = \int_{-1}^{+1}\sqrt{2W(u)}\mathrm{d}u,$$

see e.g. [2, 10, 21]. Note that by renormalizing the generic double-well potential in terms of the positive constant c_0, every value of the parameter γ can be realized. Hence we will

base our considerations on the relaxed energy

$$E_\varepsilon(u) = \int_\Omega \left(\frac{\varepsilon}{2} |\nabla u|^2 + \frac{1}{\varepsilon} W(u) \right) \mathrm{d}x + \frac{1}{2} \sum_{k \in \mathbb{Z}^2} \sigma(k) |\mathcal{F}u(k)|^2 \tag{4.2}$$

for $\varepsilon > 0$ small but fixed and the Fourier multiplier σ given by

$$\sigma(k) = (1 - \exp(-2\pi|k|)/(2\pi|k|) \quad \text{for all } k \in \mathbb{Z}^2.$$

4.3. Computation of the $\mathrm{L}^2(\Omega)$ Gradient Flow Equation

Our dynamical approach to the minimization of the energy functional E_ε on $\mathrm{H}^1(\Omega)$ is based on the study of its associated $\mathrm{L}^2(\Omega)$ gradient flow with variational formulation

$$\partial_t u + \nabla_u E_\varepsilon(u) = 0 \tag{4.3}$$

that, in its long-time asymptotics, leads to local minimizers that approximate those of the sharp-interface problem (4.1). The energy gradient can be computed explicitely. Indeed, for all $u \in \mathrm{H}^1(\Omega)$, let us decompose the energy functional as

$$E_\varepsilon(u) = G_1(u) + G_2(u)$$

with G_1 and G_2 being respectively the first and second summand in the energy formulation (4.2). Given $u \in \mathrm{H}^1(\Omega)$, $s \in \mathbb{R}$ and a test function φ on Ω, we now define

$$u_s := u + s\varphi.$$

By virtue of the chain rule, we have on a first instance that

$$\frac{\mathrm{d}}{\mathrm{d}s} E(u_s)_{|_{s=0}} = \int_\Omega \nabla_u E(u(x))\, \varphi(x) \mathrm{d}x.$$

Furthermore, there holds

$$G_1(u_s) = \int_\Omega \left(\frac{\varepsilon}{2} \big[|\nabla u(x)|^2 + 2s \nabla u(x) \cdot \nabla \varphi(x) + s^2 |\nabla \varphi(x)|^2 \big] + \frac{1}{\varepsilon} W(u_s(x)) \right) \mathrm{d}x,$$

so that

$$\begin{aligned} \frac{\mathrm{d}}{\mathrm{d}s} G_1(u_s)_{|_{s=0}} &= \varepsilon \int_\Omega \nabla u(x) \cdot \nabla \varphi(x) \mathrm{d}x + \frac{1}{\varepsilon} \int_\Omega \mathrm{D}W(u(x))\, \varphi(x) \mathrm{d}x \\ &= \varepsilon \int_\Omega (-\Delta) u(x) \varphi(x) \mathrm{d}x + \frac{1}{\varepsilon} \int_\Omega \mathrm{D}W(u(x))\, \varphi(x) \mathrm{d}x. \end{aligned}$$

Proceeding similarly with the second term of the energy, we have

$$G_2(u_s) = \frac{1}{2} \sum_{k \in \mathbb{Z}^2} \sigma(k) \big[|\mathcal{F}u(k)|^2 + 2s \mathcal{F}u(k) \mathcal{F}\varphi(k) + s^2 |\mathcal{F}\varphi(k)|^2 \big],$$

and hence

$$\frac{\mathrm{d}}{\mathrm{d}s}G_2(u_s)_{|s=0} = \sum_{k\in\mathbb{Z}^2} \sigma(k)\mathcal{F}u(k)\mathcal{F}\varphi(k).$$

By virtue of Parseval's theorem, there further holds

$$\frac{\mathrm{d}}{\mathrm{d}s}G_2(u_s(x))_{|s=0} = \int_\Omega \mathcal{F}^{-1}\big[\sigma(k)\mathcal{F}u(k)\big](x)\,\varphi(x)\mathrm{d}x$$

where $\mathcal{F}^{-1}$ denotes the inverse Fourier transform. Putting everything together, we finally obtain that for every test function φ on Ω

$$\int_\Omega \nabla_u E(u(x))\,\varphi(x)\mathrm{d}x = \int_\Omega \Big(-\varepsilon\Delta u + \frac{1}{\varepsilon}\mathrm{D}W(u) + \mathcal{F}^{-1}\big[\sigma(k)\mathcal{F}u(k)\big]\Big)(x)\,\varphi(x)\mathrm{d}x$$

and hence the expression of the energy gradient

$$\begin{aligned}\nabla_u E_\varepsilon(u) &= -\varepsilon\Delta u + \frac{1}{\varepsilon}\mathrm{D}W(u) + \mathcal{F}^{-1}\big[\sigma(k)\mathcal{F}u(k)\big] \\ &= \mathcal{F}^{-1}\big[((2\pi)^2\varepsilon|k|^2 + \sigma(k))\mathcal{F}u(k)\big] + \frac{1}{\varepsilon}\mathrm{D}W(u).\end{aligned}$$

On defining $\mathcal{L}_\varepsilon$ and $\mathcal{N}_\varepsilon$ respectively the linear and non linear operator given for $\varepsilon > 0$ by

$$\begin{aligned}\mathcal{L}_\varepsilon u &:= \mathcal{F}^{-1}\left[((2\pi)^2\varepsilon|k|^2 + \sigma(k))\mathcal{F}u(k)\right], \\ \mathcal{N}_\varepsilon(u) &:= -\mathrm{D}W_\varepsilon(u),\end{aligned}$$

with $W_\varepsilon(\cdot) := \frac{1}{\varepsilon}W(\cdot)$, the previous expression of the energy gradient decomposes as

$$\nabla_u E_\varepsilon(u) = \mathcal{L}_\varepsilon u - \mathcal{N}_\varepsilon(u).$$

Note that the linear part $\mathcal{L}_\varepsilon$ is represented in terms of a Fourier multiplier which for fixed parameter $\varepsilon > 0$, is uniformly second-order elliptic. Thus our gradient flow equation reads as the following nonlinear parabolic equation

$$u_t + \mathcal{L}_\varepsilon u = \mathcal{N}_\varepsilon(u) \quad \text{for} \quad u(\cdot,t) : \Omega \to \mathbb{R} \quad \text{and} \quad t > 0. \tag{4.4}$$

We shall assume that Equation (4.4) is subject to periodic boundary conditions and the initial condition

$$u(\cdot,0) = u_0(\cdot), \tag{4.5}$$

where u_0 is a given periodic function defined and continuous on Ω.

4.4. Existence, Regularity and Uniqueness of Solutions

In this section, we shall prove the existence of a unique global solution $u \in \mathrm{L}^\infty_t\mathrm{H}^1_x \cap \dot{\mathrm{H}}^1_t\mathrm{L}^2_x((0,\infty)\times\Omega)$ for the Cauchy problem

$$u_t + \mathcal{L}_\varepsilon u = \mathcal{N}_\varepsilon(u), \quad u(x,0) = u_0(x) \tag{4.6}$$

with initial condition $u_0 \in \mathrm{H}^1(\Omega)$ and periodic boundary conditions. For this, we shall proceed in three steps: at first, we prove the existence of weak solutions to the initial value problem (4.6). We then discuss the regularity of our weak solutions and finally show their uniqueness.

4.4.1. Existence

In order to prove the existence of a weak solution of Equation (4.6), we shall apply the Galerkin method. As the operator $\mathcal{L}_\varepsilon : \mathrm{H}^2(\Omega) \to \mathrm{L}^2(\Omega)$ is self-adjoint on $\mathrm{L}^2(\Omega)$, there exists an orthonormal basis $\{e_i\}_{i\in\mathbb{N}}$ of $\mathrm{L}^2(\Omega)$ consisting of eigenvectors for the linear operator $\mathcal{L}_\varepsilon$ with associated eigenvalues $\{\lambda_i\}_{i\in\mathbb{N}}$ such that

$$\mathcal{L}_\varepsilon e_i = \lambda_i e_i \quad \text{for all } i \in \mathbb{N}.$$

We look for approximate solutions $u_m(x,t)$ of Equation (4.6) under the form

$$u_m(x,t) = \sum_{i=1}^{m} u_m^i(t) e_i(x),$$

with the components u_m^i verifying

$$\begin{aligned} &\partial_t u_m^i + \lambda_i u_m^i - \big(\mathcal{N}_\varepsilon(u_m), e_i\big)_{\mathrm{L}^2(\Omega)} = 0 \\ &\big(u_m(x,0) - u_0(x), e_i\big)_{\mathrm{L}^2(\Omega)} = 0 \end{aligned} \tag{4.7}$$

for all $1 \le i \le m$. The above equations can be written as a linear system of ordinary differential equations

$$\begin{cases} \frac{\partial \mathrm{U}_m}{\partial t} = \mathrm{F}(\mathrm{U}_m), \\ \mathrm{U}_m(0) = \mathrm{U}_{m0}, \end{cases}$$

where $\mathrm{U}_m := (u_m^1, \dots, u_m^m)$ and U_{m0} is the projection of u_0 on $(e_1, \dots, e_m)$. The existence of a weak solution is based on standard existence theory for ODEs.

We shall now show that as we send m to infinity, a subsequence of the solutions u_m of the approximate problem (4.7) converges to a weak solution of (4.6). For this we will need some uniform estimates. On classicaly multiplying Equation (4.7) by $\partial_t u_m^i$ and summing over all $1 \le i \le m$, we obtain at first

$$\sum_{i=1}^{m} |\partial_t u_m^i|^2 + \partial_t\Big(\sum_{i=1}^{m} \lambda_i |u_m^i|^2\Big) - \sum_{i=1}^{m} \big(\mathcal{N}_\varepsilon(u_m), e_i\big)_{\mathrm{L}^2(\Omega)} \partial_t u_m^i = 0.$$

The summability of the second term in the equation implies that $|u_m|$ remains bounded in time and hence that our approximate solution can be extended to all time. Thus the solution we construct is global. The above equality can further be written

$$\int_\Omega |\partial_t u_m|^2 \mathrm{d}x + \frac{\mathrm{d}}{\mathrm{d}t}\Big[\|u_m\|_{\mathcal{L}_\varepsilon}^2 + \frac{1}{\varepsilon}\int_\Omega W(u_m)\mathrm{d}x\Big] = 0,$$

where the energy norm $\|\cdot\|_{\mathcal{L}_\varepsilon}$ is defined on $\mathrm{H}^1(\Omega)$ by

$$\|u\|_{\mathcal{L}_\varepsilon}^2 := \big(\mathcal{L}_\varepsilon u, u\big)_{\mathrm{L}^2(\Omega)} = \sum_{k\in\mathbb{Z}^2} (\varepsilon|k|^2 + \sigma(k))|\hat{u}(k)|^2, \quad u \in \mathrm{H}^1(\Omega).$$

Integrating the previous equation between times 0 and $t \in (0,T)$ yields the estimate

$$\begin{aligned}\int_{\Omega\times(0,t)} |\partial_t u_m(x,t)|^2 \mathrm{d}x\,\mathrm{d}t + \|u_m(t)\|_{\mathcal{L}_\varepsilon}^2 + \frac{1}{\varepsilon}\int_\Omega W(u_m(x,t))\mathrm{d}x \\ = \|u_m(0)\|_{\mathcal{L}_\varepsilon}^2 + \frac{1}{4\varepsilon}\int_\Omega W(u_m(x,0))\mathrm{d}x \qquad \text{for all } t \in (0,T).\end{aligned}$$

Note that for all $u \in \mathrm{H}^1(\Omega)$, we have $\|u\|_{\mathcal{L}_\varepsilon}^2 \le C(\varepsilon)\sum_{k\in\mathbb{Z}^2}(1+|k|^2)|\hat{u}(k)|^2 = C(\varepsilon)\|u\|_{\mathrm{H}^1(\Omega)}^2$. We now follow the argument of Alouges and Soyeur [3]: as $\mathrm{H}^1(\Omega)$ is compactly embedded into $\mathrm{L}^4(\Omega)$, we obtain that the right-hand member of the above equation is uniformly bounded. This implies that $\partial_t u_m$ and $(1-|u_m|^2)$ are bounded in $\mathrm{L}^2((0,T)\times\Omega)$. Furthermore, as for $u_m \in \mathrm{H}^1(\Omega)$, there holds $\|u_m\|_{\mathcal{L}_\varepsilon}^2 \ge \varepsilon\|u_m\|_{\dot{\mathrm{H}}^1(\Omega)} = \varepsilon\|\nabla u_m\|_{\mathrm{L}^2(\Omega)}$, we obtain as well that ∇u_m is bounded in $\mathrm{L}^2((0,T)\times\Omega)$. Thus (u_m) is bounded in $\mathrm{H}^1((0,T)\times\Omega)$. Consequently, we can extract a subsequence (u_{m_l}) such that

$$\begin{aligned}
&u_{m_l} \rightharpoonup u && \text{weakly in } \dot{\mathrm{H}}_t^1\mathrm{L}_x^2((0,T)\times\Omega)\\
&u_{m_l} \to u && \text{strongly in } \mathrm{L}_t^\infty\mathrm{L}_x^2((0,T)\times\Omega)\\
&1-|u_{m_l}|^2 \rightharpoonup 1-|u|^2 && \text{weakly in } \mathrm{L}_t^\infty\mathrm{L}_x^2((0,T)\times\Omega).
\end{aligned}$$

On passing to the limit $m\to\infty$, we find a weak solution $u \in \mathrm{L}_t^\infty\mathrm{H}_x^1 \cap \dot{\mathrm{H}}_t^1\mathrm{L}_x^2((0,\infty)\times\Omega)$ of Equation (4.6).

4.4.2. Regularity

In this section, we discuss the regularity of our weak solutions u to the problem (4.6). The latter depends on the regularity of the initial datum u_0. In that sense, we first take $u_0 \in \mathrm{H}^s(\Omega)$ with $s \ge 1$ to be precised in the following.

As in two dimensions, $\mathrm{H}^1(\Omega)$ is embedded into $\mathrm{L}^p(\Omega)$ for every $p<\infty$, we have in fact that

$$u \in \mathrm{L}_t^\infty\mathrm{L}_x^p((0,T)\times\Omega) \quad \text{for all } p<\infty.$$

Rewriting Equation (4.6) in form of a nonhomogeneous heat equation, we have indeed

$$u_t - \varepsilon\frac{\partial^2 u}{\partial x^2} = \mathcal{N}_\varepsilon(u) - \sigma(\mathrm{D})u, \quad u(x,0) = u_0(x),$$

with $u_0 \in \mathrm{H}^1(\Omega)$. Considering the right-hand side of the previous equation, as $u \in \mathrm{L}^p((0,T)\times\Omega)$, we have

$$f := \mathcal{N}_\varepsilon(u) - \sigma(\mathrm{D})u \in \mathrm{L}^p((0,T)\times\Omega). \tag{4.8}$$

The theory of parabolic equations, see e.g. [40], implies then that

$$u_t \in \mathrm{L}^p((0,T)\times\Omega) \quad \text{and} \quad \frac{\partial^2 u}{\partial x^2} \in \mathrm{L}^p((0,T)\times\Omega) \quad \text{for all } p<\infty.$$

Consequently we have in particular that

$$\sigma(\mathrm{D})u \in \mathrm{L}^2((0,T)\times\Omega), \quad \mathcal{N}_\varepsilon'(u) \in \mathrm{L}^4((0,T)\times\Omega) \quad \text{as well as} \quad u_t \in \mathrm{L}^4((0,T)\times\Omega).$$

This assertion implies finally implies that

$$f_t = \sigma(\mathrm{D})u_t + \mathcal{N}_\varepsilon'(u)u_t \in \mathrm{L}^2((0,T)\times\Omega). \tag{4.9}$$

From assertions (4.8) and (4.9) and regularity estimates, see Evans [26], we obtain in fact that for initial datum $u_0 \in \mathrm{H}^2(\Omega)$, the weak solutions u to (4.6) verify

$$u \in \mathrm{L}^\infty_t \mathrm{H}^2_x((0,T)\times\Omega).$$

Invoking a bootstrap argument, we finally infer that for initial datum $u_0 \in \mathrm{H}^s(\Omega)$ for any $s \geq 2$, we have

$$u \in \mathrm{C}^\infty((0,T)\times\Omega).$$

Hence in particular for given $T>0$, we obtain that u is uniformly bounded on $(0,T)\times\Omega$.

4.4.3. Uniqueness

In this section, we prove the uniqueness of the weak solution of our initial equation. To this end, we suppose that there exist u and v weak solutions of (4.6). Setting $w := u - v$, there holds in particular

$$(\partial_t w, w)_{\mathrm{L}^2(\Omega)} + (\mathcal{L}_\varepsilon w, w)_{\mathrm{L}^2(\Omega)} = (\mathcal{N}_\varepsilon(u) - \mathcal{N}_\varepsilon(v), w)_{\mathrm{L}^2(\Omega)}.$$

By virtue of the mean value theorem, there exists $\tilde{u} \in [u,v] := [\min(u,v), \max(u,v)]$ such that $\mathcal{N}_\varepsilon(u) - \mathcal{N}_\varepsilon(v) = \mathrm{D}\mathcal{N}_\varepsilon(\tilde{u})(u-v)$. The solutions u and v being uniformly bounded on $(0,T)\times\Omega$, cf. Section 4.4.2, there exists a positive constant $C = C(\varepsilon, c_0)$ depending on the paramter ε and the normalizing constant for the double well c_0 such that $|\mathrm{D}\mathcal{N}_\varepsilon(\tilde{u})| \leq C/2$. Consequently, we obtain from the above equation

$$\partial_t\Big(\frac{1}{2}\|w\|^2_{\mathrm{L}^2(\Omega)}\Big) + \|w\|^2_{\mathcal{L}_\varepsilon} = (\mathrm{D}\mathcal{N}_\varepsilon(\tilde{u})w, w)_{\mathrm{L}^2(\Omega)} \leq \frac{C}{2}\|w\|^2_{\mathrm{L}^2(\Omega)}.$$

Thus this yields in particular

$$\partial_t\Big(\frac{1}{2}\|w\|^2_{\mathrm{L}^2(\Omega)}\Big) \leq C\Big(\frac{1}{2}\|w\|_{\mathrm{L}^2(\Omega)}\Big).$$

As $\|w(x,0)\|^2_{\mathrm{L}^2(\Omega)} = 0$, we obtain from Gronwall's inequality that $w \equiv 0$ and hence uniqueness of the weak solution of (4.6).

5. Spectral Methods: Notation and Preliminary results

5.1. Introduction

The model we are considering is periodic and with a nonlinearity defined in Fourier space. Thus the use of a Fourier pseudospectral method is a very natural way to solve the problem numerically. In this section, we introduce a few notation as well as preliminary results concerning discrete Fourier transform and trigonometric interpolation. Some of these can be found in a more detailed manner for example in [15], [33] or [34]. In all the following, we shall base our considerations on the two-dimensional periodic domain

$$\Omega = (0,1)^2.$$

We shall further use the notation

$$(u,v) := (u,v)_{\mathrm{L}^2(\Omega)} = \int_\Omega u(x)\overline{v(x)}\,\mathrm{d}x \quad \text{for all } u,v \in \mathrm{L}^2(\Omega),$$

to denote the inner product on $\mathrm{L}^2(\Omega;\mathbb{C})$ as well as

$$\|u\| := \|u\|_{\mathrm{L}^2(\Omega)} = (u,u)^{1/2} \quad \text{for all } u \in \mathrm{L}^2(\Omega),$$

for the associated norm.

5.2. Fourier System

For $N \in \mathbb{N}_{>0}$ we first define the set

$$\mathbb{Z}_N := \Big\{ -\frac{N}{2}+1, \dots, \frac{N}{2} \Big\} \quad \text{for } N \text{ even},$$

and

$$\mathbb{Z}_N := \Big\{ -\frac{N-1}{2}, \dots, \frac{N-1}{2} \Big\} \quad \text{for } N \text{ odd}.$$

We denote its Cartesian product by $\mathbb{Z}_N^2$. Let us now consider the finite-dimensional linear subspace of $\mathrm{L}^2(\Omega;\mathbb{C})$ defined as

$$\mathrm{S}_N := \mathrm{span}_{\mathbb{C}}\big\{ x \in \Omega \mapsto \exp(2\mathrm{i}\pi\, k\cdot x) \in \mathbb{C} \,:\, k \in \mathbb{Z}_N^2 \big\}.$$

Since $\mathrm{card}(\mathbb{Z}_N) = N$, clearly $\dim_{\mathbb{C}}(\mathrm{S}_N) = N^2$. We denote by $P_N : \mathrm{L}^2(\Omega;\mathbb{C}) \to \mathrm{S}_N$ the orthogonal projection operator based on truncating the Fourier series at the $(N/2)$th (respectively $((N-1)/2)$th) term for N even (respectively N odd). Here $\mathrm{L}^2(\Omega;\mathbb{C})$ denotes

the set of all complex-valued square-integrable 1-periodic functions. We also introduce the subspace of S_N of real-valued functions

$$\mathrm{X}_N := \Big\{ x \in \Omega \mapsto \sum_{k \in \mathbb{Z}_N^2} c(k) \exp(2\mathrm{i}\pi\, k \cdot x) \in \mathrm{S}_N \,:\, c(-k) = \overline{c(k)} \Big\}$$

with $\dim_{\mathbb{R}}(\mathrm{X}_N) = N^2$. Note that in the case when N is even, the highest wave number in the sum $\sum_{k \in Z_N^2}$ is treated asymmetricaly and hence yields a complex exponential. Following [13], we fix this by defining the following 'symmetrized space' as a substitute for the space S_N in the case of N even

$$\Xi_N := \{ u \in \mathrm{S}_N \,:\, c(k) = c(l) \text{ for } k \sim l \},$$

where the equivalence relation $k \sim l$ means that k and l differ at most in the sign of the components k_j and l_j with $|k_j| = |l_j| = N/2$. Whenever the symmetrized space Ξ_N is concerned, we adopt the convention that summation is also symmetrized in the sense that terms whose indices are equal to the highest wave numbers are multiplied by appropriate powers of $\frac{1}{2}$; cf. [13] for details. In this case we also redefine the space X_N by setting

$$\mathrm{X}_N := \Big\{ x \in \Omega \mapsto \sum_{k \in \mathbb{Z}_N^2} c(k) \exp(2\mathrm{i}\pi\, k \cdot x) \in \Xi_N \,:\, c(-k) = \overline{c(k)} \Big\},$$

with the summation sign understood in the above symmetrized sense.

5.3. Discretization and Discrete Fourier Transform

For $N \in \mathbb{N}_{>0}$, we define the set

$$\mathbb{N}_N := \{1, 2, \ldots, N\}$$

and as in the previous section, we denote its Cartesian product by $\mathbb{N}_N^2$. On defining the spectral nodes

$$x_j := \frac{j}{N} \in \Omega, \quad j \in \mathbb{N}_N^2, \tag{5.1}$$

let $\Omega_N := \{x_j \,:\, j \in \mathbb{N}_N^2\} \subset \Omega$ denote the set of collocation points that will be used in our spatial discretization. The discrete Fourier coefficients of a function $u \in \mathrm{C}(\Omega; \mathbb{C})$ with respect to this set of collocation points are

$$\tilde{u}(k) = (\mathcal{F}_N u)(k) := \frac{1}{N^2} \sum_{j \in \mathbb{N}_N^2} u(x_j) \mathrm{e}^{-2\mathrm{i}\pi\, k \cdot x_j}, \quad k \in \mathbb{Z}_N^2.$$

The discrete Fourier inversion formula yields

$$u(x_j) = (\mathcal{F}_N^{-1} \tilde{u})(x_j) := \sum_{k \in \mathbb{Z}_N^2} \tilde{u}(k) \mathrm{e}^{2\mathrm{i}\pi\, k \cdot x_j}, \quad j \in \mathbb{N}_N^2.$$

Note again that for real-valued functions, in the case of N even, the above sum is understood in the aforementioned symmetrized sense. For complex-valued functions

$u, v \in \mathrm{C}(\Omega;\mathbb{C})$, we consider the discrete inner-product

$$\langle u, v\rangle_N := \left(\frac{1}{N}\right)^2 \sum_{j\in\mathbb{N}_N^2} u(x_j)\overline{v(x_j)},$$

and the associated norm $\|\cdot\|_N$ defined by

$$\|u\|_N^2 = \langle u, u\rangle_N.$$

Then for all $u, v \in \mathrm{S}_N$, we have that

$$\langle u, v\rangle_N = (u, v)_{\mathrm{L}^2(\Omega;\mathbb{C})},$$

and therefore also $\|u\|_N = \|u\| := \|u\|_{\mathrm{L}^2(\Omega;\mathbb{C})}$ for all $u \in \mathrm{S}_N$, cf. Appendix A for the proof. Note further that $\tilde{u}(k) = \langle u, \mathrm{e}^{2\mathrm{i}\pi\, k\cdot(\cdot)}\rangle_N$, and therefore on S_N, the exact Fourier coefficients defined in Section 2.2.2 and given by

$$\hat{u}(k) = \int_\Omega u(x)\mathrm{e}^{-2\mathrm{i}\pi\, k\cdot x}\mathrm{d}x$$

coincide with the discrete Fourier coefficients, i.e. there holds $\hat{u}(k) = \tilde{u}(k)$ for all $u \in \mathrm{S}_N$.

5.4. Trigonometric Interpolation

For $N \in \mathbb{N}_{>0}$ and collocation points x_j defined by (5.1), we can define the trigonometric interpolant $I_N u \in \mathrm{S}_N$, or Ξ_N respectively, of a function $u \in \mathrm{C}(\Omega;\mathbb{C})$ by

$$\langle I_N u, \psi\rangle_N = \langle u, \psi\rangle_N$$

for every $\psi \in \mathrm{S}_N$, respectively every $\psi \in \Xi_N$. The existence of a unique $I_N u$ is an immediate consequence of the Riesz representation theorem. More explicitely, we have the formula

$$I_N u(x) = \sum_{k\in\mathbb{Z}_N^2} \tilde{u}(k)\mathrm{e}^{2\mathrm{i}\pi\, k\cdot x}, \quad x \in \Omega,$$

where $\tilde{u}(k)$ are the discrete Fourier coefficients. Again, in the case of real-valued functions and N even, the formula needs to be symmetrized at the highest wave numbers according to the definition of Ξ_N; cf. [13] for details. The Fourier inversion formula presented previously implies that we have $I_N u(x_j) = u(x_j)$ for all $j \in \mathbb{N}_N^2$. In particular for the restriction to real-valued functions we have

$$u \in \mathrm{C}(\Omega;\mathbb{R}) \mapsto I_N u \in \mathrm{X}_N,$$

and I_N can be regarded as an orthogonal projection upon the space X_N with respect to the discrete inner-product $\langle\cdot,\cdot\rangle_N$. For any given $u \in \mathrm{C}(\Omega;\mathbb{C})$, the function $I_N u$ represents an approximation of u. In fact, $I_N u$ converges to u in the $\mathrm{L}^2(\Omega;\mathbb{C})$ norm, i.e.

$$\lim_{N\to\infty} \|u - I_N u\| = 0, \quad u \in \mathrm{C}(\Omega,\mathbb{C}).$$

We also define the aliasing error $R_N u := P_N u - I_N u$, which is $\mathrm{L}^2(\Omega;\mathbb{C})$-orthogonal to the truncation error $u - P_N u$ with P_N being the $\mathrm{L}^2(\Omega;\mathbb{C})$-orthogonal projection onto X_N, see [15]. Thus for $u \in \mathrm{C}(\Omega;\mathbb{C})$, there holds

$$\|u - I_N u\|^2 = \|u - P_N u\|^2 + \|R_N u\|^2;$$

hence, in the $\mathrm{L}^2(\Omega)$-norm, the error due to the truncation is always smaller than the error due to the interpolation. However, both errors decay at the same rate if the genuine solution of the differential equation is sufficiently smooth. Indeed, extending results from [13] and [14] to two dimensions, there holds the following estimates: for $u \in \mathrm{H}^s(\Omega;\mathbb{C})$, and with $\mathrm{H}^s(\Omega;\mathbb{C})$ equipped with the norm $\|\cdot\|_s$ defined by

$$\|u\|_s := \left[\sum_{k\in\mathbb{Z}^2} (1 + |k|^{2s})|\hat{u}(k)|^2\right]^{\frac{1}{2}},$$

we have, for $s \geq 1$,

$$\|u - P_N u\| \leq C N^{-s} \|u\|_s, \tag{5.2}$$

with $C = C(s)$ a positive constant depending on the parameter s. In higher Sobolev norms, the truncation error can be estimated as follows

$$\|u - P_N u\|_l \leq C N^{l-s} \|u\|_s \quad \text{for } 1 \leq l \leq s.$$

Concerning the interpolation error, the estimate

$$\|u - I_N u\| \leq C N^{-s} \|u\|_s \tag{5.3}$$

shows that the interpolation and truncation error have the same asymptotic behaviour in the $\mathrm{L}^2(\Omega;\mathbb{C})$ norm. In terms of the $\mathrm{L}^\infty(\Omega)$ norm, there holds further

$$\|u - I_N u\|_{\mathrm{L}^\infty(\Omega)} \leq C(\log N) N^{-s} \|u\|_s.$$

Finally, as for the truncation error, an estimation in the Sobolev norms yields

$$\|u - I_N u\|_l \leq C N^{l-s} \|u\|_s \quad \text{for } 1 \leq l \leq s.$$

Consequently, in terms of the aliasing error, there holds as well the estimate

$$\|R_N u\| \leq C(s) N^{-s} \|u\|_s. \tag{5.4}$$

For a better overview, all the estimates are gathered together in Table 5.1.

5.5. Discrete Fourier Integral Operators

Recall that for a function $m : \mathbb{Z}^2 \to \mathbb{C}$ the associated Fourier integral operator $m(\mathrm{D})$ is for sufficiently regular functions $u : \Omega \to \mathbb{C}$ defined by

$$m(\mathrm{D}) \,:\, u \mapsto \mathcal{F}^{-1}(m\hat{u}).$$

Table 5.1.: Estimates for the truncation, interpolation and aliasing errors for $s \geq 1$.

Error	**Estimates**
Truncation Error	$\|u - P_N u\| \leq CN^{-s}\|u\|_s$
	$\|u - P_N u\|_l \leq CN^{l-s}\|u\|_s$
Interpolation error	$\|u - I_N u\| \leq CN^{-s}\|u\|_s$
	$\|u - I_N u\|_l \leq CN^{l-s}\|u\|_s$
	$\|u - I_N u\|_{L^\infty(\Omega)} \leq C(\log N)N^{-s}\|u\|_s$
Aliasing error	$\|R_N u\| \leq CN^{-s}\|u\|_s$

Note that if m is symmetric in the aforementioned sense that $m(-k) = \overline{m(k)}$ for $k \in \mathbb{Z}^2$ and u is real-valued then $m\hat{u}$ shares this symmetry and $m(\mathrm{D})u$ is also real-valued. One of the main properties of the Fourier integral operator $m(\mathrm{D})$ is that it commutes with the $\mathrm{L}^2(\Omega;\mathbb{C})$-orthogonal projection operator P_N, i.e. there holds

$$P_N\big(m(\mathrm{D})u\big) = m(\mathrm{D})P_N u$$

for all sufficiently regular functions u. However, this is generally not the case for the interpolation operator I_N. In fact, for a generic function $u \in \mathrm{C}^\infty(\Omega,\mathbb{C})$

$$I_N\big(m(\mathrm{D})u\big) \neq m(\mathrm{D})I_N u,$$

so that an aliasing error needs to be taken into account. For $N \in \mathbb{N}_{>0}$ the corresponding discrete Fourier integral on S_N is simply the restriction of $m(\mathrm{D})$ to trigonometric polynomials in S_N. On still denoting it by $m(\mathrm{D})$, it can be expressed in terms of the discrete Fourier transform as follows:

$$m(\mathrm{D}) \,:\, u \in \mathrm{S}_N \mapsto \mathcal{F}_N^{-1}(m\tilde{u}) \in \mathrm{S}_N.$$

As in the 'continuous' case, if m is symmetric and $u \in \mathrm{X}_N$ then $(m\tilde{u})(-k) = \overline{(m\tilde{u})(k)}$ for $k \in \mathbb{Z}_N^2$, and hence $m(\mathrm{D}))u \in \mathrm{X}_N$. Since the Fourier multiplier σ is real-valued with $\sigma(k) = \sigma(-k)$, the action of the operator $\mathcal{L}_\varepsilon$ on the space X_N given by

$$\mathcal{L}_\varepsilon \,:\, u \in \mathrm{X}_N \mapsto \mathcal{L}_\varepsilon u = \mathcal{F}_N^{-1}\left[((2\pi)^2\varepsilon|\cdot|^2 + \sigma(\cdot))\tilde{u}(\cdot)\right] \in \mathrm{X}_N$$

is well-defined. Finally, we define the energy-norm $\|\cdot\|_{\mathcal{L}_\varepsilon}$ on X_N as follows:

$$\|u\|_{\mathcal{L}_\varepsilon}^2 := \langle \mathcal{L}_\varepsilon u, u\rangle_N = \langle \mathcal{L}_\varepsilon^{\frac{1}{2}} u, \mathcal{L}_\varepsilon^{\frac{1}{2}} u\rangle_N = \sum_{k\in\mathbb{Z}_N^2} \left((2\pi)^2\varepsilon|k|^2 + \sigma(k)\right)|\tilde{u}(k)|^2, \quad u \in \mathrm{X}_N.$$

5.6. Estimates for Trigonometric Polynomials

In our numerical approach to the problem, cf. Section 6.3, we shall seek for solutions of a numerical scheme in terms of real-valued trigonometric polynomials. In particular, we shall prove, under a condition on the initial energy, that these solutions are bounded in $\mathrm{H}^1(\Omega)$. However, the classical Sobolev embedding fails to ensure the uniform boundedness

of these solutions in dimension ≥ 1. We shall therefore use estimates of the $\mathrm{L}^\infty(\Omega)$ norm of elements of the space S_N in terms of either the $\mathrm{L}^2(\Omega)$ or the $\mathrm{H}^1(\Omega)$ norm. An estimation of the L^q norm of an element of S_N in terms of the L^p norm for $1 \leq p \leq q \leq \infty$ is given in the one-dimensional case in [15]. In the following lemma, we shall extend this estimate to two dimensions for the case $q = \infty$, $p = 2$.

Lemma 5.1. *Let $u \in \mathrm{S}_N$. There holds the estimate*

$$\|u\|_{\mathrm{L}^\infty(\Omega)} \leq N \|u\|_{\mathrm{L}^2(\Omega)}.$$

Proof. Let $x \in \Omega$ and $u(x) = \sum_{k \in \mathbb{Z}_N^2} a_k \mathrm{e}^{2\mathrm{i}\pi\, k \cdot x} \in \mathrm{S}_N$. Then we have

$$\|u\|_{\mathrm{L}^\infty(\Omega)} = \sup_{x \in \Omega} \Big| \sum_{k \in \mathbb{Z}_N^2} a_k \mathrm{e}^{2i\pi k \cdot x} \Big| \leq \sup_{x \in \Omega} \sum_{k \in \mathbb{Z}_N^2} |a_k| \left| \mathrm{e}^{2i\pi k \cdot x} \right| \leq \big(N^2\big)^{\frac{1}{2}} \Big(\sum_{k \in \mathbb{Z}_N^2} |a_k|^2 \Big)^{\frac{1}{2}}.$$

For a trigonometric polynomial $u \in \mathrm{S}_N$, there holds $\|u\|^2_{\mathrm{L}^2(\Omega)} = \|u\|^2_N = \sum_{k \in \mathbb{Z}_N^2} |a_k|^2$, see Appendix A. Thus, we obtain from the above inequality that

$$\|u\|_{\mathrm{L}^\infty(\Omega)} \leq N \|u\|_{\mathrm{L}^2(\Omega)}.$$

□

Under assumptions of $\mathrm{H}^1(\Omega)$ regularity of the trigonometric polynomial u, we can obtain a sharper estimate for the $\mathrm{L}^\infty(\Omega)$ norm, namely:

Lemma 5.2. *Let $u \in \mathrm{S}_N$. Then there exists a constant $C > 0$ such that, for N sufficiently large, we have*

$$\|u\|_{\mathrm{L}^\infty(\Omega)} \leq C (\log N)^{1/2} \|u\|_{\mathrm{H}^1(\Omega)}.$$

Proof. Let $u \in \mathrm{S}_N$, then

$$\|u\|_{\mathrm{L}^\infty(\Omega)} = \sup_{x \in \Omega} \Big| \sum_{k \in \mathbb{Z}_N^2} a_k \mathrm{e}^{2i\pi k \cdot x} \Big| \leq \Big(\sum_{k \in \mathbb{Z}_N^2} \frac{1}{1 + |k|^2} \Big)^{\frac{1}{2}} \Big(\sum_{k \in \mathbb{Z}^2} (1 + |k|^2) \, |a_k|^2 \Big)^{\frac{1}{2}}.$$

The last term in the right-hand side of the above equation directly yields $\|u\|_{\mathrm{H}^1(\Omega)}$. Concerning the first term, we use the following upper bound:

$$\begin{aligned} \sum_{k \in \mathbb{Z}_N^2} \frac{1}{1 + |k|^2} = 1 + \sum_{k \in \mathbb{Z}_N^2 \setminus (0,0)} \frac{1}{1 + |k|^2} &\leq 1 + \int_{-\frac{N}{2}}^{\frac{N}{2}} \int_{-\frac{N}{2}}^{\frac{N}{2}} \frac{1}{1 + x^2 + y^2} \, \mathrm{d}x \, \mathrm{d}y \\ &\leq 1 + \int_0^{2\pi} \int_0^N \frac{r}{1 + r^2} \, \mathrm{d}r \, \mathrm{d}\theta \\ &\leq C \, \log N \qquad \text{with } C > 0. \end{aligned}$$

Using this estimate in the first inequality finally yields

$$\|u\|_{\mathrm{L}^\infty(\Omega)} \leq C \, (\log N)^{1/2} \|u\|_{\mathrm{H}^1(\Omega)}.$$

□

6. Approximation by a Fourier Collocation Method

6.1. Introduction

In this chapter, we derive a numerical scheme based on a Fourier collocation method in order to approximate the solutions of the continuous problem (4.4). We prove the stability of the scheme by stating an energy inequality and then present some convergence results. This includes an existence result for the solutions of the iteration procedure, a proof of the convergence of the numerical solutions towards solutions of the initial continuous problem (4.4) as well as the derivation of a-priori error estimates. Recall that in our approach, we consider the classical double-well potential

$$W(u) = c_0(1-u^2)^2, \quad c_0 > 0.$$

Furthermore, in all the following, we shall consider the parameter $\varepsilon > 0$ to be small but fixed. We begin first with a short review on spectral methods.

6.2. Short Review on Spectral Methods

Spectral methods involve seeking the solution of a differential equation in terms of a series of known, smooth functions. They are, along with finite differences and finite elements, one of the main techniques for solving partial differential equations numerically and have become a prevailing tool in certain fields of numerical fluid dynamics where large scale calculations are needed, for example to study numerical weather predictions or ocean dynamics. They are also an interesting alternative to finite-elements and finite-differences techniques in other applications, such as heat transfer, boundary layers or compressible flows, cf. [16], and appear to be one of the best tools in terms of accuracy and memory requirements when the data defining the problem are smooth. In fact, their acuracy is very much related to the regularity of the genuine solution of the differential equation: the smoother the solution, the higher the convergence rate. In that sense, they are typically well suited to problems with smooth data and simple geometries. Finite-element methods are, on the other hand, a more efficient tool for problems displaying very complex geometries.

The main component in the formulation of a numerical method lies in the choice of the trial functions that are used to provide the approximate representation of the solution. A key feature to distinguish finite-differences and finite-elements methods from spectral methods lies in the choice of these trial functions. While finite differences and finite elements use trial functions that are defined in a local sense, spectral methods are global: the trial functions are chosen in order to form an orthogonal basis of smooth global functions. The most usual ones are for example trigonometric functions and Chebyshev

or Legendre polynomials. Spectral methods also involve the use of test functions in order to ensure that the partial differential equation and possibly the boundary conditions are satisfied as closely as possible by the truncated series expansion. This is carried out by minimzation, in a suitable norm, of the residual produced after substituting the truncated expansion into the differential equation. Practically, one wants the residual to be orthogonal to the set of chosen weight functions. In that sense, spectral methods can be considered as a special case of the method of weighted residuals, cf. [29].

Within the framework of spectral methods, one usually distinguishes three different techniques, depending on the choice of the test functions: the Tau, Galerkin and pseudospectral (or collocation) methods. For the Galerkin method, one sets the test functions to be equal to the trial functions, the latter which have furthermore to satisfy the boundary conditions of the differential equation. The approach is similar with the Tau method, but the trial functions need not to satisfy the boundary conditions. These are then enforced by an additional set of equations.
By opposition to the two aforementioned approaches, the pseudospectral method can be considered as an interpolating method. Indeed, in this case, the test functions are chosen to be Dirac delta functions centered at the so-called interpolation (or collocation) points, and at which the approximate solution has to satisfy exactly the differential equation. The boundary conditions are imposed by a new set of equations as in the Tau method. The choice of the trial functions used is very much depending on the characteristics of the differential equation. In case of periodic problems, one usually picks trigonometric functions because they show a good convergence rate for the approximated functions, the derivatives are easy to determine and finally, due to the Fast Fourier Transformation, the conversion between the expansion coefficients of the function and the value at specific nodes is fast. In the case of non periodic problems, orthogonal polynomials of Jacobi type (e.g. Chebyshev or Legendre polynomials) have proven to be the most successful, and are in fact the most commonly used.

The basic idea of spectral methods stems from Fourier analysis, but their first use to solve numerically ordinary differential equations goes back to the 1930s, with the works of Lanczos [41] and also Slater [49] or Kantorovic [37] for specific applications. Despite their many advantages, spectral methods were not used for a long time to solve partial differential equations because of their expensive cost of computational time. But their popularity raised around the 1970s thanks mainly to the Fast Fourier Transform algorithm of Cooley and Tukey [20]. Kreiss and Oliger [39] were then the first to apply collocation methods to partial differential equations. In 1977, Gottlieb and Orszag [33] published a survey summarizing the state of the art in spectral methods, tackling theoretical as well as applicational aspects. A non exhaustive list of literature on the topic includes the book of Mercier [44] which provides an elementary discussion on the mathematical aspects of spectral methods, including introductions to the theories of Fourier series and polynomial expansions. In [8], Bernardi and Maday give an introduction to the numerical analysis of spectral methods in the solution of elliptic boundary value problems. From a more applied aspect, the book of Fornberg [30] lays the emphasis on practical implementations of pseudospectral methods over a wide range of problem types including turbulence modeling, nonlinear wave equations or weather predictions. In [34], Guo presents the basic algorithms, the main theoretical results as well as applications of spectral methods. The book of Boyd [9] focuses on the application of spectral method to eigenvalue, boundary value and time-dependent problems. It provides a survey of all the necessary fundamentals for

the application of spectral methods to various disciplines of computational engineering but also delves deep into various advanced topics. The first of a two-volume monograph on spectral methods of Canuto, Hussaini, Quarteroni and Zang [15] provides a comprehensive discussion of the generic aspects of classical spectral methods in single domains, from a theoretical as well as computational aspect. The second volume [16] focuses more on applications to fluid dynamics and multidomain spectral methods. Trefethen gives in [51] an intuitive and excellent introduction to some of the fundamental ideas and techniques of spectral methods from a computational point of view.

6.3. Fully Discrete Scheme

The problem we are considering is periodic and with a nonlinearity defined in terms of a Fourier multiplier. The use of a Fourier collocation method is therefore in this case particularly convenient. One commonly admits that a reasonable numerical approximation should preserve as much as possible the features of the genuine solution of the original problem. Thus, we have formulated a fully discrete scheme using a Fourier spectral decomposition for the space variable and a modified Crank–Nicolson method for the time variable. This scheme has the important feature of inheriting the energy dissipation property of the initial continuous problem.

Given $T > 0$ and $J \in \mathbb{N}_{>0}$, let $0 = t^0 < t^1 < \cdots < t^{J-1} < t^J = T$ be a partition of $[0, T]$ with constant time step

$$\Delta t := T/J.$$

Let furthermore $\mathcal{I}_n := [t^n, t^{n+1})$ for $n \in \{0, \ldots, J-1\}$ denote the consecutive time intervals of our partition. For more simplicity, we shall use the notation $u_N^n(x_j) := u_N(t^n, x_j)$ to denote our numerical solution at time t^n.

Let us suppose that $u_0 \in \mathrm{C}(\Omega, \mathbb{R})$, and let $u_N^0 := I_N u_0$ where $N \in \mathbb{N}_{>0}$. For $n \in 0, 1, \ldots, J-1$, our numerical scheme at time iteration $n+1$ reads as follows: find $u_N^{n+1} \in \mathrm{X}_N$ such that for all $j \in \mathbb{N}_N^2 = \{1, 2, \ldots, N\}^2$

$$\frac{u_N^{n+1}(x_j) - u_N^n(x_j)}{\Delta t} + \mathcal{L}_\varepsilon \left(\frac{u_N^{n+1}(x_j) + u_N^n(x_j)}{2} \right) = I_N \mathcal{N}_\varepsilon(u_N^{n+1}(x_j), u_N^n(x_j)) \tag{6.1}$$

where in our case

$$\mathcal{N}_\varepsilon(u_N^{n+1}(x_j), u_N^n(x_j)) := \frac{c_0}{\varepsilon} \Big(1 - \frac{|u_N^{n+1}(x_j)|^2 + |u_N^n(x_j)|^2}{2} \Big) \Big(\frac{u_N^{n+1}(x_j) + u_N^n(x_j)}{2} \Big).$$

More generally, the nonlinear operator $\mathcal{N}_\varepsilon$ is in fact defined as the first-order difference quotient of the nonlinear potential $W_\varepsilon(u) = \frac{1}{\varepsilon} W(u)$ i.e.

$$\mathcal{N}_\varepsilon(u, v) := -\frac{W_\varepsilon(u) - W_\varepsilon(v)}{u - v} \quad \text{for} \quad u \neq v \tag{6.2}$$

with

$$\mathcal{N}_\varepsilon(u, u) := \mathcal{N}_\varepsilon(u) = -\mathrm{D}W_\varepsilon(u). \tag{6.3}$$

Note that this last notation matches with the definition of the nonlinear operator $\mathcal{N}_\varepsilon$ initially given in Section 4.3 and will be used throughout the rest of the manuscript.

On using the condensed notation

$$u_N^{n+1/2} = \frac{u_N^{n+1} - u_N^n}{2}, \quad n = 0, 1, \ldots, J-1,$$

our discretized problem (6.1) can be restated as follows:

$$\frac{u_N^{n+1}(x_j) - u_N^n(x_j)}{\Delta t} + \mathcal{L}_\varepsilon u_N^{n+1/2}(x_j) = I_N \mathcal{N}_\varepsilon(u_N^{n+1}(x_j), u_N^n(x_j)) \quad \text{for all } j \in \mathbb{N}_N^2.$$

Out of the sequence of functions u_N^n defined pointwise in time, we build a function continuous in time by linearly interpolating between the nodal values u_N^n and u_N^{n+1} as follows:

$$u_N(t) := u_N^{n+1} + (t - t^{n+1})\frac{u_N^{n+1} - u_N^n}{\Delta t}, \qquad t \in [t^n, t^{n+1}], \quad n = 0, \ldots, J-1. \tag{6.4}$$

With this definition, the time derivative of u_N is a function defined for a.e. $t \in (0, T)$ as

$$\partial_t u_N(t) = \frac{u_N^{n+1} - u_N^n}{\Delta t}, \qquad t \in \mathcal{I}_n = [t^n, t^{n+1}), \quad n = 0, \ldots, J-1. \tag{6.5}$$

In that sense, we shall up from now use an extended definition for the set X_N: we define it as the set of real-valued trigonometric polynomials in space that are extended piecewise affinely in time on the interval $(0, T)$ according to (6.4). Notice that $\mathrm{X}_N \subset \mathrm{X} := L^\infty((0,T); H^1(\Omega)) \cap H^1((0,T); L^2(\Omega))$, so this interpretation of the discrete solution is conforming with the continuous problem.

6.4. Discrete Energy Functional and Stability of the Numerical Scheme

Given $u \in \mathrm{X}_N$, we define the associated discrete energy functional $E_N(u)$ by

$$E_N(u) := \frac{1}{2}\langle \mathcal{L}_\varepsilon u, u\rangle_N + \frac{1}{\varepsilon}\langle 1, W(u)\rangle_N \tag{6.6}$$

as a discretized version of the energy functional E_ε associated to our gradient flow equation (4.3). As for its continuous counterpart, the discrete energy functional has the particularity of inheriting the energy dissipation property of the gradient flow. This is one of the main features of the scheme.

Lemma 6.1 (Discrete energy law)**.** *Consider the sequence $(u_N^n)_{n=0}^J \subset \mathrm{X}_N$ with $N \in \mathbb{N}_{>0}$, defined by the numerical scheme* (6.1) *with initial value $u_N^0 := I_N u_0 \in \mathrm{X}_N$, where $u_0 \in \mathrm{C}(\Omega; \mathbb{R})$. Then, considering the discretized energy functional* (6.6)*, the following discrete energy law holds:*

$$\frac{1}{\Delta t}\|u_N^{n+1} - u_N^n\|_N^2 + E_N(u_N^{n+1}) = E_N(u_N^n), \quad n = 0, 1, \ldots, J-1. \tag{6.7}$$

Proof. Multiplication of (6.1) by $u_N^{n+1} - u_n^n$ and summation over the collocation points

yields

$$\frac{1}{\Delta t}\|u_N^{n+1}-u_N^n\|_N^2+\langle\mathcal{L}_\varepsilon u_N^{n+1/2},u_N^{n+1}-u_N^n\rangle_N=\langle\mathcal{N}_\varepsilon(u_N^{n+1},u_N^n),u_N^{n+1}-u_N^n\rangle_N \tag{6.8}$$

The operator $\mathcal{L}_\varepsilon$ being self adjoint, we have in fact

$$\langle\mathcal{L}_\varepsilon u_N^{n+1/2},u_N^{n+1}-u_N^n\rangle_N=\frac{1}{2}\langle\mathcal{L}_\varepsilon u_N^{n+1},u_N^{n+1}\rangle_N-\frac{1}{2}\langle\mathcal{L}_\varepsilon u_N^n,u_N^n\rangle_N.$$

Furthermore, on developing the right-hand member of Equation (6.8), we obtain

$$\begin{aligned}\langle\mathcal{N}_\varepsilon(u_N^{n+1},u_N^n),u_N^{n+1}-u_N^n\rangle_N&=-\frac{1}{\varepsilon}\Big\langle\frac{W(u_N^{n+1})-W(u_N^n)}{u_N^{n+1}-u_N^n},u_N^{n+1}-u_N^n\Big\rangle_N\\&=\frac{1}{\varepsilon}\big[\langle 1,W(u_N^n)\rangle_N-\langle 1,W(u_N^{n+1})\rangle_N\big].\end{aligned}$$

Finally putting everything together yields the discrete energy law

$$\frac{1}{\Delta t}\|u_N^{n+1}-u_N^n\|_N^2+E_N(u_N^{n+1})=E_N(u_N^n),\quad n=0,1,\dots,J-1.$$

□

The above energy equality ensures the stability of the numerical scheme. Indeed, for given initial condition $u_0\in\mathrm{C}(\Omega;\mathbb{R})$, solutions of the Crank–Nicolson scheme (6.1) generate on long-time asymptotics local minimizers for the discrete energy E_N.

Corollary 6.2. *Considering the piecewise affine extension u_N of the numerical solution on the time interval $(0,T)$, there further holds the extended energy law*

$$\int_0^T\|\partial_t u_N(t)\|_{\mathrm{L}^2(\Omega)}^2\mathrm{d}t+E_N(u_N(T))=E_N(u_N^0). \tag{6.9}$$

Proof. Let $t\in\mathcal{I}_n=[t^n,t^{n+1})$. Recall the expression of the time derivative of u_N given in (6.5)

$$\partial_t u_N(t)=\frac{u_N^{n+1}-u_N^n}{\Delta t}\quad\text{for } t^n\le t<t^{n+1}.$$

Consequently, our energy law (6.7) can equivalently be formulated

$$\|\partial_t u_N(t)\|_{\mathrm{L}^2(\Omega)}^2+\frac{1}{\Delta t}E_N(u_N^{n+1})=\frac{1}{\Delta t}E_N(u_N^n),\quad\text{for all } n=0,1,\dots,J-1.$$

Integrating in time between t^n and t^{n+1} yields

$$\int_{t^n}^{t^{n+1}}\|\partial_t u_N(t)\|_{\mathrm{L}^2(\Omega)}^2\mathrm{d}t+E_N(u_N^{n+1})=E_N(u_N^n),\quad\text{for all } n=0,1,\dots,J-1.$$

On summing from $n=0$ to $J-1$, we finally obtain

$$\int_0^T\|\partial_t u_N(t)\|_{\mathrm{L}^2(\Omega)}^2\mathrm{d}t+E_N(u_N(T))=E_N(u_N^0).$$

□

The above formulation of the energy law will be useful in the following in order to derive a-priori bounds on the numerical solution.

6.5. Preliminary Results

Next we present some preliminary results for the numerical solution that will be used throughout this chapter.

6.5.1. A-priori Bounds on the Numerical Solution

In this section, we derive some a-priori bounds on the numerical solution under the assumption that the initial discrete energy is bounded. Let $u_N \in \mathrm{X}_N$ be a solution of the numerical scheme (6.1) on $(0,T)\times\Omega$ with initial datum $u_N^0 = I_N u_0$. We assume that

$$E_N(u_N^0) \leq M_0, \tag{6.10}$$

where M_0 denotes a positive constant independent of the gridsize N and the time step Δt. We shall now show that under this assumption, our numerical solution u_N is uniformly bounded in $\mathrm{H}^1((0,T)\times\Omega)$. For this, we shall proceed in three steps: first, we show that ∇u_N is uniformly bounded in $\mathrm{L}^2((0,T)\times\Omega)$. Then we prove that $\partial_t u_N$ and finally u_N are bounded as well in $\mathrm{L}^2((0,T)\times\Omega)$.

The bound on the initial energy combined to the energy dissipation property of Lemma 6.1 and Corollary 6.2 imply that $E_N(u_N(t)) \leq M_0$ for every $t \in (0,T)$. Hence, each separate term of the discrete energy functional is bounded. As we consider the parameter ε to be fixed, we have in particular that

$$\sum_{k\in\mathbb{Z}_N^2} |k|^2 |\tilde{u}_N(k)|^2 \leq C,$$

with $C = C(M_0,\varepsilon)$ a positive constant depending only on M_0 and ε. Thus, using Parseval's theorem for the discrete Fourier transform

$$\sum_{k\in\mathbb{Z}_N^2} |k|^2 |\tilde{u}_N(k)|^2 = \frac{1}{N^2} \sum_{j\in\mathbb{N}_N^2} |\nabla u_N(x_j)|^2 = \|\nabla u_N\|^2_{\mathrm{L}^2(\Omega)} \quad \text{for } u_N \in \mathrm{H}^1(\Omega),$$

we obtain the following inequality

$$\|\nabla u_N(t)\|^2_{\mathrm{L}^2(\Omega)} \leq C \quad \text{for all } t \in (0,T).$$

It immediately follows that ∇u_N is uniformly bounded in $\mathrm{L}^\infty((0,T);\mathrm{L}^2(\Omega))$. This implies in particular for $T < \infty$ that

$$\nabla u_N \text{ is uniformly bounded in } \mathrm{L}^2((0,T)\times\Omega). \tag{6.11}$$

From the energy law (6.9), we also directly obtain that

$$\int_0^T \|\partial_t u_N(t)\|^2_{\mathrm{L}^2(\Omega)} \mathrm{d}t \leq M_0,$$

and thus that

$$\partial_t u_N \text{ is uniformly bounded in } \mathrm{L}^2((0,T)\times\Omega). \tag{6.12}$$

We shall now show that u_N is bounded in $\mathrm{L}^2((0,T)\times\Omega)$. Proceeding similarly as before, it follows from (6.10) that

$$\langle 1, W(u_N(t))\rangle_N = \frac{1}{N^2}\sum_{j\in\mathbb{N}_N^2} W(u_N(t,x_j)) \leq C(M_0,\varepsilon) \quad \text{for all } t\in(0,T).$$

On using the fact that $(|x|^2-4)\leq(1-|x|^2)^2$ for all $x\in\mathbb{R}$, we have that

$$\frac{1}{N^2}\sum_{j\in\mathbb{N}_N^2}\big(|u_N(t,x_j)|^2-4\big) \leq \frac{1}{N^2}\sum_{j\in\mathbb{N}_N^2}(1-u_N(t,x_j)^2)^2 \quad \text{for all } t\in(0,T).$$

It follows from the two above inequalities that

$$\|u_N(t)\|^2_{\mathrm{L}^2(\Omega)} = \frac{1}{N^2}\sum_{j\in\mathbb{N}_N^2}|u_N(t,x_j)|^2 \leq C \quad \text{for all } t\in(0,T),$$

and hence that u_N is uniformly bounded in $\mathrm{L}^\infty((0,T);\mathrm{L}^2(\Omega))$. As precedently, this implies in particular for $T<\infty$ that

$$u_N \text{ is uniformly bounded in } \mathrm{L}^2((0,T)\times\Omega). \tag{6.13}$$

On gathering the bounds (6.11),(6.12) and (6.13), we directly obtain that

$$u_N \text{ is uniformly bounded in } \mathrm{H}^1((0,T)\times\Omega). \tag{6.14}$$

By virtue of the Sobolev embedding theorem, cf. Section 2.3, we have indeed that $\mathrm{H}^1((0,T)\times\Omega)$ is compactly embedded in $\mathrm{L}^p((0,T)\times\Omega)$ for all $p\leq 6$. This finally implies that

$$u_N \text{ is uniformly bounded in } \mathrm{L}^p((0,T)\times\Omega) \quad \text{for all } p\leq 6. \tag{6.15}$$

These different bounds on the numerical solution will be particularly useful in the following sections in order to prove convergence of the numerical scheme. In addition, we present here a further estimate for the numerical solution in terms of the initial discrete energy.

Lemma 6.3. *Let $u_N\in \mathrm{X}_N$ be a solution of the numerical scheme (6.1) on $(0,T)\times\Omega$ with initial datum $u_N^0 = I_N u_0$. Then there holds the estimate*

$$\|u_N^{n+1}-u_N^n\|^2_{\mathrm{L}^2(\Omega)} \leq \Delta t E_N(u_N^0) \quad \textit{for all } n=0,1,\dots J-1. \tag{6.16}$$

Proof. Let $u_N \in \mathrm{X}_N$ and $n \in \{0, 1, \ldots, J-1\}$. By definition, we have first

$$\|u_N^{n+1} - u_N^n\|_{\mathrm{L}^2(\Omega)} = \Big\| \int_{t^n}^{t^{n+1}} \partial_t u_N(t) \mathrm{d}t \Big\|_{\mathrm{L}^2(\Omega)} \leq \int_{t^n}^{t^{n+1}} \|\partial_t u_N(t)\|_{\mathrm{L}^2(\Omega)} \mathrm{d}t.$$

On applying the Cauchy–Schwarz inequality on the last term of the above inequality, we obtain

$$\|u_N^{n+1} - u_N^n\|_{\mathrm{L}^2(\Omega)} \leq (t^{n+1} - t^n)^{\frac{1}{2}} \Big(\int_{t^n}^{t^{n+1}} \|\partial_t u_N(t)\|_{\mathrm{L}^2(\Omega)} \mathrm{d}t \Big)^{\frac{1}{2}}.$$

From the energy law (6.9) of Corollary 6.2, we obtain that $\int_0^T \|\partial_t u(t)\|^2_{\mathrm{L}^2(\Omega)} \leq E_N(u_N^0)$ and hence in particular

$$\|u_N^{n+1} - u_N^n\|^2_{\mathrm{L}^2(\Omega)} \leq \Delta t E_N(u_N^0).$$

□

6.5.2. Estimates of the Nonlinearity

We shall present in this section two lemmas that provide us with estimates on the nonlinear operator $\mathcal{N}_\varepsilon$ that we shall use througout the following sections.

Lemma 6.4. *Let $u, v \in \mathrm{X}_N$, we write $u = u(t,x)$ for $(t,x) \in (0,T) \times \Omega$. Then we have*

$$|\mathcal{N}_\varepsilon(u) - \mathcal{N}_\varepsilon(v)| \leq \sup \big\{ |\mathcal{N}_\varepsilon'(z)| : z \in [\min(u,v), \max(u,v)] \big\} |u - v|,$$

where $\mathcal{N}_\varepsilon$ denotes the nonlinear operator defined in (6.2) *and* (6.3).

Proof. This is a direct consequence of the mean value theorem. □

Corollary 6.5. *On considering the parameter ε fixed and the classical double-well potential $W(u) := c_0(1-u^2)^2$, we have in fact*

$$|\mathcal{N}_\varepsilon(u) - \mathcal{N}_\varepsilon(v)| \leq C(1 + u^2 + v^2)|u - v| \quad \textit{for } u, v \in \mathrm{X}_N,$$

with $C = C(\varepsilon, c_0)$ a positive constant depending on the parameter ε and the normalization constant c_0.

We now generalize the above lemma to three variables.

Lemma 6.6. *Let u_1, u_2 and $v \in \mathrm{X}_N$. Then we have*

$$|\mathcal{N}_\varepsilon(u_1, v) - \mathcal{N}_\varepsilon(u_2, v)| \leq \frac{1}{\varepsilon} \sup_{z \in [u_1, u_2]} \Big\{ \sup_{y \in [v,z]} |\mathrm{D}^2 W(y)| \Big\} |u_1 - u_2|,$$

where, by convention, we use the notation $[u_1, u_2] := [\min(u_1, u_2), \max(u_1, u_2)]$.

Proof. Using definition (6.2), we have for $u > v$, that

$$\begin{aligned} -\frac{\partial \mathcal{N}_\varepsilon}{\partial u}(u,v) &= \frac{\frac{1}{\varepsilon}\mathrm{D}W(u) + \mathcal{N}_\varepsilon(u,v)}{u - v} \\ &= \frac{1}{\varepsilon} \frac{1}{(u-v)^2} \int_v^u \big(\mathrm{D}W(u) - \mathrm{D}W(z) \big) \mathrm{d}z \\ &= \frac{1}{\varepsilon} \frac{1}{(u-v)^2} \int_v^u \int_z^u \mathrm{D}^2 W(y) \mathrm{d}y \, \mathrm{d}z, \end{aligned}$$

and similarly for $u < v$. Thus

$$\left|\frac{\partial \mathcal{N}_\varepsilon}{\partial u}(u,v)\right| \leq \frac{1}{\varepsilon}\sup\{|\mathrm{D}^2 W(y)| : y \in [\min(u,v), \max(u,v)]\}.$$

Now, by the mean value theorem,

$$|\mathcal{N}_\varepsilon(u_1,v) - \mathcal{N}_\varepsilon(u_2,v)| \leq \sup\left\{\left|\frac{\partial \mathcal{N}_\varepsilon}{\partial u}(z,v)\right| : z \in [\min(u_1,u_2), \max(u_1,u_2)]\right\}|u_1 - u_2|$$

for all u_1, $u_2 \in \mathrm{X}_N$. Putting the two above inequalities together, we finally obtain

$$|\mathcal{N}_\varepsilon(u_1,v) - \mathcal{N}_\varepsilon(u_2,v)| \leq \frac{1}{\varepsilon}\sup_{z\in[u_1,u_2]}\Big\{\sup_{y\in[v,z]}|\mathrm{D}^2 W(y)|\Big\}|u_1 - u_2| \quad \text{for all } u_1, u_2 \in \mathrm{X}_N.$$

□

Corollary 6.7. *As for Corollary 6.5, considering the parameter ε fixed and the double well $W(u) := c_0(1-u^2)^2$, we have*

$$|\mathcal{N}_\varepsilon(u_1,v) - \mathcal{N}_\varepsilon(u_2,v)| \leq C(1 + u_1^2 + u_2^2 + v^2)|u_1 - u_2| \quad \textit{for all } u_1, u_2 \textit{ and } v \in \mathrm{X}_N.$$

6.6. Residual

In this section, we compute the residual obtained after substituting our numerical solution into the intial continuous model and then derive an $\mathrm{H}^{-1}(\Omega)$ bound on it.

6.6.1. Computation of the Residual

Let $u_N \in \mathrm{X}_N$ be a solution of the numerical scheme (6.1) on $(0,T)\times\Omega$ with initial datum $u_N^0 = I_n u_0$. We define the trigonometric polynomial f_N on $(0,T)\times\Omega$ by

$$f_N(t^n,x) := \partial_t u_N^n(x) + \mathcal{L}_\varepsilon u_N^{n+1/2}(x) - I_N\mathcal{N}_\varepsilon(u_N^n(x), u_N^{n+1}(x))$$

for all $n = 0,1,\ldots,J-1$ and all $x \in \Omega$. As $f_N(t^n,\cdot) \in \mathrm{X}_N$, we have in fact

$$\|f_N(t^n,\cdot)\|_{\mathrm{L}^2(\Omega)} = \|f_N(t^n,\cdot)\|_N \quad \text{for all } n = 0,1,\ldots,J-1.$$

Furthermore, as u_N is a solution of the numerical scheme (6.1), there holds indeed for all $n = 0,1,\ldots,J-1$,

$$f_N(t^n,x_j) = 0 \quad \text{for all } j \in \mathbb{N}_N^2,$$

so that $\|f_N(t^n,\cdot)\|_N^2 = \sum_{j\in\mathbb{N}_N^2} f_N^2(t^n,x_j)/N^2 = 0$ and thus $\|f_N(t^n,\cdot)\|_{\mathrm{L}^2(\Omega)} = 0$. This then implies that

$$f_N(t^n,x) = 0 \quad \text{for all } x \in \Omega \text{ and all } n = 0,1,\ldots,J-1.$$

Consequently, u_N is in fact a solution of the numerical scheme (6.1) not only at the collocation points x_j, but on the whole domain Ω i.e., there holds

$$\partial_t u_N^n(x) + \mathcal{L}_\varepsilon u_N^{n+1/2}(x) - I_N\mathcal{N}_\varepsilon(u_N^n(x), u_N^{n+1}(x)) = 0, \tag{6.17}$$

for all $x \in \Omega$ and all $n = 0, 1, \ldots, J-1$.

Let now $t \in \mathcal{I}_n = [t^n, t^{n+1})$ be fixed. On substituting the solution u_N of the discrete problem into the initial nonlinear equation (4.4), we have

$$\partial_t u_N(t,x) + \mathcal{L}_\varepsilon u_N(t,x) - \mathcal{N}_\varepsilon(u(t,x)) = \partial_t u_N(t^n,x) + \mathcal{L}_\varepsilon u_N(t,x) - \mathcal{N}_\varepsilon(u_N(t,x))$$

for all $x \in \Omega$. On substracting Equation (6.17) to the right-hand member of the above equality, we obtain

$$\begin{aligned}\partial_t u_N(t,x) + \mathcal{L}_\varepsilon u_N(t,x) - \mathcal{N}_\varepsilon(u_N(t,x)) \\ = \mathcal{L}_\varepsilon\big(u_N(t,x) - u_N^{n+1/2}(x)\big) - \big(\mathcal{N}_\varepsilon(u_N(t,x)) - I_N\mathcal{N}_\varepsilon(u_N^n(x), u_N^{n+1}(x))\big),\end{aligned}$$

for all $x \in \Omega$. Based on this equation, we define the residual R at time $t \in \mathcal{I}_n$ and $x \in \Omega$ by

$$\mathrm{R}(t,x) := \mathcal{L}_\varepsilon\big(u_N(t,x) - u_N^{n+1/2}(x)\big) - \big(\mathcal{N}_\varepsilon(u_N(t,x)) - I_N\mathcal{N}_\varepsilon(u_N^n(x), u_N^{n+1}(x))\big). \quad (6.18)$$

The residual denotes the amount by which the approximate solution u_N misses being an exact solution of the continuous initial equation (4.4).

6.6.2. H^{-1} Bound on the Residual

Let $t \in \mathcal{I}_N$ be fixed and $\phi \in \mathrm{H}^1(\Omega)$. Recall that for a solution $u_N \in \mathrm{X}_N$ of the numerical scheme (6.1), we have

$$(\mathrm{R},\phi)_{\mathrm{L}^2(\Omega)} = \big(\mathcal{L}_\varepsilon(u_N(t) - u_N^{n+1/2}), \phi\big)_{\mathrm{L}^2(\Omega)} - \big(\mathcal{N}_\varepsilon(u_N(t) - I_N\mathcal{N}_\varepsilon(u_N^n, u_N^{n+1}), \phi\big)_{\mathrm{L}^2(\Omega)}. \quad (6.19)$$

We shall now look for estimates of the right-hand members of the above equation. In that purpose, we shall need the following $\mathrm{L}^2(\Omega)$ estimate for the linear operator $\mathcal{L}_\varepsilon$.

Lemma 6.8. *Let $u \in \mathrm{H}^1(\Omega)$. Then we have*

$$\|\mathcal{L}_\varepsilon^{1/2} u\|^2_{\mathrm{L}^2(\Omega)} \leq C\|u\|^2_{\mathrm{H}^1(\Omega)},$$

where $C = C(\varepsilon)$ denotes a positive constant depending on the parameter ε and where we set by convention $\|\mathcal{L}_\varepsilon^{1/2} u\|^2_{\mathrm{L}^2(\Omega)} := \|u\|^2_{\mathcal{L}_\varepsilon} = \sum_{k\in\mathbb{Z}^2_N}((2\pi)^2\varepsilon|k|^2 + \sigma(k))|\tilde{u}(k)|^2$.

Proof. Let $u \in \mathrm{H}^1(\Omega)$. We have

$$\|\mathcal{L}_\varepsilon^{1/2} u\|^2_{\mathrm{L}^2(\Omega)} \leq \max((2\pi)^2\varepsilon, 1) \sum_{k\in\mathbb{Z}^2_N} (1+|k|^2)|\tilde{u}(k)|^2 \leq C(\varepsilon)\|u\|_{\mathrm{H}^1(\Omega)}.$$

□

As a first step, we consider the first term of the right-hand side of (6.19). By virtue of the Cauchy–Schwarz inequality, there holds

$$\big|\big(\mathcal{L}_\varepsilon(u_N(t) - u_N^{n+1/2}), \phi\big)_{\mathrm{L}^2(\Omega)}\big| \leq \big\|\mathcal{L}_\varepsilon^{1/2}(u_N(t) - u_N^{n+1/2})\big\|_{\mathrm{L}^2(\Omega)} \big\|\mathcal{L}_\varepsilon^{1/2}\phi\big\|_{\mathrm{L}^2(\Omega)}.$$

On using the previously derived estimate of Lemma 6.8, we obtain

$$\left|\left(\mathcal{L}_\varepsilon(u_N(t)-u_N^{n+1/2}),\phi\right)_{\mathrm{L}^2(\Omega)}\right| \leq C\|u_N(t)-u_N^{n+1/2}\|_{\mathrm{H}^1(\Omega)}\|\phi\|_{\mathrm{H}^1(\Omega)}.$$

The numerical solution u_N being piecewise affine in time according to extension (6.4), we have indeed that

$$|u_N(t)-u_N^n| = |u_N^{n+1}-u_N^n+(t-t^{n+1})\partial_t u_N^n| \leq |u_N^{n+1}-u_N^n|,$$

as well as

$$|u_N(t)-u_N^{n+1}| = |(t-t^{n+1})\partial_t u_N^n| \leq |u_N^{n+1}-u_N^n|.$$

Thus, there holds

$$\|u_N(t)-u_N^{n+1/2}\|_{\mathrm{H}^1(\Omega)} \leq C[\|u_N^{n+1}\|_{\mathrm{H}^1(\Omega)}+\|u_N^n\|_{\mathrm{H}^1(\Omega)}].$$

Finally, we obtain the following estimate

$$\left|\left(\mathcal{L}_\varepsilon(u_N(t)-u_N^{n+1/2}),\phi\right)_{\mathrm{L}^2(\Omega)}\right| \leq C[\|u_N^{n+1}\|_{\mathrm{H}^1(\Omega)}+\|u_N^n\|_{\mathrm{H}^1(\Omega)}]\|\phi\|_{\mathrm{H}^1(\Omega)}. \tag{6.20}$$

We shall now estimate the second term of the right-hand member of (6.19). Due to the treatment of the nonlinearity, the computation is not as straightforward as previously. We first decompose the considered quantity into four contributions

$$\begin{aligned}
&\left(\mathcal{N}_\varepsilon(u_N(t))-I_N\mathcal{N}_\varepsilon(u_N^n,u_N^{n+1}),\phi\right)_{\mathrm{L}^2(\Omega)} = \\
&\quad\left(\mathcal{N}_\varepsilon(u_N(t))-P_N\mathcal{N}_\varepsilon(u_N(t)),\phi\right)_{\mathrm{L}^2(\Omega)}+\left(P_N[\mathcal{N}_\varepsilon(u_N(t))-\mathcal{N}_\varepsilon(u_N^n)],\phi\right)_{\mathrm{L}^2(\Omega)} \\
&+\left(P_N[\mathcal{N}_\varepsilon(u_N^n)-\mathcal{N}_\varepsilon(u_N^n,u_N^{n+1})],\phi\right)_{\mathrm{L}^2(\Omega)}+\left((P_N-I_N)\mathcal{N}_\varepsilon(u_N^n,u_N^{n+1}),\phi\right)_{\mathrm{L}^2(\Omega)}
\end{aligned} \tag{6.21}$$

that we will each estimate separately. On considering the first contribution, we have

$$\left|\left(\mathcal{N}_\varepsilon(u_N(t))-P_N\mathcal{N}_\varepsilon(u_N(t)),\phi\right)_{\mathrm{L}^2(\Omega)}\right| \leq \|\mathcal{N}_\varepsilon(u_N(t))\|_{L^2(\Omega)}\|\phi-P_N\phi\|_{L^2(\Omega)}.$$

As $\phi\in\mathrm{H}^1(\Omega)$, on applying estimate (5.2), there holds on the one hand

$$\|\phi-P_N\phi\|_{\mathrm{L}^2(\Omega)} \leq \frac{C}{N}\|\phi\|_{\mathrm{H}^1(\Omega)}.$$

On the other hand, we have

$$\|\mathcal{N}_\varepsilon(u_N(t))\|_{\mathrm{L}^2(\Omega)} = \frac{c_0}{\varepsilon}\|u_N(t)(1-u_N^2(t))\|_{\mathrm{L}^2(\Omega)} \leq C(\varepsilon,c_0)\|u_N(t)\|_{\mathrm{L}^\infty(\Omega)}\|1-u_N^2(t)\|_{\mathrm{L}^2(\Omega)}.$$

Lemma 5.2 yields an estimate of the $\mathrm{L}^\infty(\Omega)$ norm of u_N in terms of the $\mathrm{H}^1(\Omega)$ norm, namely

$$\|u_N\|^2_{\mathrm{L}^\infty(\Omega)} \leq C\log(N)\|u_N\|^2_{\mathrm{H}^1(\Omega)}.$$

Considering the second term in the right-hand member of the previous inequality, we have

$$\|1-u_N^2(t)\|^2_{\mathrm{L}^2(\Omega)} \leq C(\varepsilon)E_N(u_N(t)) \leq CE_N(u_N^0),$$

so that finally, we obtain the following estimate

$$\big|\big(\mathcal{N}_\varepsilon(u_N(t)) - P_N\mathcal{N}_\varepsilon(u_N(t)), \phi\big)_{\mathrm{L}^2(\Omega)}\big| \leq C\,\frac{(\log N)^{1/2}}{N}(E_N(u_N^0))^{1/2}\|u\|_{\mathrm{H}^1(\Omega)}\|\phi\|_{\mathrm{H}^1(\Omega)}. \tag{6.22}$$

with $C > 0$ a constant depending on the parameter ε and the normalization constant c_0.

We now consider the second contribution in equation (6.21) and proceed similarly as before. Since trivially $\|P_N\phi\|_{\mathrm{L}^2(\Omega)} \leq \|\phi\|_{\mathrm{L}^2(\Omega)}$, we have in fact that

$$\begin{aligned}\big|\big(P_N[\mathcal{N}_\varepsilon(u_N(t)) - \mathcal{N}_\varepsilon(u_N^n)], \phi\big)_{\mathrm{L}^2(\Omega)}\big| &= \big|\big(\mathcal{N}_\varepsilon(u_N(t)) - \mathcal{N}_\varepsilon(u_N^n), P_N\phi\big)_{\mathrm{L}^2(\Omega)}\big| \\ &\leq C\|\mathcal{N}_\varepsilon(u_N(t)) - \mathcal{N}_\varepsilon(u_N^n)\|_{\mathrm{L}^2(\Omega)}\|\phi\|_{\mathrm{H}^1(\Omega)}.\end{aligned}$$

Corollary 6.7 yields the estimate

$$\|\mathcal{N}_\varepsilon(u_N(t)) - \mathcal{N}_\varepsilon(u_N^n)\|_{\mathrm{L}^2(\Omega)} \leq C\big(1 + \|u_N(t)\|^2_{\mathrm{L}^\infty(\Omega)} + \|u_N^n\|^2_{\mathrm{L}^\infty(\Omega)}\big)\|u_N(t) - u_N^n\|_{\mathrm{L}^2(\Omega)}.$$

On using the estimates of Lemma 5.2 and Lemma 6.3, we obtain

$$\|\mathcal{N}_\varepsilon(u_N(t)) - \mathcal{N}_\varepsilon(u_N^n)\|_{\mathrm{L}^2(\Omega)} \leq C(\Delta t)^{1/2}(\log N)E_N(u_N^0)\big(\|u_N(t)\|^2_{\mathrm{H}^1(\Omega)} + \|u_N^n\|^2_{\mathrm{H}^1(\Omega)}\big).$$

Consequently, there finally holds

$$\begin{aligned}&\big|\big(P_N[\mathcal{N}_\varepsilon(u_N(t)) - \mathcal{N}_\varepsilon(u_N^n)], \phi\big)_{\mathrm{L}^2(\Omega)}\big| \\ &\qquad \leq C(\Delta t)^{1/2}(\log N)(E_N(u_N^0))^{1/2}(\|u_N(t)\|^2_{\mathrm{H}^1(\Omega)} + \|u_N^n\|^2_{\mathrm{H}^1(\Omega)})\|\phi\|_{\mathrm{H}^1(\Omega)}.\end{aligned} \tag{6.23}$$

The procedure is exactly identical for the third term of the right-hand member of (6.21) and yields the estimate

$$\begin{aligned}&\big|\big(P_N[\mathcal{N}_\varepsilon(u_N^n) - \mathcal{N}_\varepsilon(u_N^n, u_N^{n+1})], \phi\big)_{\mathrm{L}^2(\Omega)}\big| \\ &\qquad \leq C(\Delta t)^{1/2}(\log N)(E_N(u_N^0))^{1/2}(\|u_N^{n+1}\|^2_{\mathrm{H}^1(\Omega)} - \|u_N^n\|^2_{\mathrm{H}^1(\Omega)})\|\phi\|_{\mathrm{H}^1(\Omega)}.\end{aligned} \tag{6.24}$$

Concerning the last contribution in (6.21), we have

$$\big|\big((P_N - I_N)\mathcal{N}_\varepsilon(u_N^n, u_N^{n+1}), \phi\big)_{\mathrm{L}^2(\Omega)}\big| \leq \|\mathcal{N}_\varepsilon(u_N^n, u_N^{n+1})\|_{\mathrm{L}^2(\Omega)}\|(I_N - P_N)\phi\|_{\mathrm{L}^2(\Omega)}.$$

The operator $R_N = I_N - P_N$ has been defined in Section 5.4 as the aliasing error. Using the estimate (5.4), we have in fact that

$$\|R_N\phi\|_{\mathrm{L}^2(\Omega)} \leq \frac{C}{N}\|\phi\|_{\mathrm{H}^1(\Omega)} \quad \text{for all } \phi \in \mathrm{H}^1(\Omega).$$

Consequently, this implies that

$$\big|\big((P_N - I_N)\mathcal{N}_\varepsilon(u_N^n, u_N^{n+1}), \phi\big)_{\mathrm{L}^2(\Omega)}\big| \leq \frac{C}{N}\|\mathcal{N}_\varepsilon(u_N^n, u_N^{n+1})\|_{\mathrm{L}^2(\Omega)}\|\phi\|_{\mathrm{H}^1(\Omega)}.$$

It now remains to derive an estimate for $\|\mathcal{N}_\varepsilon(u_N^n, u_N^{n+1})\|_{\mathrm{L}^2(\Omega)}$. On decomposing the

quantity as

$$\mathcal{N}_\varepsilon(u_N^n, u_N^{n+1}) = \mathcal{N}_\varepsilon(u_N^n, u_N^{n+1}) - \mathcal{N}_\varepsilon(u_N^n, u_N^n) + \mathcal{N}_\varepsilon(u_N^n, u_N^n),$$

and applying the triangle inequality, there holds

$$\|\mathcal{N}_\varepsilon(u_N^n, u_N^{n+1})\|_{\mathrm{L}^2(\Omega)} \le C\|\mathcal{N}_\varepsilon(u_N^n, u_N^{n+1}) - \mathcal{N}_\varepsilon(u_N^n, u_N^n)\|_{\mathrm{L}^2(\Omega)} + \|\mathcal{N}_\varepsilon(u_N^n)\|_{\mathrm{L}^2(\Omega)}.$$

Quantities similar to the contributions in the right-hand side of the above inequality have already been estimated previously. On using the corresponding estimates, we finally obtain

$$\begin{aligned}
&\big|\big((P_N - I_N)\mathcal{N}_\varepsilon(u_N^n, u_N^{n+1}), \phi\big)_{\mathrm{L}^2(\Omega)}\big| \\
&\quad \le C(E_N(u_N^0))^{1/2}\Big((\Delta t)^{1/2}\frac{\log(N)}{N}(\|u_N^{n+1}\|_{\mathrm{H}^1(\Omega)}^2 + \|u_N^n\|_{\mathrm{H}^1(\Omega)}^2) \\
&\qquad\qquad + \frac{\log(N)^{1/2}}{N}\|u_N^n\|_{\mathrm{H}^1(\Omega)}\Big)\|\phi\|_{\mathrm{H}^1(\Omega)}.
\end{aligned} \tag{6.25}$$

On now merging the estimates (6.22), (6.23),(6.24) and (6.25) together, we obtain the following estimate

$$\begin{aligned}
&\big|\big(\mathcal{N}_\varepsilon(u_N(t)) - I_N\mathcal{N}_\varepsilon(u_N^n, u_N^{n+1}), \phi\big)_{\mathrm{L}^2(\Omega)}\big| \\
&\qquad \le C(E_N(u_N^0))^{1/2}\Big[\frac{\log(N)^{1/2}}{N}(\|u_N(t)\|_{\mathrm{H}^1(\Omega)} + \|u_N^n\|_{\mathrm{H}^1(\Omega)}) \\
&\qquad\quad + (\Delta t)^{1/2}\log(N)(\|u_N(t)\|_{\mathrm{H}^1(\Omega)}^2 + \|u_N^n\|_{\mathrm{H}^1(\Omega)}^2 + \|u_N^{n+1}\|_{\mathrm{H}^1(\Omega)}^2) \\
&\qquad\quad + (\Delta t)^{1/2}\frac{\log(N)}{N}(\|u_N^n\|_{\mathrm{H}^1(\Omega)}^2 + \|u_N^{n+1}\|_{\mathrm{H}^1(\Omega)}^2)\Big]\|\phi\|_{\mathrm{H}^1(\Omega)}.
\end{aligned} \tag{6.26}$$

As we have shown in Section 6.5.1, assuming that the initial discrete energy $E_N(u_N^0)$ is bounded, cf. (6.10), implies the uniform boundedness of the numerical solution u_N in $\mathrm{H}^1(\Omega)$, and hence yields simplified estimates for (6.20) and (6.26), namely

$$\big|\big(\mathcal{L}_\varepsilon(u_N(t) - u_N^{n+1/2}), \phi\big)_{\mathrm{L}^2(\Omega)}\big| \le C\|\phi\|_{\mathrm{H}^1(\Omega)},$$

and

$$\big|\big(\mathcal{N}_\varepsilon(u_N(t)) - I_N\mathcal{N}_\varepsilon(u_N^n, u_N^{n+1}), \phi\big)_{\mathrm{L}^2(\Omega)}\big| \le C\Big(\frac{\log(N)^{1/2}}{N} + (\Delta t)^{1/2}\log(N)\Big)\|\phi\|_{\mathrm{H}^1(\Omega)}.$$

Finally, under Assumption (6.10), we obtain the following estimate for the residual

$$|(\mathrm{R}, \phi)_{\mathrm{L}^2(\Omega)}| \le C\Big(\frac{\log(N)^{1/2}}{N} + (\Delta t)^{1/2}\log(N)\Big)\|\phi\|_{\mathrm{H}^1(\Omega)} \quad \text{for all } \phi \in \mathrm{H}^1(\Omega). \tag{6.27}$$

Our aim in this section though is to derive a uniform bound for the $\mathrm{H}^{-1}(\Omega)$ norm of the residual. By definition, we have

$$\|\mathrm{R}\|_{\mathrm{H}^{-1}(\Omega)} := \sup\{(\mathrm{R}, \phi)_{\mathrm{L}^2(\Omega)} : \|\phi\|_{\mathrm{H}^1(\Omega)} \le 1\}.$$

Hence we get from Equation (6.27) the following $\mathrm{H}^{-1}(\Omega)$ estimate for the residual

$$\|\mathrm{R}\|_{\mathrm{H}^{-1}(\Omega)} \leq C\Big(\frac{\log(N)^{1/2}}{N} + (\Delta t)^{1/2}\log(N)\Big).$$

The above inequality is indeed verified at every time $t \in (0,T)$. Thus there holds the uniform bound

$$\sup_{t\in(0,T)} \|\mathrm{R}(t)\|_{\mathrm{H}^{-1}(\Omega)} \leq C\Big(\frac{\log(N)^{1/2}}{N} + (\Delta t)^{1/2}\log(N)\Big). \tag{6.28}$$

Note that this estimate only holds under the assumption that the initial discrete energy is a bounded quantity.

6.7. Existence and Uniqueness of the Numerical Solutions

We present in this section an existence theorem for the solutions $(u_N^n)_{n=0}^J$ of the numerical scheme. More precisely, we shall show, using a fixed point argument, that, for each $n \in \{0,1,\ldots,J-1\}$ and $u_N^n \in \mathrm{X}_N$ given, there exists a unique solution $u_N^{n+1} \in \mathrm{X}_N$ to (6.1). On writing $u = u_N^{n+1}$ and $v = u_N^n$, Equation (6.1) can be rewritten in the following equivalent form: given $v \in \mathrm{X}_N$, find $u \in \mathrm{X}_N$ such that

$$\langle u,\phi\rangle_N + \frac{\Delta t}{2}\langle u, \mathcal{L}_\varepsilon\phi\rangle_N = \langle v,\phi\rangle_N - \frac{\Delta t}{2}\langle v,\mathcal{L}_\varepsilon\phi\rangle_N + \Delta t\langle \mathcal{N}_\varepsilon(u,v),\phi\rangle_N \tag{6.29}$$

for all $\phi \in \mathrm{X}_N$. On defining the adapted inner product

$$\langle u,v\rangle_{\Delta t} := \langle u,v\rangle_N + \frac{\Delta t}{2}\langle \mathcal{L}_\varepsilon u, v\rangle_N$$

with associated time-increment dependent norm

$$\|v\|_{\Delta t}^2 := \langle v,v\rangle_{\Delta t} = \|v\|_N^2 + \frac{\Delta t}{2}\|v\|_{\mathcal{L}_\varepsilon}^2,$$

Equation (6.29) can conveniently be written as follows:

$$\langle u,\phi\rangle_{\Delta t} = \langle v,\phi\rangle_{\Delta t} + \langle \mathcal{N}_\varepsilon(u,v) - \mathcal{L}_\varepsilon v,\phi\rangle_N \quad \text{for all } \phi \in \mathrm{X}_N. \tag{6.30}$$

Note that the inner-product $\langle\cdot,\cdot\rangle_{\Delta t} = \langle\cdot,\cdot\rangle_{\Delta t,\varepsilon}$ depends on the parameter ε too, but we shall drop this dependence in the notation for more simplicity. Motivated by the form of the previous equation, we define, for a given $v \in \mathrm{X}_N$, the mapping $T_v : \mathrm{X}_N \mapsto \mathrm{X}_N$ such that for $u \in \mathrm{X}_N$, $U = T_v u$ satisfies

$$\langle U,\phi\rangle_{\Delta t} = \langle v,\phi\rangle_{\Delta t} + \langle \mathcal{N}_\varepsilon(u,v) - \mathcal{L}_\varepsilon v,\phi\rangle_N \quad \text{for all } \phi \in \mathrm{X}_N. \tag{6.31}$$

By virtue of the Riesz representation theorem, the operator T_v is well defined. The task of showing the existence of a unique $u_N^{n+1} \in \mathrm{X}_N$, given $u_N^n \in \mathrm{X}_N$, is then equivalent to showing the existence of a unique fixed point u of T_v for $v := u_N^n$ given, and then defining $u_N^{n+1} := u$.

In order to prove existence and uniqueness of the numerical solution we shall proceed

in two steps: considering $v \in \mathrm{X}_N$ to be fixed, we first show that the mapping T_v maps a specific ball centered in v into itself. Then we show that under some appropriate rate conditions between the time step Δt and the gridsize N, this mapping is contractive. Based on these two statements and invoking finally a fixed point argument, we infer the existence and uniqueness result.

Bound on $T_v v - v$

Lemma 6.9. *Let $v \in \mathrm{X}_N$. There exists a constant $C > 0$ such that*

$$\|T_v v - v\|_{\Delta t}^2 \leq C\big((\Delta t)^2 N^2 (E_N(v))^2 + \Delta t E_N(v)\big).$$

Corollary 6.10. *Suppose $E_N(v) < \infty$. Then there exists a constant $\alpha > 0$ such that if $\Delta t N < \alpha$, there holds*

$$\|T_v v - v\|_{\Delta t} \leq \frac{1}{4}.$$

Proof. Let $v \in \mathrm{X}_N$. On setting $u = v$ (and hence $U = T_v v$) and $\phi = T_v v - v$ in equation (6.31), we obtain

$$\langle T_v v, T_v v - v\rangle_{\Delta t} = \langle v, T_v v - v\rangle_{\Delta t} + \Delta t \langle \mathcal{N}_\varepsilon(v) - \mathcal{L}_\varepsilon v, T_v v - v\rangle_N,$$

and hence

$$\|T_v v - v\|_{\Delta t}^2 = \Delta t \langle \mathcal{N}_\varepsilon(v) - \mathcal{L}_\varepsilon v, T_v v - v\rangle_N.$$

On separating the terms appearing on the right-hand side of the above equation, there holds in particular

$$\|T_v v - v\|_{\Delta t}^2 \leq \Delta t |\langle \mathcal{N}_\varepsilon(v), T_v v - v\rangle_N| + \Delta t |\langle \mathcal{L}_\varepsilon v, T_v v - v\rangle_N|.$$

By virtue of Young's inequality, there further holds

$$|\langle \mathcal{N}_\varepsilon(v), T_v v - v\rangle_N| \leq \frac{1}{2\Delta t}\|T_v v - v\|_N^2 + \frac{\Delta t}{2}\|\mathcal{N}_\varepsilon(v)\|_N^2,$$

as well as

$$|\langle \mathcal{L}_\varepsilon v, T_v v - v\rangle_N| \leq \frac{1}{4}\|T_v v - v\|_{\mathcal{L}_\varepsilon}^2 + \|v\|_{\mathcal{L}_\varepsilon}^2,$$

so that, on merging both estimates together, we obtain

$$\|T_v v - v\|_{\Delta t}^2 \leq (\Delta t)^2 \|\mathcal{N}_\varepsilon(v)\|_N^2 + 2\Delta t \|v\|_{\mathcal{L}_\varepsilon}.$$

The second term of the right-hand side of the above inequality can be estimated by the associated discrete energy. Indeed, there holds trivially

$$\|v\|_{\mathcal{L}_\varepsilon} \leq C E_N(v).$$

Concerning the first term, we have

$$\|\mathcal{N}_\varepsilon(v)\|_N^2 = \frac{c_0^2}{\varepsilon^2}\frac{1}{N^2}\sum_{j \in \mathbb{N}_N^2} v^2(x_j)(1 - v^2(x_j))^2 \leq C(\varepsilon, c_0)\|v\|_{\mathrm{L}^\infty(\Omega)}^2 E_N(v).$$

On using the estimate of Lemma 5.1, we obtain further

$$\|\mathcal{N}_\varepsilon(v)\|_N^2 \leq CN^2\|v\|_{\mathrm{L}^2(\Omega)}^2 E_N(v).$$

The term $\|v\|_{\mathrm{L}^2(\Omega)}^2$ can also easily be bounded by the discrete energy. Indeed, by virtue of Parseval's theorem, we have

$$\|v\|_{\mathrm{L}^2(\Omega)}^2 = \sum_{k\in\mathbb{Z}_N^2} |\hat{v}(k)|^2 \leq CE_N(v),$$

so that finally we obtain the bound on $T_v v - v$

$$\|T_v v - v\|_{\Delta t}^2 \leq C\big((\Delta t)^2 N^2 (E_N(v))^2 + \Delta t E_N(v)\big).$$

On taking $\Delta t \lesssim 1/N$ with N sufficiently large, we obtain the result of the corollary. □

Bound on $T_v u - T_v v$

Lemma 6.11. *Let $v \in \mathrm{X}_N$. For all $u \in \mathrm{X}_N$, we have*

$$\|T_v u - T_v v\|_{\Delta t} \leq C\Delta t\big(1 + N^2\|u - v\|_{\Delta t}^2 + N^2 E_N(v)\big)\|u - v\|_{\Delta t}.$$

Corollary 6.12. *Suppose $E_N(v) < \infty$. Then there exists a constant $\beta_1 > 0$ such that if $\Delta t N^2 < \beta_1$, then there holds*

$$\|T_v u - T_v v\|_{\Delta t} \leq \frac{1}{4} + \frac{1}{4}\|u - v\|_{\Delta t}^3 + \frac{1}{4}\|u - v\|_{\Delta t} \quad \textit{for all } u \in \mathrm{X}_N.$$

Proof. Let $v \in \mathrm{X}_N$. By Young's inequality, setting $\phi = U - U'$ and substracting the identities (6.31) obtained respectively for $U = T_v u$ and $U' = T_v v$ yields

$$\|T_v u - T_v v\|_{\Delta t}^2 \leq (\Delta t)^2 \|\mathcal{N}_\varepsilon(u, v) - \mathcal{N}_\varepsilon(v)\|_N^2.$$

Using the estimate of Corollary 6.7, we obtain

$$\begin{aligned}\|\mathcal{N}_\varepsilon(u, v) - \mathcal{N}_\varepsilon(v)\|_N^2 &\leq C\big(1 + \|u\|_{\mathrm{L}^\infty(\Omega)}^2 + \|v\|_{\mathrm{L}^\infty(\Omega)}^2\big)^2 \|u - v\|_N^2 \\ &\leq C\big(1 + \|u - v\|_{\mathrm{L}^\infty(\Omega)}^2 + \|v\|_{\mathrm{L}^\infty(\Omega)}^2\big)^2 \|u - v\|_N^2.\end{aligned}$$

We shall now estimate the quantities of the above inequality. Taking the estimate of Lemma 5.1, we first have

$$\|u - v\|_{\mathrm{L}^\infty(\Omega)}^2 \leq N^2\|u - v\|_{\mathrm{L}^2(\Omega)}^2 \leq N^2\|u - v\|_{\Delta t}^2,$$

while, as mentioned previously, there holds $\|v\|_{\mathrm{L}^\infty(\Omega)}^2 \leq CN^2 E_N(v)$. Merging the different estimates together, we finally obtain

$$\|T_v u - T_v v\|_{\Delta t} \leq C\Delta t\big(1 + N^2\|u - v\|_{\Delta t}^2 + N^2 E_N(v)\big)\|u - v\|_{\Delta t}.$$

On taking $\Delta t \lesssim 1/N^2$ with N sufficiently large, we have

$$\|T_v u - T_v v\|_{\Delta t} \leq \frac{1}{4} + \frac{1}{4}\|u - v\|_{\Delta t}^3 + \frac{1}{4}\|u - v\|_{\Delta t}.$$

□

Bound on $T_v u - v$

Proposition 6.13. *Let $v \in \mathrm{X}_N$ with $E_N(v) < \infty$. There exists a constant $\beta_2 > 0$ such that for $\Delta t N^2 < \beta_2$, there holds*

$$\|T_v u - v\|_{\Delta t} \leq \frac{1}{2} + \frac{1}{4}\|u - v\|_{\Delta t}^3 + \frac{1}{4}\|u - v\|_{\Delta t} \quad \textit{for all } u \in \mathrm{X}_N.$$

Proof. Using the triangle inequality and the results of Corollary 6.10 and Corollary 6.12 yields the result. □

On defining

$$\mathrm{B}_r^{\Delta t}(v) := \{u \in \mathrm{X}_N : \|u - v\|_{\Delta t} < r\}$$

the ball of radius $r > 0$ centered at v in $(\mathrm{X}_N, \|\cdot\|_{\Delta t})$, the previous proposition shows that T_v maps the ball $\mathrm{B}_1^{\Delta t}$ into itself. More precisely we infer:

Corollary 6.14. *Consider the sequence $(u_k)_{k=0}^{\infty} \subset \mathrm{X}_N$ where $u_{k+1} := T_v u_k$ with $u_0 := v$. Then for $\Delta t N^2 < \beta_2$, we have*

$$u_k \in \mathrm{B}_1^{\Delta t}(v) \quad \textit{for all } k \in \mathbb{N}.$$

Proof. Trivially, we have $u_0 := v \in \mathrm{B}_1^{\Delta t}(v)$. Let now $u_k \in \mathrm{B}_1^{\Delta t}(v)$ for given $k \in \mathbb{N}$. On using the estimate of Proposition 6.13, we obtain

$$\|u_{k+1} - v\|_{\Delta t} = \|T_v u_k - v\|_{\Delta t} \leq \frac{1}{2} + \frac{1}{4}\|u_k - v\|_{\Delta t}^3 + \frac{1}{4}\|u_k - v\|_{\Delta t} < 1,$$

and hence $u_{k+1} \in \mathrm{B}_1^{\Delta t}(v)$. □

Contraction Property of T_v

We shall now prove that the mapping T_v is a contraction; we infer the following proposition:

Proposition 6.15. *Let $v \in \mathrm{X}_N$ with $E_N(v) < \infty$. There exists a constant $\beta_3 > 0$ such that for $\Delta t N^2 < \beta_3$, we have*

$$\big(\|U - U'\|_N \leq\big) \qquad \|U - U'\|_{\Delta t} \leq \frac{1}{2}\|u - u'\|_N \qquad \Big(\leq \frac{1}{2}\|u - u'\|_{\Delta t}\Big)$$

for all $u, u' \in \mathrm{B}_1^{\Delta t}(v)$, where $U = T_v u$ and $U' = T_v u'$.

Proof. Let $v \in \mathrm{X}_N$. We consider u and $u' \in \mathrm{B}_1^{\Delta t}(v)$. As previously, on setting $\phi = U - U'$ and substracting the inequalities (6.31) obtained respectively for $U = T_v u$ and for $U' =$

$T_v u'$ and then applying Young's inequality, we obtain

$$\|U - U'\|_{\Delta t}^2 \leq (\Delta t)^2 \|\mathcal{N}_\varepsilon(u, v) - \mathcal{N}_\varepsilon(u', v)\|_N^2.$$

On using again the estimate of Corollary 6.7, there holds

$$\|\mathcal{N}_\varepsilon(u, v) - \mathcal{N}_\varepsilon(u', v)\|_N^2 \leq C\big(1 + N^2\|u - v\|_{\Delta t}^2 + N^2\|u' - v\|_{\Delta t}^2 + N^2 E_N(v)\big)^2 \|u - u'\|_N^2.$$

Since u and $u' \in \mathrm{B}_1^{\Delta t}$, we obtain

$$\|U - U'\|_{\Delta t}^2 \leq C\big(\Delta t + \Delta t N^2 + \Delta t N^2 E_N(v)\big)^2 \|u - u'\|_N^2.$$

Consequently, taking $\Delta t \lesssim 1/N^2$ and N sufficiently large, we have

$$\|U - U'\|_{\Delta t}^2 \leq \frac{1}{2}\|u - u'\|_N^2.$$

□

Existence Theorem

On setting $\beta = \min(\beta_1, \beta_2, \beta_3)$, using the results of Proposition 6.13 and Proposition 6.15 as well as the Banach fixed point theorem, we infer the following existence theorem.

Theorem 6.16. *Let $v \in \mathrm{X}_N$ with $E_N(v) < \infty$. There exists a constant β depending only on v and the parameter ε such that for $\Delta t N^2 < \beta$, the mapping T_v has a unique fixed point $u \in \mathrm{X}_N$.*

From a more constructive point of view, let us consider the sequence $(u_k)_{k=0}^\infty \subset \mathrm{X}_N$, where $u_{k+1} := T_v u_k$ with $u_0 := v$. Then for $\ell > k + 1$ we have

$$\|u_\ell - u_{k+1}\|_{\Delta t} \leq \sum_{i=k+1}^{\ell-1} \|u_{i+1} - u_i\|_{\Delta t}.$$

On using the bound of Proposition 6.15, there holds for $\Delta t N^2 < \beta$

$$\|u_\ell - u_{k+1}\|_{\Delta t} \leq \left(\left(\frac{1}{2}\right)^k - \left(\frac{1}{2}\right)^{\ell-1}\right) \|u_1 - u_0\|_{\Delta t}$$

for all $\ell > k + 1$. Thus $(u_k)_{k=1}^\infty$ is a Cauchy sequence in the finite-dimensional normed linear space X_N, with respect to the norm $\|\cdot\|_{\Delta t}$. Hence, by completeness of X_N with respect to the norm $\|\cdot\|_{\Delta t}$, the sequence $(u_k)_{k=0}^\infty \subset \mathrm{X}_N$, where $u_{k+1} := T_v u_k$ with initial value $u_0 := v$, converges in $\mathrm{L}^2(\Omega)$ to a fixed point $u \in \mathrm{X}_N$ for any $v \in \mathrm{X}_N$. On passing to the limit $\ell \to \infty$ in the above inequality, we obtain that

$$\|u - u_{k+1}\|_{\Delta t} \leq 2^{-k}\|u_1 - v\|_{\Delta t}$$

On using the bound on the initial step $u_1 - u_0$ given in Lemma 6.9 and provided $\Delta t N^2 < \beta$, we deduce that there exists a constant $C > 0$ such that

$$\|u - u_{k+1}\|_{\Delta t}^2 \leq 4^{-k} C \Delta t\big((E_N(v))^2 + E_N(v)\big) \quad \text{for any } k \geq 0.$$

Denoting by u_N^{n+1} the unique fixed point in X_N of T_v with $v = u_N^n$, for $\Delta t N^2 < \beta$ and $N \geq 1$, Theorem 6.16 implies the existence of a unique solution to the $(n+1)$st step of the numerical scheme (6.1). Proceeding inductively for $n = 0, 1, \ldots, J-1$, we deduce, for all $\Delta t N^2 < \beta$ and all $N \geq 1$, the existence of a unique solution $(u_N^n)_{n=0}^J \subset \mathrm{X}_N$ to the scheme for a given initial value $u_N^0 = I_N u_0 \in \mathrm{X}_N$ with $E_N(u_N^0) < \infty$.

6.8. Convergence of the Numerical Solutions

A sine qua non condition for a numerical scheme is that its solutions converge in some sense to the solutions of its continuous counterpart, in our case equation (4.4). Therefore we infer the following theorem:

Theorem 6.17 (Convergence theorem)**.** *Let $u_N \in \mathrm{X}_N$ be a solution of the numerical scheme* (6.1) *on $(0,T) \times \Omega$ with initial datum $u_N^0 = I_N u_0$. Suppose furthermore that the initial discrete energy associated to u_N is bounded by a positive constant M_0 independent of N and Δt i.e.,*

$$E_N(u_N^0) \leq M_0.$$

Then as we send the gridsize $N \to \infty$ and the time step $\Delta t \to 0$ with $(\Delta t)^{1/2} \leq 1/\log N$, u_N subconverges to a weak solution of the continuous equation (4.4)*.*

Corollary 6.18. *Given initial datum $u_0 \in \mathrm{H}^1(\Omega)$, then as $N \to \infty$ and $\Delta t \to 0$ with $(\Delta t)^{1/2} \leq 1/\log N$, weak solutions of the approximate initial value problem with initial datum $u_N^0 = I_N u_0$ subconverge to weak solutions of the continuous initial value problem* (4.4),(4.5)*.*

Proof. The proof of the convergence theorem is composed of two steps: at first, we show that the numerical solution has a converging subsequence. Then, we prove that the residual R obtained after substituting the numerical solution into the initial continuous problem converges weakly to 0 in the space $\mathcal{D}'((0,T)\times\Omega)$ of all distributions on $(0,T)\times\Omega$.

Subconvergence of the Numerical Solution

As we proved in Section 6.5.1, the boundedness of the initial discrete energy $E_N(u_N^0)$ implies that our numerical solution u_N is uniformly bounded in $\mathrm{H}^1((0,T)\times\Omega)$. By virtue of the Rellich–Kondrachov theorem, $\mathrm{H}^1((0,T)\times\Omega)$ is compactly embedded in $\mathrm{L}^p((0,T)\times\Omega)$ for all $1 < p < 6$. Thus we infer that u_N has a subsequence that converges strongly to u in $\mathrm{L}^p((0,T)\times\Omega)$, $1 < p < 6$. Hence, in terms of the residual, there holds up to a subsequence

$$\lim_{\substack{\Delta t \to 0 \\ N \to \infty}} \int_0^T \left| \left(\partial_t u_N + \mathcal{L}_\varepsilon u_N - \mathcal{N}_\varepsilon(u_N), \phi \right)_{\mathrm{L}^2(\Omega)} \right| \mathrm{d}t = \int_0^T \left| \left(\partial_t u + \mathcal{L}_\varepsilon u - \mathcal{N}_\varepsilon(u), \phi \right)_{\mathrm{L}^2(\Omega)} \right| \mathrm{d}t$$

for all $\phi \in \mathrm{C}_0^\infty((0,T)\times\Omega)$.

Weak Convergence of the Residual

Let at first $t \in \mathcal{I}_n = [t^n, t^{n+1})$ be fixed for $n \in \{0, 1, \ldots, J-1\}$ and let $\phi \in \mathrm{C}_0^\infty((0,T)\times\Omega)$.We first have

$$|(\mathrm{R}, \phi)_{\mathrm{L}^2(\Omega)}| \leq \|\mathrm{R}\|_{\mathrm{H}^{-1}(\Omega)} \|\phi\|_{\mathrm{H}^1(\Omega)}.$$

The above equation holds for every $t \in (0,T)$, thus in fact there holds

$$\int_0^T |(\mathrm{R},\phi)_{\mathrm{L}^2(\Omega)}|\mathrm{d}t \leq \Big(\sup_{t\in(0,T)} \|\mathrm{R}\|_{\mathrm{H}^{-1}(\Omega)}\Big)\Big(\int_0^T \|\phi\|_{\mathrm{H}^1(\Omega)}\mathrm{d}t\Big) \quad \text{for all } \phi \in \mathrm{C}_0^\infty((0,T)\times\Omega).$$

Using the estimate on the residual (6.28), we obtain

$$\int_0^T |(\mathrm{R},\phi)_{\mathrm{L}^2(\Omega)}|\mathrm{d}t \leq C\left(\frac{(\log N)^{1/2}}{N} + (\Delta t)^{1/2}(\log N)\right)\Big(\int_0^T \|\phi\|_{\mathrm{H}^1(\Omega)}\mathrm{d}t\Big)$$

for all $\phi \in \mathrm{C}_0^\infty((0,T)\times\Omega)$.The second term of the right-hand side of the above inequality is finite while the first term vanishes as we send $N \to \infty$ and $\Delta t \to 0$ with $(\Delta t)^{1/2} \leq 1/\log N$. This proves the weak convergence of the residual to 0 in $\mathcal{D}'((0,T)\times\Omega)$ and thus that the limit of our numerical solution u_N is a weak solution of the continuous equation (4.4).

□

6.9. A Priori Error Estimates

In this section, we keep the parameter ε fixed. The argument below is inspired by the one of Du and Nicolaides in [25]. Yet the problem they treat is only one-dimensional and a part of their analysis to derive the estimate is based on the uniform boundedness in L^∞ of both the exact and numerical solution of the problem. In Section 6.5.1, we proved the uniform boundedness of our numerical solution u_N in $\mathrm{H}^1((0,T)\times\Omega)$ under the assumption of bounded initial energy. Yet in two dimensions, the Sobolev embedding fails to ensure the uniform boundedness of u_N in $\mathrm{L}^\infty((0,T)\times\Omega)$. We shall therefore use the estimate of the $\mathrm{L}^\infty(\Omega)$ norm in terms of the full $\mathrm{H}^1(\Omega)$ norm of Lemma 5.2.

We let u be the solution of the exact equation

$$u_t + \mathcal{L}_\varepsilon u = \mathcal{N}_\varepsilon(u)$$

and u_N be the solution of the numerical scheme (6.1). Let now

$$e_N^n := u_N^n - P_N u(t^n)$$

denote the error at time t^n and $e_N^{n+1/2} = \frac{1}{2}(e_N^n + e_N^{n+1})$. Concerning the initial continuous equation (4.4), there holds in a weak form

$$\langle \partial_t u(t), \phi\rangle_N + \langle \mathcal{L}_\varepsilon u(t), \phi\rangle_N = \langle \mathcal{N}_\varepsilon(u(t)), \phi\rangle_N \quad \text{for all } t \in (0,T) \text{ and all } \phi \in X_N. \quad (6.32)$$

Similarly, in terms of the fully discretized scheme, a weak formulation reads

$$\frac{1}{\Delta t}\langle u_N^{n+1} - u_N^n, \phi\rangle_N + \frac{1}{2}\langle \mathcal{L}_\varepsilon(u_N^{n+1} + u_N^n), \phi\rangle_N = \langle \mathcal{N}_\varepsilon(u_N^n, u_N^{n+1}), \phi\rangle_N \quad \text{for all } \phi \in \mathrm{X}_N. \quad (6.33)$$

In terms of the error, there holds by definition

$$\frac{1}{\Delta t}\langle e_N^{n+1} - e_N^n, \phi\rangle_N = \frac{1}{\Delta t}\langle u_N^{n+1} - u_N^n, \phi\rangle_N - \big(u(t^{n+1}) - u(t^n), \phi\big)_{\mathrm{L}^2(\Omega,\mathbb{C})}$$

as well as

$$\langle \mathcal{L}_\varepsilon e_N^{n+1/2}, \phi\rangle_N = \frac{1}{2}\langle \mathcal{L}_\varepsilon(u_N^n + u_N^{n+1}), \phi\rangle_N - \frac{1}{2}\big(\mathcal{L}_\varepsilon(u(t^n) + u(t^{n+1})), \phi\big)_{\mathrm{L}^2(\Omega,\mathbb{C})}$$

for all $\phi \in \mathrm{X}_N$. On putting the two previous equations together and using the weak formulations (6.32) and (6.33), we obtain

$$\begin{aligned}\frac{1}{\Delta t}\langle e_N^{n+1} - e_N^n, \phi\rangle_N + \langle \mathcal{L}_\varepsilon e_N^{n+1/2}, \phi\rangle_N \\ = \langle \mathcal{N}_\varepsilon(u_N^n, u_N^{n+1}), \phi\rangle_N - \frac{1}{\Delta t}\big(u(t^{n+1}) - u(t^n), \phi\big)_{\mathrm{L}^2(\Omega)} \\ - \frac{1}{2}\big(\mathcal{L}_\varepsilon(u(t^n) + u(t^{n+1})), \phi\big)_{\mathrm{L}^2(\Omega)}\end{aligned} \tag{6.34}$$

for all $\phi \in \mathrm{X}_N$. Furthermore, on applying Equation (6.32) with $t = t^{n+1/2} := (t^n + t^{n+1})/2$, we obtain

$$\langle \partial_t u(t^{n+1/2}), \phi\rangle_N + \langle \mathcal{L}_\varepsilon u(t^{n+1/2}), \phi\rangle_N - \langle \mathcal{N}_\varepsilon(u(t^{n+1/2})), \phi\rangle_N = 0 \quad \text{for all } \phi \in \mathrm{X}_N.$$

Adding this quantity to Equation (6.34) yields

$$\begin{aligned}\frac{1}{\Delta t}\langle e_N^{n+1} - e_N^n, \phi\rangle_N + \langle \mathcal{L}_\varepsilon e_N^{n+1/2}, \phi\rangle_N \\ = \langle \mathcal{N}_\varepsilon(u_N^n, u_N^{n+1}) - P_N\mathcal{N}_\varepsilon(u(t^{n+1/2})), \phi\rangle_N \\ + \big(u_t(t^{n+1/2}) - \frac{u(t^{n+1}) - u(t^n)}{\Delta t}, \phi\big)_{\mathrm{L}^2(\Omega,\mathbb{C})} \\ + (\mathcal{L}_\varepsilon u(t^{n+1/2}) - \mathcal{L}_\varepsilon\big(\frac{u(t^{n+1}) + u(t^n)}{2}\big), \phi\big)_{\mathrm{L}^2(\Omega,\mathbb{C})}\end{aligned}$$

for all $\phi \in \mathrm{X}_N$. On taking $\phi = e_N^{n+1/2}$ as a test function in the above equation and using the Cauchy–Schwarz inequality, we obtain

$$\begin{aligned}\frac{1}{2\Delta t}\left(\|e_N^{n+1}\|^2 - \|e_N^n\|^2\right) + \|e_N^{n+1/2}\|_{\mathcal{L}_\varepsilon}^2 \\ \leq \bigg(\|\mathcal{N}_\varepsilon(u_N^n, u_N^{n+1}) - \mathcal{N}_\varepsilon(u(t^{n+1/2}))\|_N + \Big\|\frac{u(t^{n+1}) - u(t^n)}{\Delta t} - u_t(t^{n+1/2})\Big\| \\ + \|R_N\mathcal{N}_\varepsilon(u(t^{n+1/2})\|\bigg)\|e_N^{n+1/2}\| + \Big\|\frac{u(t^n) + u(t^{n+1})}{2} - u(t^{n+1/2})\Big\|_{\mathcal{L}_\varepsilon}\|e_N^{n+1/2}\|_{\mathcal{L}_\varepsilon},\end{aligned}$$

with the energy norm $\|f\|_{\mathcal{L}_\varepsilon} := (\mathcal{L}_\varepsilon f, f)_{\mathrm{L}^2(\Omega,\mathbb{C})}$ and where $R_N := P_N - I_N$ denotes the aliasing error. Therefore, by Young's inequality,

$$\begin{aligned}\frac{1}{\Delta t}\big(\|e_N^{n+1}\|^2 - \|e_N^n\|^2\big) + \|e_N^{n+1/2}\|_{\mathcal{L}_\varepsilon}^2 \leq 3\|e_N^{n+1/2}\|^2 \\ + \Big(\|\mathcal{N}_\varepsilon(u_N^n, u_N^{n+1}) - \mathcal{N}_\varepsilon(u(t^{n+1/2}))\|_N^2 + \|R_N\mathcal{N}_\varepsilon(u(t^{n+1/2})\|^2\Big) \\ + \Big\|\frac{u(t^n) + u(t^{n+1})}{2} - u(t^{n+1/2})\Big\|_{\mathcal{L}_\varepsilon}^2 + \Big\|\frac{u(t^{n+1}) - u(t^n)}{\Delta t} - u_t(t^{n+1/2})\Big\|^2.\end{aligned} \tag{6.35}$$

By virtue of Taylor's theorem the last two terms can be bounded by

$$c(\Delta t)^3 \int_{t^n}^{t^{n+1}} \Big(\|u_{tt}(t)\|_{\mathcal{L}_\varepsilon}^2 + \|u_{ttt}(t)\|^2 \Big) \mathrm{d}t. \tag{6.36}$$

Concerning the second term in the right-hand side of inequality (6.35), we infer the following lemma, which is in fact adapted from Lemma 4.3 in [25].

Lemma 6.19. *There exists a constant $C > 0$ such that*

$$\begin{aligned}
&\|\mathcal{N}_\varepsilon(u_N^n, u_N^{n+1}) - \mathcal{N}_\varepsilon(u(t^{n+1/2}))\|_N^2 \\
&\qquad \le C \Big(\|u_N^{n+1} - u(t^{n+1})\|_N^2 \big(1 + \|u_N^{n+1}\|_{\mathrm{L}^\infty(\Omega)}^2 + \|u_N^n\|_{\mathrm{L}^\infty(\Omega)}^2\big)^2 \\
&\qquad\qquad + \|u_N^n - u(t^n)\|_N^2 \big(1 + \|u_N^n\|_{\mathrm{L}^\infty(\Omega)}^4\big) + \|(u(t^{n+1}) - u(t^n))^2\|_N^2 \\
&\qquad\qquad + \Big\| \frac{u(t^{n+1}) + u(t^n)}{2} - u(t^{n+1/2}) \Big\|_N^2 \Big).
\end{aligned}$$

Proof. We proceed almost identically as in Lemma 4.3 in [25], except that we do a priori not have uniform boundedness of our numerical solution u_N on $\mathrm{L}^\infty(\Omega)$. By the triangle inequality, we first have

$$\begin{aligned}
&\|\mathcal{N}_\varepsilon(u_N^n, u_N^{n+1}) - \mathcal{N}_\varepsilon(u(t^{n+1/2}))\|_N^2 \\
&\qquad \le C \Big(\|\mathcal{N}_\varepsilon(u_N^n, u_N^{n+1}) - \mathcal{N}_\varepsilon(u_N^n, u(t^{n+1}))\|_N^2 \\
&\qquad\qquad + \|\mathcal{N}_\varepsilon(u_N^n, u(t^{n+1})) - \mathcal{N}_\varepsilon(u(t^n), u(t^{n+1}))\|_N^2 \\
&\qquad\qquad\qquad + \|\mathcal{N}_\varepsilon(u(t^n), u(t^{n+1})) - \mathcal{N}_\varepsilon\big(\frac{u(t^n) + u(t^{n+1})}{2}\big)\|_N^2 \\
&\qquad\qquad\qquad\qquad + \|\mathcal{N}_\varepsilon\big(\frac{u(t^n) + u(t^{n+1})}{2}\big) - \mathcal{N}_\varepsilon(u(t^{n+1/2}))\|_N^2 \Big).
\end{aligned}$$

We shall now bound separately all the terms of the right-hand side of the above inequality. On using the estimate of Corollary 6.7, as our exact solution u is bounded in $\mathrm{L}^\infty(\Omega)$, we obtain for the first two terms

$$\begin{aligned}
&\|\mathcal{N}_\varepsilon(u_N^n, u_N^{n+1}) - \mathcal{N}_\varepsilon(u_N^n, u(t^{n+1}))\|_N^2 \\
&\qquad \le C \|u_N^{n+1} - u(t^{n+1})\|_N^2 \big(1 + \|u_N^{n+1}\|_{\mathrm{L}^\infty(\Omega)}^2 + \|u_N^n\|_{\mathrm{L}^\infty(\Omega)}^2\big)^2,
\end{aligned}$$

as well as

$$\|\mathcal{N}_\varepsilon(u_N^n, u(t^{n+1})) - \mathcal{N}_\varepsilon(u(t^n), u(t^{n+1}))\|_N^2 \le C \|u_N^{n+1} - u(t^{n+1})\|_N^2 (1 + \|u_N^n\|_{\mathrm{L}^\infty(\Omega)}^2)^2.$$

Concerning the third term, on considering the double well $W(u) := (1 - u^2)^2$, we obtain in fact by computation

$$\mathcal{N}_\varepsilon(u(t^n), u(t^{n+1})) - \mathcal{N}_\varepsilon\big(\frac{u(t^n) + u(t^{n+1})}{2}\big) = -\frac{1}{8\varepsilon} \big(u(t^{n+1}) + u(t^n)\big) \big(u(t^{n+1}) - u(t^n)\big)^2,$$

so that we get immediately

$$\|\mathcal{N}_\varepsilon(u(t^n),u(t^{n+1}))-\mathcal{N}_\varepsilon\big(\frac{u(t^n)+u(t^{n+1})}{2}\big)\|_N^2\le C\|(u(t^{n+1})-u(t^n))^2\|_N^2.$$

Proceeding similarly with the last remaining term, we obtain the following estimate

$$\|\mathcal{N}_\varepsilon\big(\frac{u(t^n)+u(t^{n+1})}{2}\big)-\mathcal{N}_\varepsilon(u(t^{n+1/2}))\|_N^2\le C\Big\|\frac{u(t^{n+1})+u(t^n)}{2}-u(t^{n+1/2})\Big\|_N^2.$$

Finally putting the four bounds together yields the result. □

The bound provided in the lemma can be extended further. Indeed, Lemma 5.2 gives an estimate of the $\mathrm{L}^\infty(\Omega)$ norm of the numerical solution u_N in terms of the full $\mathrm{H}^1(\Omega)$ norm which itself can be estimated in terms of the associated initial discrete energy $E_N(u_N^0)$, see Section 6.5.1. This yields

$$\begin{aligned}&\|\mathcal{N}_\varepsilon(u_N^n,u_N^{n+1})-\mathcal{N}_\varepsilon(u(t^{n+1/2}))\|_N^2\\&\quad\le C\Big(\big[\|e_N^{n+1}\|_N^2+\|e_N^n\|_N^2+\|R_Nu(t^{n+1})\|_N^2+\|R_Nu(t^n)\|_N^2\big](\log N)^2(E_N(u_N^0))^4\\&\qquad+\|(u(t^{n+1})-u(t^n))^2\|_N^2+\Big\|\frac{u(t^{n+1})+u(t^n)}{2}-u(t^{n+1/2})\Big\|_N^2\Big),\end{aligned}\tag{6.37}$$

where R_Nu denotes the aliasing error. Furthermore, by virtue of Taylor's theorem, the last two terms in the above inequality can be estimated by

$$C(\Delta t)^3\int_{t^n}^{t^{n+1}}\Big(\|u_{tt}(t)\|_N^2+\|(u_t(t))^2\|_N^2\Big)\mathrm{d}t.\tag{6.38}$$

Finally, we obtain from (6.35), (6.36), (6.37) and (6.38):

$$\begin{aligned}&\|e_N^{n+1}\|^2-\|e_N^n\|^2+\Delta t\|e_N^{n+1/2}\|_{\mathcal{L}_\varepsilon}^2\\&\quad\le c(\Delta t)^4\int_{t^n}^{t^{n+1}}\Big(\|u_{ttt}(t)\|^2+\|u_{tt}(t)\|_{\mathcal{L}_\varepsilon}^2+\|u_{tt}(t)\|_N^2+\|(u_t(t))^2\|_N^2\Big)\mathrm{d}t\\&\qquad+c\Delta t(\log N)^2(E_N(u_N^0))^4\Big(\|e_N^{n+1}\|^2+\|e_N^{n+1/2}\|^2+\|e_N^n\|^2\\&\qquad\quad+\|R_Nu(t^{n+1})\|^2+\|R_Nu(t^n)\|^2+\|R_N\mathcal{N}_\varepsilon(u(t^{n+1/2}))\|^2\Big),\end{aligned}$$

and after summation from $n=0$ to $k-1$, where $1\le k\le J$,

$$\begin{aligned}&\|e_N^k\|^2-\|R_Nu_0\|^2+\Delta t\sum_{n=0}^{k-1}\|e_N^{n+1/2}\|_{\mathcal{L}_\varepsilon}^2\\&\le c(\Delta t)^4\int_0^T\Big(\|u_{ttt}(t)\|^2+\|u_{tt}(t)\|_{\mathcal{L}_\varepsilon}^2+\|u_{tt}(t)\|_N^2+\|(u_t(t))^2\|_N^2\Big)\mathrm{d}t\\&+c\Delta t(\log N)^2(E_N(u_N^0))^4\sum_{n=0}^{k}\Big(\|e_N^n\|^2+\|R_Nu(t^n)\|^2+\|R_N\mathcal{N}_\varepsilon(u(t^{n+1/2}))\|^2\Big).\end{aligned}\tag{6.39}$$

In view of Sobolev embedding $\|u\|_N\lesssim\|u\|_{\mathrm{L}^\infty(\Omega)}\lesssim\|u\|_{\mathrm{H}^s(\Omega)}$ for $s>1$. Since $\mathrm{H}^s(\Omega)$ is a

Banach algebra for $s > 1$, we also have that $\|u^2\|_{\mathrm{H}^s(\Omega)} = \|u\|^2_{\mathrm{H}^s(\Omega)}$. Therefore the integral terms in the above inequality are finite provided

$$u_t \in \mathrm{H}^2_t\mathrm{L}^2_x \cap \mathrm{H}^1_t\mathrm{H}^2_x((0,T)\times\Omega).$$

According to (5.4), in two-dimensional space we have

$$\|R_N u\| \lesssim cN^{-2}\|u\|_{\mathrm{H}^2(\Omega)}.$$

Hence, as the exact solution u is bounded in $\mathrm{L}^\infty(\Omega)$, the terms related to the aliasing error can be estimated provided $u \in \mathrm{H}^1_t\mathrm{H}^2_x((0,T)\times\Omega)$, and decay as $\mathcal{O}(N^{-2})$. More generally, if $s \geq 2$ and $u \in \mathrm{L}^\infty_t\mathrm{H}^s_x((0,T)\times\Omega)$, then

$$\|R_N u\| \lesssim cN^{-s}\|u\|_{\mathrm{H}^s(\Omega)}.$$

We can now apply the discrete Gronwall inequality to (6.39) and obtain the following result.

Theorem 6.20. *Suppose that $u \in \mathrm{H}^3_t\mathrm{L}^2_x \cap \mathrm{H}^2_t\mathrm{H}^2_x \cap \mathrm{L}^\infty_t\mathrm{H}^s_x((0,T)\times\Omega)$, $s \geq 2$; then there exists a positive constant $C = C(s,T,\varepsilon)$ such that*

$$\max_{0\leq n\leq J} \|u_N^n - u(t^n)\| \leq C\big(N^{-s}\log N + (\Delta t)^2\big).$$

7. Numerical Experiments

7.1. Introduction

This chapter is devoted to numerical experiments aimed at assessing the practical performance of the numerical method and to undertaking a parameter study of the energy functional (4.1). The numerical scheme (6.1) has been implemented in MATLAB. Our numerical experiments focus on the two-dimensional periodic domain $\Omega = (0,1)^2$. For the purpose of our parameter studies we reintroduce the parameter $\gamma > 0$, the interfacial energy per unit length, which balances the strength of domain wall against dipolar energy. We consider, for $\varepsilon > 0$, the linear and nonlinear operators

$$u \mapsto \mathcal{L}_\varepsilon u = \gamma\varepsilon(-\Delta)u + \sigma(\mathrm{D})u$$

and

$$u \mapsto \mathcal{N}_\varepsilon(u) = -\frac{\gamma}{\varepsilon}\mathrm{D}W(u),$$

where $\sigma : k \in \mathbb{Z}^2 \mapsto \sigma(k) \in \mathbb{R}_{\geq 0}$ is a Fourier multiplier

$$\sigma(k) = \frac{1-\exp(-2\pi|k|)}{2\pi|k|} \quad \text{for} \quad k \neq 0 \quad \text{and} \quad \sigma(0) = 1,$$

and $W : u \in \mathbb{R} \mapsto W(u) \in \mathbb{R}_{\geq 0}$ is the classical double-well potential

$$W(u) = c_0(1-u^2)^2 \quad \text{where} \quad c_0 = \frac{1}{2}\left(\int_{-1}^{1} |1-v^2|\mathrm{d}v\right)^{-2} = \frac{9}{32}.$$

As indicated in Section 4.1, the original model (which stems from micromagnetics) includes an additional dilation parameter $\delta > 0$ which corresponds to the relative film thickness. The precise energy scaling and morphology, depending on all system parameters, is subtle and is hard to capture in a rigorous analytic fashion. Current investigations reported in physics literature mainly rely on further reductions and optimization through a special ansatz; cf. [31, 38]. Our numerical experiments provide an adequate account of characteristic patterns and structures in more generality and support the latter results.

7.2. Procedure

The implementation is based on the nonlinear system

$$u_N^{n+1}(x_j) = \big(1+\frac{\Delta t}{2}\mathcal{L}_\varepsilon\big)^{-1}\big[\big(1-\frac{\Delta t}{2}\mathcal{L}_\varepsilon\big)u_N^n(x_j) + \Delta t I_N \mathcal{N}_\varepsilon(u_N^{n+1}(x_j), u_N^n(x_j))\big],$$
$$j \in \mathbb{N}_N^2 = \{0,1,2,\ldots,N-1\}^2,$$

that we solve at each time-step by a fixed-point iteration. Inspection in Fourier space shows that the inverse $(1 + \frac{\Delta t}{2}\mathcal{L}_\varepsilon)^{-1}$ is well-defined. In order to compute the numerical solution at time iteration $n+1$, we use the following predictor-corrector algorithm:

$$u_{N,[0]}^{n+1}(x_j) = \big(1 + \frac{\Delta t}{2}\mathcal{L}_\varepsilon\big)^{-1}\big[\big(1 - \frac{\Delta t}{2}\mathcal{L}_\varepsilon\big)u_N^n(x_j) + \Delta t I_N \mathcal{N}_\varepsilon(u_N^n(x_j), u_N^n(x_j))\big], \quad j \in \mathbb{N}_N^2 = \{0, 1, 2, \ldots, N-1\}^2,$$

$$u_{N,[k+1]}^{n+1}(x_j) = \big(1 + \frac{\Delta t}{2}\mathcal{L}_\varepsilon\big)^{-1}\big[\big(1 - \frac{\Delta t}{2}\mathcal{L}_\varepsilon\big)u_N^n(x_j) + \Delta t I_N \mathcal{N}_\varepsilon(u_{N,[k]}^n(x_j), u_N^n(x_j))\big], \quad j \in \mathbb{N}_N^2 = \{0, 1, 2, \ldots, N-1\}^2, \quad k = 0, 1, 2, \ldots.$$

The iterations to solve the system at each time-step are considered to have converged when the discrete $\mathrm{L}^2(\Omega)$ norm of the difference of two successive iterates becomes smaller than a chosen positive tolerance; in our case the stopping tolerance was set to 10^{-8}. The quantities on the right-hand side of the above equations are computed by applying the following procedure:

1. Evaluation of $\big(1 - \frac{\Delta t}{2}\mathcal{L}_\varepsilon\big)u_N^n(x_j)$ in Fourier space;
2. Evaluation of the quantity $\Delta t I_N \mathcal{N}_\varepsilon(u_{N,[k]}^n(x_j), u_N^n(x_j))$ in physical space, followed by switching to Fourier space using Fast Fourier Transform (FFT);
3. Evaluation of $\big(1 + \frac{\Delta t}{2}\mathcal{L}_\varepsilon\big)^{-1}\big[\big(1 - \frac{\Delta t}{2}\mathcal{L}_\varepsilon\big)u_N^n(x_j) + \Delta t I_N \mathcal{N}_\varepsilon(u_{N,[k]}^n(x_j), u_N^n(x_j))\big]$ in Fourier space, followed by an Inverse Fast Fourier Transform (IFFT) to return to physical space.

The terminal time $T = J\,\Delta t$ for the evolution, i.e. the total number of time-steps J, is determined through a smallness condition for the energy gradient, which indicates that a local minimum has been reached approximately.

Remark 7.1. *Our numerical analysis shows the convergence of the numerical scheme for temporal meshes with uniform spacing Δt, once Δt is sufficiently small relative to ε and possibly N. However, with regard to the different time-scales involved in the morphological evolution of the patterns (quick formation of domains at the beginning, much slower evolution afterwards), adaptive time-stepping based on the number of iterations needed to solve the fixed point iteration was also implemented in the algorithm. This allows us to locally (in time) adapt the time-step to the evolution of the solution: on time intervals of slow/fast evolution the time-step is increased/decreased, respectively. This simple step-size selection process reduces drastically the computing time needed to reach a local minimum of the free energy.*

7.3. Implementation and Interpretation

Figures 7.1(a)–(e) and Figures 7.2(a)–(e) show typical examples of temporal evolution of morphological patterns during spinodal decomposition and subsequent growth. The gray levels represent the local compositions of the solution, black representing positive values typically around $+1$ and white representing negative values around -1. During the spinodal decomposition, we observe the formation of domains on a relatively short

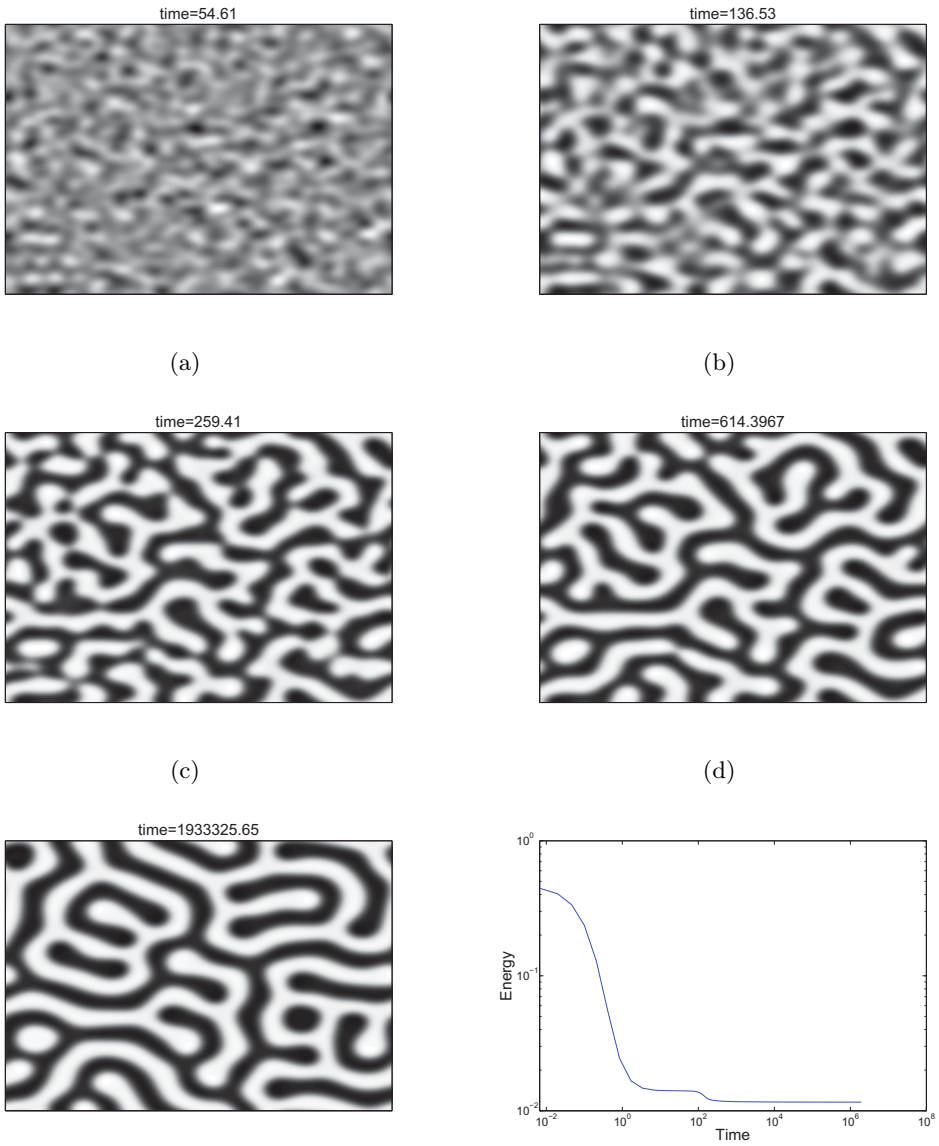

Figure 7.1.: (a)–(e) Formation and temporal evolution of a labyrinth-pattern obtained for a randomly distributed initial condition. (f) Temporal evolution of the associated discrete energy.

time-scale and with a corresponding substantial drop in the value of the discretized free energy of the system. During the succeeding growth period, we observe domain expansion and possibly nucleation on a much longer time-scale. The decrease of the energy on that period is also much smaller.

Figures 7.1(a)–(e) show the formation and evolution of a so-called labyrinth-pattern that typically arises in the study of magnetic garnet films. It was obtained for randomly distributed initial values on a lattice of 512×512 grid points and for parameter values $\gamma = 1/400$ and $\varepsilon = 1/20$.

Figures 7.2(a)–(e) show the evolution obtained for the initial condition u_0 defined by

$$u_0(x_1, x_2) := \sin(8\pi x_1)\sin(8\pi x_2) \tag{7.1}$$

discretized on a lattice of 512×512 grid points and parameter values $\gamma = 1/100$ and $\varepsilon = 1/20$. The drops of the energy seen in Figure 7.2(f) each correspond to topological changes in the pattern: the first drop occurs during the transition from the initial state to the checkerboard-pattern, the second one during the transition from the checkerboard-pattern to the stripe-pattern.

Based on a reduction of (4.1) through corresponding trial functions and an optimization argument Gehring and Kaplan [31] showed that a stripe-pattern is a lower energy state than a checkerboard-pattern. The numerical results shown on Figure 7.2 are consistent with these predictions. Indeed, the checkerboard-pattern obtained on Figure 7.2(b) appears as an unstable configuration, as we observe a further evolution of the system into an energetically lower, stripe-pattern, configuration; cf. Figure 7.2(d).

7.4. Parameter-Dependence

We have investigated the influence of the interfacial energy parameter γ on the domain morphology and the scaling of the asymptotic energy. Qualitatively, a decrease in the typical domain wall energy γ triggers the influence of the dipolar interaction, and therefore tends to favour oscillating solutions and eventually microstructure. Consequently, as displayed in Figure 7.3, we observe a decrease of the typical size of the domains. In the opposite regime, for increasing values of the interfacial energy parameter, the dipolar interaction has a declining influence. For sufficiently large γ, the problem almost reduces to the minimal interface problem. In that case, the absolute minimizer is a single domain state taking the value either $+1$ or -1 everywhere. This statement is illustrated in Figure 7.5. The pattern-evolution was obtained for a random initial condition (7.1), but with the parameter value $\gamma = 1000$.

In a more quantitative study we have investigated the precise scaling law for the energy as γ varies. As pointed out earlier, real micromagnetic applications involve a second parameter δ that corresponds to the film thickness relative to the dimension of the periodicity cell. Formal results have been obtained in the physics literature: the theory of Kooy and Enz [38] predicts an algebraic energy scaling of order $(\gamma/\delta)^{1/2}$ for $\gamma \ll \delta$, whereas for $\gamma \gg \delta$ the approach of Gehring and Kaplan [31] predicts an exponential dependence of type $C_1\,\delta(1 - C_2\exp[-C_3(\gamma/\delta)])$ with positive constants C_1, C_2 and C_3.

In our model problem we bypass the additional complexity arising from the presence of

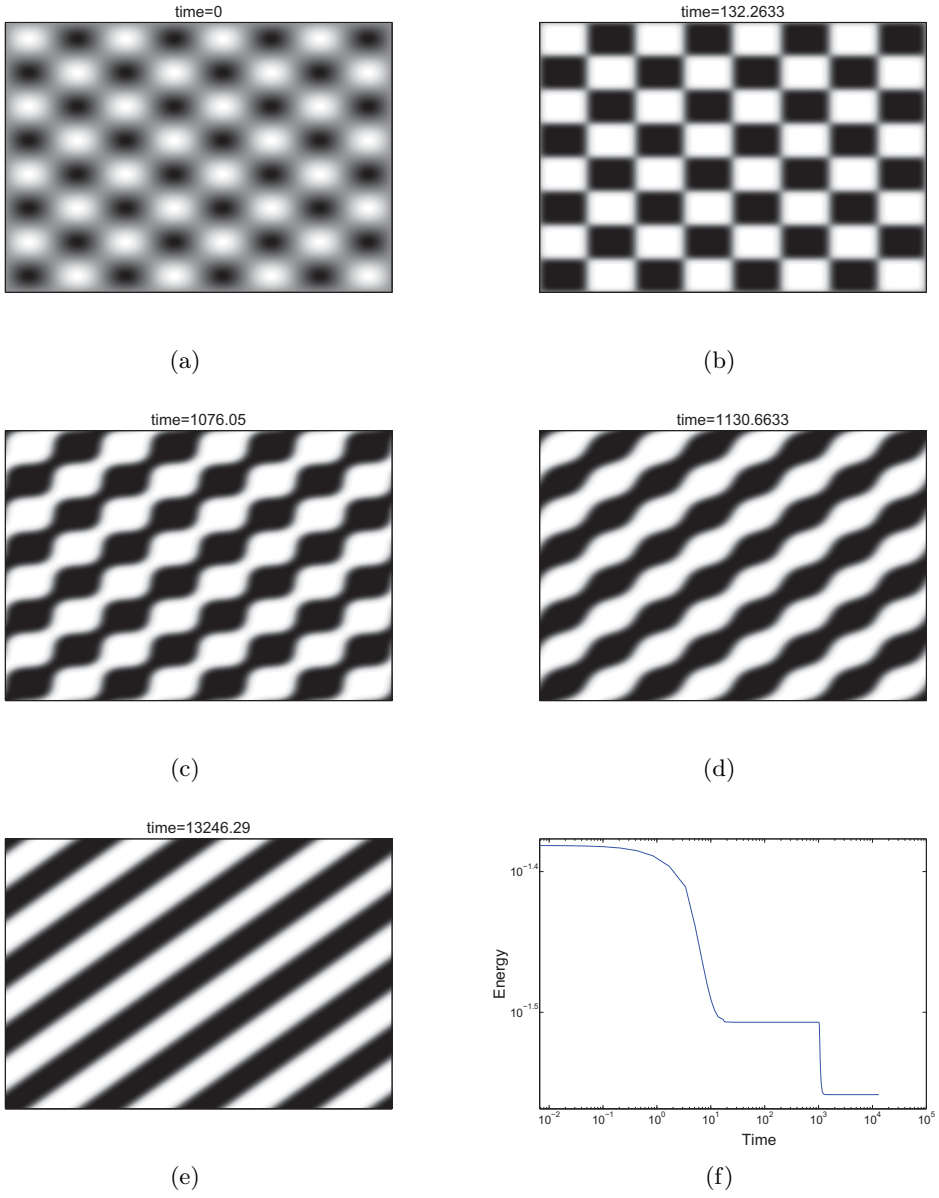

Figure 7.2.: (a)–(e) Formation of a checkerboard-pattern and subsequent evolution towards a stripe-pattern. (f) The corresponding energy profile.

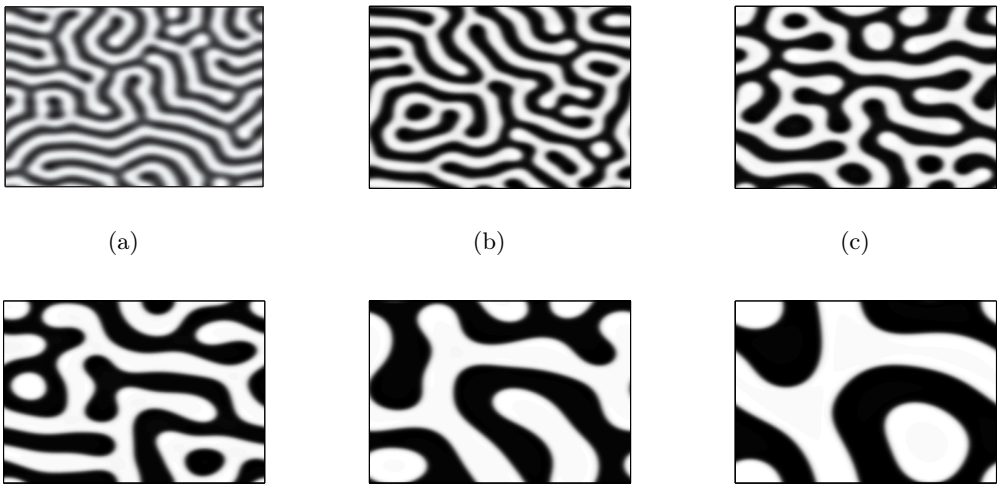

(a) (b) (c)

(d) (e) (f)

Figure 7.3.: Typical domain sizes observed for increasing values of the interfacial energy parameter, respectively (a) $\gamma = 0.00125$, (b) $\gamma = 0.002$, (c) $\gamma = 0.005$, (d) $\gamma = 0.008$, (e) $\gamma = 0.0175$ and (f) $\gamma = 0.035$.

a thickness parameter δ by setting it to 1 for convenience. Accordingly, we have studied the evolution of the asymptotic energy as a function of the interfacial energy parameter γ only. Taking a random initial condition and $\varepsilon = 1/20$, we ran the algorithm for values of γ ranging from $1/800$ to $1/2$ in the first instance, and subsequently for values ranging from 10 to 1000. For the small values of the interfacial energy parameter, we obtain a scaling of the asymptotic energy as an algebraic power of γ; cf. Figure 7.4(a). For larger values of γ, the solutions converge towards a single domain state. The energy fluctuations are much less prominent than in the previous case, nevertheless the plot of the asymptotic energy as a function of γ suggests a scaling law of exponential type, as predicted by Kaplan and Gehring; cf. Figure 7.4(b). These scaling laws are consistent with the formal results predicted in [38] and [31], and a cross-over in the energy scaling can be observed.

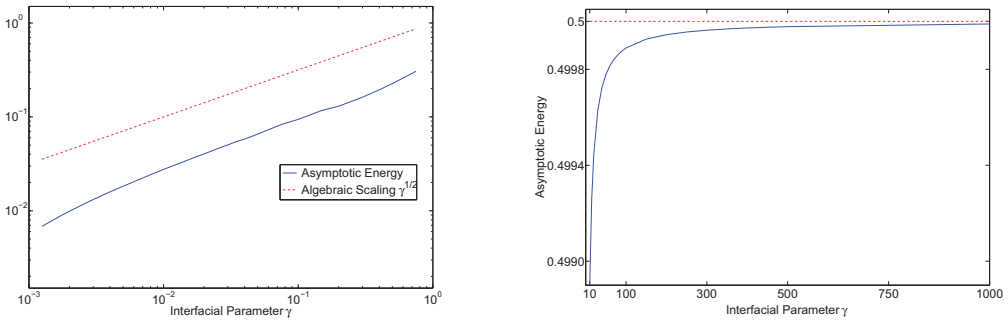

(a) (b)

Figure 7.4.: Evolution of the asymptotic discrete energy as a function of the interfacial energy parameter γ. (a) Logarithmic plot for values of γ ranging from 1/800 to 1/2 and comparison with the algebraic scaling $\gamma^{1/2}$ predicted by [38]. (b) Plot of the asymptotic discrete energy for values of γ ranging from 10 to 1000.

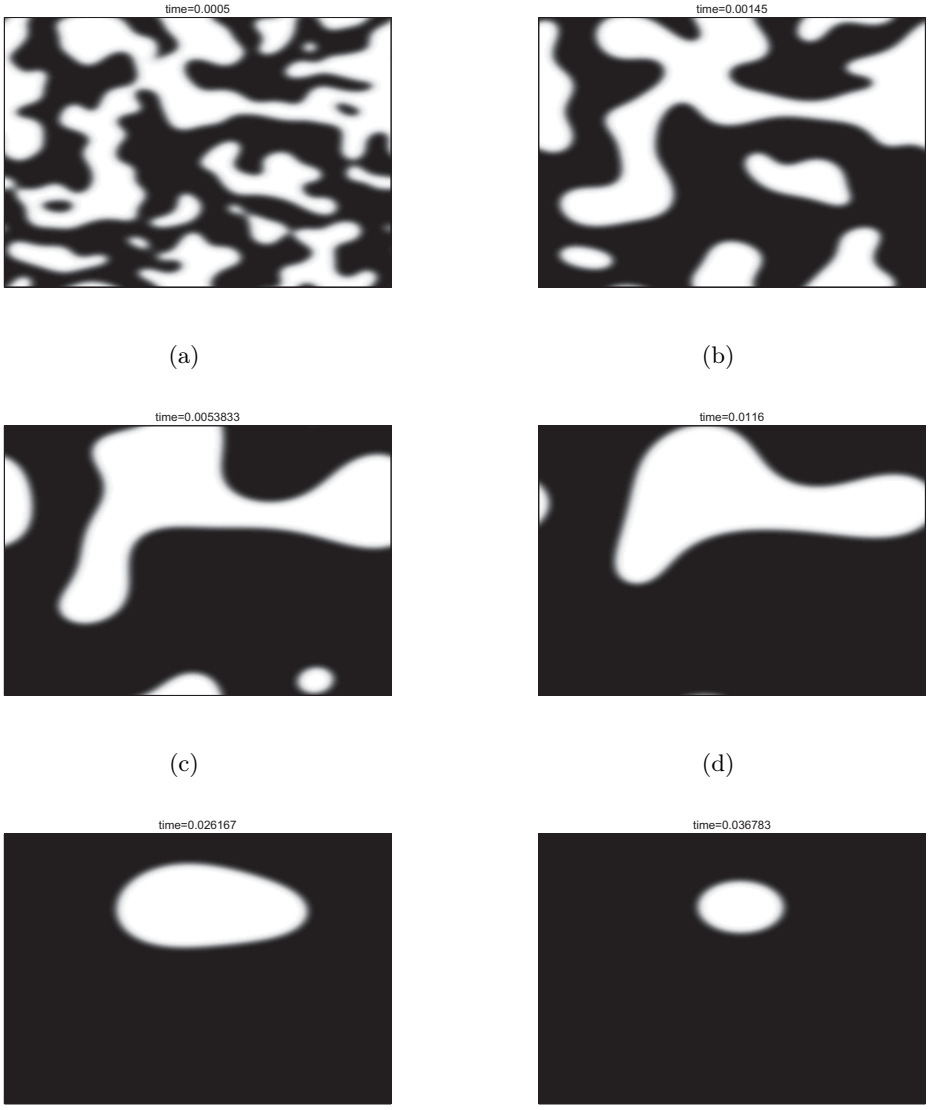

Figure 7.5.: Temporal evolution towards a single-domain state. The patterns were obtained on a 512×512 grid for random initial condition and the parameter value $\gamma = 1000$.

A. Norm Equivalence for Trigonometric Polynomials

We shall show here that on the space S_N, the norms $\|\cdot\|_N$ and $\|\cdot\|_{\mathrm{L}^2(\Omega)}$ coincide. Let then $N \in \mathbb{N}_{>0}$ be fixed and let $u, v \in \mathrm{S}_N$ be two trigonometric polynomials given by

$$u(x) = \sum_{k \in \mathbb{Z}_N^2} a(k)\, \mathrm{e}^{2\mathrm{i}\pi\, k\cdot x} \quad \text{and} \quad v(x) = \sum_{k' \in \mathbb{Z}_N^2} b(k')\, \mathrm{e}^{2\mathrm{i}\pi\, k'\cdot x}$$

for all $x \in \Omega$. On considering the discrete inner-product $\langle \cdot, \cdot \rangle_N$ defined in Section 6.3, we have

$$\begin{aligned}
\langle u, v \rangle_N &= \frac{1}{N^2} \sum_{j \in \mathbb{N}_N^2} \Big[\sum_{k \in \mathbb{Z}_N^2} a(k)\, \mathrm{e}^{2\mathrm{i}\pi\, k\cdot x_j} \sum_{k' \in \mathbb{Z}_N^2} b(k')\, \mathrm{e}^{-2\mathrm{i}\pi\, k'\cdot x_j} \Big] \\
&= \frac{1}{N^2} \sum_{k \in \mathbb{Z}_N^2} \sum_{k' \in \mathbb{Z}_N^2} a(k) b(k') \Big[\sum_{j \in \mathbb{N}_N^2} \mathrm{e}^{2\mathrm{i}\pi\, (k-k')\cdot x_j} \Big] \\
&= \frac{1}{N^2} \sum_{k \in \mathbb{Z}_N^2} \sum_{k' \in \mathbb{Z}_N^2} a(k) b(k') \Big[\sum_{j \in \mathbb{N}_N^2} \mathrm{e}^{\frac{2\mathrm{i}\pi}{N}\, (k-k')\cdot j} \Big].
\end{aligned}$$

On using the notation $j = (j_1, j_2)$, $k = (k_1, k_2)$ and $k' = (k_1', k_2')$, developing the last term of the right-hand side of the previous equation yields

$$\begin{aligned}
\frac{1}{N^2} \sum_{j \in \mathbb{N}_N^2} \mathrm{e}^{\frac{2\mathrm{i}\pi}{N}\, (k-k')\cdot j} &= \Big[\frac{1}{N} \sum_{j_1=1}^{N} \mathrm{e}^{\frac{2\mathrm{i}\pi}{N}\, (k_1-k_1')j_1} \Big] \Big[\frac{1}{N} \sum_{j_2=1}^{N} \mathrm{e}^{\frac{2\mathrm{i}\pi}{N}\, (k_2-k_2')j_2} \Big] \\
&= \begin{cases} 1 & \text{if } k_1 = k_1' \text{ and } k_2 = k_2' \\ 0 & \text{else} \end{cases},
\end{aligned}$$

so that finally we obtain

$$\langle u, v \rangle_N = \sum_{k \in \mathbb{Z}_N^2} a(k) b(k).$$

Similarly, in terms of the $\mathrm{L}^2(\Omega)$ inner-product $(\cdot, \cdot)_{\mathrm{L}^2(\Omega;\mathbb{C})}$, we have

$$(u, v)_{\mathrm{L}^2(\Omega;\mathbb{C})} = \int_\Omega u(x)\overline{v(x)}\, \mathrm{d}x = \sum_{k \in \mathbb{Z}_N^2} \sum_{k' \in \mathbb{Z}_N^2} a(k) b(k') \int_\Omega \mathrm{e}^{2\mathrm{i}\pi\, (k-k')\cdot x}\, \mathrm{d}x.$$

On proceeding as in the discrete case and developing the last term of the previous equation with $x = (x_1, x_2)$, we obtain

$$\begin{aligned}\int_\Omega \mathrm{e}^{2\mathrm{i}\pi\,(k-k')\cdot x}\,\mathrm{d}x &= \Big[\int_0^1 \mathrm{e}^{2\mathrm{i}\pi\,(k_1-k_1')x_1}\,\mathrm{d}x_1\Big]\Big[\int_0^1 \mathrm{e}^{2\mathrm{i}\pi\,(k_2-k_2')x_2}\,\mathrm{d}x_2\Big] \\ &= \begin{cases} 1 & \text{if } k_1 = k_1' \text{ and } k_2 = k_2' \\ 0 & \text{else} \end{cases},\end{aligned}$$

so that as expected we have

$$(u, v)_{\mathrm{L}^2(\Omega;\mathbb{C})} = \sum_{k\in\mathbb{Z}_N^2} a(k)b(k) = \langle u, v\rangle_N.$$

Consequently, there holds as well

$$\|u\|_N = \|u\|_{\mathrm{L}^2(\Omega)} \quad \text{for all } u \in \mathrm{S}_N.$$

B. Implementation Code (MATLAB)

The following programm and functions realize the implementation in MATLAB of the numerical scheme (6.1) as presented in Chapter 7.

Implicit Scheme Implementation

```
%-- CUSTOM SET UP --
gridsize=1;
N=512; % Number of Gridpoints
dt=1/3000; % Time step
c0=9/32; % Normalization constant for double well
epsilon=1/20;
gamma=1/100;
th=1; % Thickness parameter
Nmax=40; % Maximum iterations for finding fixed point
tol=10^(-8); % Tolerance for finding fixed point
stop_crit=10^(-8); %Stopping criterion for time iteration
max_it=50000;

%-- GENERIC SET UP --
x=gridsize/N*(0:N-1);
k=[0:N/2 -N/2+1:-1]'; % Wave numbers 1D
[xi,eta]=ndgrid(k,k); % 2D Wave numbers
modk2=xi.^2+eta.^2;
modk=sqrt(modk2);
L=(2*pi)^2*gamma*epsilon*(modk2)+sigma(th*modk); % Linear
   operator in Fourier Space
Mult=ones(N)-dt/2*L; % Multiplicating operator in Fourier
   Space (1-dt/2*L)
Inv=ones(N)+dt/2*L; %Invert operator in Fourier Space (1+dt/2*
   L)

%-- TIME STEPPING LOOP INITIALIZATION --
n_it=1;
time=0;
i=1;
time=time+dt;
u_int=u0;
Du=1;
Denergy=1000;
%-- Time Vector Values --
```

```
time_vector=zeros(max_it,1);
time_vector(1)=0;

%-- ENERGY COMPUTATION - INITIALIZATION --
[Energy(1,i)]=energy_value(gamma,epsilon,N,u0,th,modk,modk2,c0
   );
i=i+1;

%-- TIME STEPPING LOOP --
while (Denergy>stop_crit)
    % Computation of fixed point
    [k,u,err,conv]=fixpt(u_int,L,dt,N,epsilon, gamma,Nmax,tol,
       c0);
    if (conv==1)
        %-- Energy Computation --
        [Energy(1,i)]=energy_value(gamma,epsilon,N,u,th,modk,
           modk2,c1);
        %-- Error in L-infinity norm --
        Du=max(max(abs(u-u_int)));
        %-- Energy Decay
        Denergy=Energy(1,i-1)-Energy(1,i);

        %-- Time Vector --
        time_vector(i)=time_vector(i-1)+dt;

        %-- Pattern visualization --
        imagesc(x,x,u); colormap(gray);
        title(['time=' num2str(time)]);
        Frames(:,i-1)=getframe;

        %-- Incrementation --
        u_int=u;
        time=time+dt;
        n_it=n_it+1;
        i=i+1;

    elseif (conv==0)
        dt=dt/4; %try with reduced time step
    end
end
```

Computation of Fixed Point

The following function computes the solution of the numerical scheme (6.1) using the procedure explained in Section 7.2. Arguments of the algorithm are the initial guess for the fixed point, the linear operator $\mathcal{L}_\varepsilon$, the time step Δt and the gridsize N, the parameters γ and ε as well as the normalizing factor c_0 for the double-well potential and the tolerance for finding the fixed point. It returns the number of iterations needed to reach the fixed

point, the fixed point itself, the error in the approximation as well as a boolean taking the value 0 if a fixed point has not been reached within a chosen number of iterations.

```
function [k,u_n,err,conv]=fixpt(u0,L,dt,N,epsilon,gamma,Nmax,
   tol,c0)
% k=number of iterations needed to obtain fixed point
% u_n=approximation to fixed point
% err=error in approximation (L-inf norm)
% u0=initial guess for fixed point
% L=Linear operator of gradient flow equation (in Fourier
   Space)
% dt=time step
% N=grid size
% eps= epsilon
% gamma
% Nmax= maximum number of iterations
% tol= error tolerance

%-- Nonlinear function --
NL=inline('2*gamma*c0/(epsilon)*(u+v).*(1-(abs(u).^2+abs(v)
   .^2)/2)','u','v','epsilon','gamma','c0');

%-- Calculation of constant term [(1-dt/2 L)/(1+dt/2 L) U_n]
CT=real(ifft2((ones(N)-dt/2*L)./(ones(N)+dt/2*L).*fft2(u0)));

%-- Initialization of Iteration step --
j=1;
u_int2=N*ones(N,N);
u_int=u0;
error=10;
convergence=0;

%-- Fixed Point Iteration Loop --
while (j<Nmax) && (error>tol)
    test=NL(u_int,u0,epsilon,gamma,c0);
    u_int2=real((ifft2(fft2(dt*test)./(ones(N)+dt/2*L))+CT));
    error=max(max(abs(u_int2-u_int)));
    u_int=u_int2;
    j=j+1;
end
if (error<tol)
    convergence=1;
end

k=j;
err=error;
u_n=u_int2;
```

```
conv=convergence;
```

Evaluation of Discrete Energy

The following function computes the value of the discrete energy

$$E_N(u) = \frac{\gamma}{\varepsilon}\langle 1, W(u)\rangle_N + \frac{1}{2}\langle u, \mathcal{L}_\varepsilon u\rangle_N$$

for a given solution $u \in \mathrm{X}_N$. Parameters taken in entry are γ, ε, the gridsize N, the solution u, the thickness parameter th, the normalizing constant c_0 for the double well and the matrices $modk$ and $modk2$ composed of the values of $|k|$, respectively $|k|^2$, for all $k \in \mathbb{Z}_N^2$.

```
function [discrete_energy_value]=energy_value(gamma,epsilon,N,
   u,th,modk,modk2,c0)
W=double_well(u,c0);
ftu=1/N^2*(fft2(u));
discrete_energy_value=(gamma/epsilon)*1/N^2*(sum(sum(W)))+1/2*
   sum(sum((sigma(th*modk)+gamma*epsilon*(modk2)).*((abs(ftu))
   .^2)));
```

Double Well

The function `double_well` evaluates in this case the quantity $W(u) = c_0(1-u^2)^2$ for a given solution u. It is needed for the evaluation of the discrete energy. Included in the entries are the solution u and the normalizing parameter for the double well c_0.

```
function W=double_well(u,c0)
u2=1-(abs(u)).^2;
W=c0*((u2).^2);
```

Fourier Multiplier σ

The following function computes the quantities $\sigma(k) = \frac{1-\exp(-2\pi|k|)}{2\pi|k|}$ for frequencies k given in entry.

```
function sig=sigma(A)
if (abs(A)<1.0e-12)
    B=1-(pi*abs(A));
else
    B=(1-exp(-2*pi*abs(A)))./(2*pi*abs(A));
end
sig=B;
```

Bibliography

[1] R. A. Adams. *Sobolev spaces*. Academic Press [A subsidiary of Harcourt Brace Jovanovich, Publishers], New York-London, 1975. Pure and Applied Mathematics, Vol. 65.

[2] G. Alberti. Variational models for phase transitions, an approach via Γ-convergence. In *Calculus of variations and partial differential equations (Pisa, 1996)*, 7, pages 95–114. Springer, Berlin, 2000.

[3] F. Alouges and A. Soyeur. On global weak solutions for Landau-Lifshitz equations: existence and nonuniqueness. *Nonlinear Anal.*, 18(11):1071–1084, 1992. ISSN 0362-546X.

[4] H. W. Alt. *Lineare Funktionalanalysis*. Springer, fourth edition, 2002.

[5] L. Ambrosio, N. Fusco, and D. Pallara. *Functions of bounded variation and free discontinuity problems*. Oxford Mathematical Monographs. The Clarendon Press Oxford University Press, New York, 2000. ISBN 0-19-850245-1.

[6] H. Attouch. *Variational convergence for functions and operators*. Applicable Mathematics Series. Pitman (Advanced Publishing Program), Boston, MA, 1984. ISBN 0-273-08583-2.

[7] M. Bahiana and Y. Oono. Cell dynamical system approach to block copolymers. *Phys. Rev. A*, 41(12):6763–6771, Jun 1990. doi: 10.1103/PhysRevA.41.6763.

[8] C. Bernardi and Y. Maday. *Approximations spectrales de problèmes aux limites elliptiques*, volume 10 of *Mathématiques & Applications (Berlin) [Mathematics & Applications]*. Springer-Verlag, Paris, 1992. ISBN 2-287-00387-8.

[9] J. P. Boyd. *Chebyshev and Fourier spectral methods*. Dover Publications Inc., Mineola, NY, second edition, 2001. ISBN 0-486-41183-4.

[10] A. Braides. *Γ-convergence for beginners*, volume 22 of *Oxford Lecture Series in Mathematics and its Applications*. Oxford University Press, Oxford, 2002. ISBN 0-19-850784-4.

[11] H. Brezis. *Analyse fonctionnelle*. Collection Mathématiques Appliquées pour la Maîtrise. [Collection of Applied Mathematics for the Master's Degree]. Masson, Paris, 1983. ISBN 2-225-77198-7. Théorie et applications. [Theory and applications].

[12] I. N. Bronstein and K. A. Semendjajew. *Taschenbuch der Mathematik*. B. G. Teubner Verlagsgesellschaft mbH, Stuttgart, fifth edition, 1991. ISBN 3-8154-2000-8. Translated from the Russian, Translation edited and with a foreword by G. Grosche, V. Ziegler and D. Ziegler.

[13] C. Canuto and A. Quarteroni. Approximation results for orthogonal polynomials in Sobolev spaces. *Math. Comp.*, 38(157):67–86, 1982. ISSN 0025-5718.

[14] C. Canuto, M. Y. Hussaini, A. Quarteroni, and T. A. Zang. *Spectral methods in fluid dynamics*. Springer Series in Computational Physics. Springer-Verlag, New York, 1988. ISBN 0-387-17371-4.

[15] C. Canuto, M. Y. Hussaini, A. Quarteroni, and T. A. Zang. *Spectral methods*. Scientific Computation. Springer-Verlag, Berlin, 2006. ISBN 978-3-540-30725-9; 3-540-30725-7. Fundamentals in single domains.

[16] C. Canuto, M. Y. Hussaini, A. Quarteroni, and T. A. Zang. *Spectral methods*. Scientific Computation. Springer, Berlin, 2007. ISBN 978-3-540-30727-3. Evolution to complex geometries and applications to fluid dynamics.

[17] R. Choksi. Scaling laws in microphase separation of diblock copolymers. *J. Nonlinear Sci.*, 11(3):223–236, 2001. ISSN 0938-8974.

[18] R. Choksi and X. Ren. On the derivation of a density functional theory for microphase separation of diblock copolymers. *J. Statist. Phys.*, 113(1-2):151–176, 2003. ISSN 0022-4715.

[19] N. Condette, C. Melcher, and E. Süli. Spectral approximation of pattern-forming nonlinear evolution equations with double-well potentials of quadratic growth. *Math. Comp.*, 80:205–223, 2011.

[20] J. W. Cooley and J. W. Tukey. An algorithm for the machine calculation of complex Fourier series. *Math. Comp.*, 19:297–301, 1965. ISSN 0025-5718.

[21] G. Dal Maso. *An introduction to* Γ*-convergence*. Progress in Nonlinear Differential Equations and their Applications, 8. Birkhäuser Boston Inc., Boston, MA, 1993. ISBN 0-8176-3679-X.

[22] E. De Giorgi and T. Franzoni. Su un tipo di convergenza variazionale. *Atti Accad. Naz. Lincei Rend. Cl. Sci. Fis. Mat. Natur. (8)*, 58(6):842–850, 1975.

[23] A. Desimone, R. V. Kohn, S. Müller, and F. Otto. A reduced theory for thin-film micromagnetics. *Comm. Pure Appl. Math.*, 55(11):1408–1460, 2002. ISSN 0010-3640.

[24] A. DeSimone, R. V. Kohn, S. Müller, and F. Otto. Recent analytical developments in micromagnetics. In G. Bertotti and I. Mayergoyz, editors, *The Science of Hysteresis*, volume 2, chapter 4, pages 269–381. Elsevier Academic Press, 2005. ISBN 0-12-480874-3.

[25] Q. Du and R. A. Nicolaides. Numerical analysis of a continuum model of phase transition. *SIAM J. Numer. Anal.*, 28(5):1310–1322, 1991. ISSN 0036-1429.

[26] L. C. Evans. *Partial differential equations*, volume 19 of *Graduate Studies in Mathematics*. American Mathematical Society, Providence, RI, 1998. ISBN 0-8218-0772-2.

[27] L. C. Evans and R. F. Gariepy. *Measure theory and fine properties of functions*. Studies in Advanced Mathematics. CRC Press, Boca Raton, FL, 1992. ISBN 0-8493-7157-0.

[28] H. Federer. *Geometric measure theory*. Die Grundlehren der mathematischen Wissenschaften, Band 153. Springer-Verlag New York Inc., New York, 1969.

[29] A. Finlayson and L. Scriven. The method of weighted residuals: a review. *Applied Mechanics Review*, 19:735–748, 1966.

[30] B. Fornberg. *A practical guide to pseudospectral methods*, volume 1 of *Cambridge Monographs on Applied and Computational Mathematics*. Cambridge University Press, Cambridge, 1996. ISBN 0-521-49582-2.

[31] G. Gehring and B. Kaplan. The domain structure in ultrathin magnetic films. *J. Magn. Magn. Mat.*, 128:111–116, 1993.

[32] G. Gioia and R. James. Micromagnetics of very thin films. *Proc. R. Soc. Lond. A*, 453:213–223, 1997.

[33] D. Gottlieb and S. A. Orszag. *Numerical analysis of spectral methods: theory and applications*. Society for Industrial and Applied Mathematics, Philadelphia, Pa., 1977. CBMS-NSF Regional Conference Series in Applied Mathematics, No. 26.

[34] B.-Y. Guo. *Spectral methods and their applications*. World Scientific Publishing Co. Inc., River Edge, NJ, 1998. ISBN 981-02-3333-7.

[35] A. Hubert. Statics and dynamics of domain walls in bubble materials. *J. Appl. Phys.*, 46(5):2276–2287, 1975.

[36] A. Hubert and R. Schäfer. *Magnetic Domains: The Analysis of Magnetic Microstructures*. Springer Verlag, 1998.

[37] L. Kantorovic. On a new method of approximate solution of partial differential equation. *Dokl. Akad. Nauk SSSR*, 2:532–536, 1934.

[38] C. Kooy and U. Enz. Kooy-enz theory. *Philips Res. Rep.*, 15(7), 1960.

[39] H.-O. Kreiss and J. Oliger. Comparison of accurate methods for the integration of hyperbolic equations. *Tellus*, 24:199–215, 1972. ISSN 0040-2826.

[40] O. A. Ladyženskaja, V. A. Solonnikov, and N. N. Ural′ceva. *Linear and quasilinear equations of parabolic type*. Translated from the Russian by S. Smith. Translations of Mathematical Monographs, Vol. 23. American Mathematical Society, Providence, R.I., 1967.

[41] C. Lanczos. Trigonometric interpolation of empirical and analytical functions. *J. Math. Phys.*, 17:123–199, 1938.

[42] L. Landau and E. Lifshitz. On the theory of the dispersion of magnetic permeability in ferromagnetic bodies. *Phys. Z. Sowjetunion*, 8:153–169, 1935.

[43] C. Melcher. The logarithmic tail of Néel walls. *Arch. Ration. Mech. Anal.*, 168(2): 83–113, 2003. ISSN 0003-9527.

[44] B. Mercier. *An introduction to the numerical analysis of spectral methods*, volume 318 of *Lecture Notes in Physics*. Springer-Verlag, Berlin, 1989. ISBN 3-540-51106-7.

[45] L. Modica. The gradient theory of phase transitions and the minimal interface criterion. *Arch. Rational Mech. Anal.*, 98(2):123–142, 1987. ISSN 0003-9527.

[46] Y. Nishiura and I. Ohnishi. Some mathematical aspects of the micro-phase separation in diblock copolymers. *Phys. D*, 84(1-2):31–39, 1995. ISSN 0167-2789.

[47] T. Ohta and K. Kawasaki. Equilibrium morphology of block copolymer melts. *Macromolecules*, 19:2621–2632, 1986.

[48] E. Schlömann. Domain walls in bubble films. i. general theory of static properties. *J. Appl. Phys.*, 44(4):1837–1849, 1973.

[49] J. Slater. Electronic energy bands in metal. *Phys. Rev.*, 45:794–801, 1934.

[50] J. Slonczewski. Theory of domain wall motion in magnetic films and platelets. *J. Appl. Phys.*, 44:1759–1770, 1973.

[51] L. N. Trefethen. *Spectral methods in MATLAB*, volume 10 of *Software, Environments, and Tools*. Society for Industrial and Applied Mathematics (SIAM), Philadelphia, PA, 2000. ISBN 0-89871-465-6.

Selbständigkeitserklärung

Hiermit versichere Ich, meine Dissertation *Pattern Formation in Magnetic Thin Films: Analysis and Numerics* selbstständig und ohne unerlaubte Hilfsmittel erstellt zu haben.

Die verwendte Literatur und die Hilfsmittel sind in der Arbeit angegeben. Die Promotionsordnung der Mathematisch-Naturwissenschaftlichen Fakultät II ist mir bekannt. Ich habe mich nicht anderwärts um einen Doktorgrad beworben und ich besitze noch keinen Doktorgrad im Promotionsfach.

Berlin, den 29.01.2010 Nicolas Condette